Alma Mater Studiorum – Università di Bologna

DOTTORATO DI RICERCA IN

SCIENZE BIOMEDICHE E NEUROMOTORIE

Ciclo XXXVI

Settore Concorsuale: 05/D1 - FISIOLOGIA

Settore Scientifico Disciplinare: BIO/09 - FISIOLOGIA

CATEGORIZATION OF SLEEP APNEAS IN DIFFERENT MOUSE MODELS OF HUMAN DISEASES

Presentata da: GABRIELE MATTEOLI

Coordinatore Dottorato

PROF.SSA MATILDE YUNG FOLLO

Supervisore

PROF.SSA GIOVANNA ZOCCOLI

Co- Supervisore

PROF. FRANCO TREVISANI

Esame finale anno 2023

INDEX

ABSTRACT

Introduction. Sleep apneas represent the most common and hazardous form of sleep-related breathing disorders (SBD). Depending on their origin, sleep apneas can be categorized as central sleep apneas (CSA), when they arise from a disruption in the central transmission of the signal for inspiration, or as obstructive sleep apneas (OSA), when an obstruction of the airways occurs. Regardless of their nature, they produce a series of life-threatening cardiovascular, metabolic, and neurocognitive dysfunctions. However, despite the evident clinical significance, our understanding of the mechanisms and genetic factors contributing to these conditions, particularly OSA, remains limited. Moreover, current therapies are not fully efficacious or targeted and this challenge is further exacerbated in individuals with craniofacial abnormalities, such as in Down Syndrome (DS), CDKL5 deficiency disorder (CDD), and Pierre Robin sequence (PRS), where SBDs are even more prevalent.

Aim. To investigate whether the genetic mouse models of DS (Ts65Dn mice, TS), CDD (CDKL5-knockout mice, CDKL5-KO), and PRS (BMP7-knockout, BMP7-KO mice) could replicate the respiratory disturbances observed in human patients.

Methods. Experiments were performed on age-matched male mice. Specifically, we employed 12 TS mice and 14 euploid controls (EU) for the model of DS, 14 CDKL5-KO and 10 wild-type mice (CDKL5-WT) for the model of CDD, and 3 BMP7-KO and 3 control mice (BMP7-WT) for the model of PRS. Each mouse was implanted with specific electrodes for sleep stage discrimination and diaphragmatic activity (DIA) detection and was recorded twice inside a whole-body plethysmograph (WBP) for 8 hours during the light (resting) period. Then, the hypnic and respiratory phenotypes were assessed and apneas occurring during sleep were categorized as either CSA or OSA according to the DIA and WBP signals.

Results on the DS mouse model. We observed a decreased occurrence of CSA during non-rapid-eye-movements (NREM) sleep in TS mice when compared to EU controls. TS mice also exhibited a higher frequency of apneas with an obstructive element during rapid-eye-movements (REM) sleep, which was accompanied by an increased amplitude of diaphragmatic bursts, likely indicating a greater diaphragm effort. Finally, we found that all apneic events, regardless of their type, were associated with bradycardia.

Results on the CDD mouse model. CDKL5-KO mice showed a reduced occurrence of sighs during NREM sleep and a heightened frequency of apneas with an obstructive component during REM sleep when compared to CDKL5-WT mice. While there is a lack of direct evidence for OSAs in human CDD pathology, these findings suggest a potential link

between CDKL5 kinase and the regulation of breathing, possibly involving the control of upper airway musculature.

Results on the PRS mouse model. Preliminary data indicated that almost all apneic events occurring during NREM sleep were CSA in both BMP7-KO and BMP7-WT mice, whereas both CSA and OSA occurred during REM sleep. Moreover, despite considerable variability among mice within the same experimental group, BMP7-KO mice appeared to exhibit an augmented increased occurrence rate of CSA during NREM sleep, as well as an augmented frequency of both CSA and OSA during REM sleep in comparison to BMP7-WT mice.

Conclusions. We demonstrated that mice are valuable models for the investigation of SBDs, as they exhibited OSAs and varying degrees of airway obstruction like humans. Notably, we found that TS and CDKL5-KO mice, which respectively recapitulate the core aspects of DS and CDD, can be used as valid models of OSA, whereas BMP7-KO mice, model of PRS, require further investigation. Therefore, this insight will help not only to enhance our comprehension of the mechanisms underlying the genesis of obstructive events, but also holds the potential to expedite the development of targeted therapies.

INTRODUCTION

1. SLEEP

1.1 DEFINITION OF SLEEP

Sleep is a spontaneous, cyclically occurring, and reversible brain process characterized by a loss of responsiveness to the environment, unconsciousness, and absence of voluntary movements[1,2].

Sleep, in the strictest sense of the word, had been historically set aside only for mammals and birds because its different stages could be easily distinguished by clear behavioral schemes and specific brain electrical activity[2,3]. However, sleep is a fundamental and ubiquitous behavior in the animal kingdom[4] and sleep-like states are highly conserved during evolution[3]. Therefore, thanks to the advent of the molecular revolution, the investigation of the mechanisms and genetics of sleep has been extended to simpler models (e.g., *Drosophila melanogaster*, *Caenorhabditis elegans*, and *Danio rerio*), which required new criteria for the definition of this phenomenon[2,5]. Notably, these include a behavioral quiescence with loss of locomotion, a species-specific posture or a resting place aimed at minimizing sensory stimulation, the need for an elevated arousal threshold to environmental stimuli, an homeostatic regulation following circadian mechanisms, a rapid reversibility, and the presence of state-related changes in neural function[1,2,5,6].

1.2 SLEEP FUNCTIONS

The intrinsic biological importance of sleep is evidently demonstrated by the high conservation of a sort of rest behavior throughout the entire animal kingdom[4] and by the fact that humans usually spend up to one-third of their lives sleeping[7]. Furthermore, sleep appears even more vital when focusing on the deleterious effects of sleep deprivation, which is associated with a higher risk of premature mortality due to cardiovascular diseases, malignant neoplasms, cerebrovascular diseases, accidents, diabetes, septicemia, and hypertension[8,9]. Indeed, as confirmed by numerous studies on the effects of sleep loss, sleep is evidently involved in various and numerous physiological body functions, such as glucose and lipid metabolism, energy expenditure/intake, respiration, DNA repair, hormone homeostasis, arterial blood pressure, inflammation, vigilance, memory, learning, brain development, response to stress, and mood[8–15]. However, notwithstanding extensive efforts

have been made to investigate mechanisms, molecular pathways, and specific processes associated with sleep, there is still little scientific consensus regarding the actual function of sleep, which remains one of the biggest enigmas of neurobiology[2,12,16].

During the last decades, a lot of different hypotheses about the function of sleep have been developed and discussed by the major experts in the field. These theories are not mutually exclusive and consider several and different aspects, ranging from high-order activities (learning and memory) to housekeeping and homeostatic functions (detoxification and restoration).

The **cognitive hypothesis** proposes that sleep is essential for learning and memory. Indeed, it has been demonstrated that information and memories encoded during the wake period are transferred from the hippocampus (i.e., the temporary store) to the neocortex (i.e., the long-term store) during non-rapid-eye-movements (NREM) sleep[17]. This process, necessary for long-term memory consolidation, is enabled by coupling between electrical events in these two regions[2] and by the consolidation of synapses[18].

In line with the previous theory, the **synaptic homeostasis hypothesis** concerns that sleep is fundamental for the maintenance of cerebral synaptic plasticity, which, in turn, is essential for high-order functions. During normal wakefulness, the interaction with the environment and the acquisition of information induces an increase in the number and size of synapses, changes in dendritic spines and synaptic boutons, and a potentiation of existing synapses[2]. Thus, this imposes a great cost on the brain in terms of energy consumption, delivery of cellular supplies, cellular stress, and increased support from glial cells[19]. Therefore, sleep aims to restore normal brain function by selectively downscaling specific subsets of synapses to a baseline level that is energetically sustainable and by saving space in the gray matter[19,20] in order to prevent learning saturation.

The **restorative hypothesis** suggests that sleep is necessary for re-equilibrating a cumulative condition occurring during the waking state, which mainly involves brain energy, macromolecular synthesis, and/or detoxification[2].

In 1995, Benington and Heller first developed the **brain energy hypothesis**, according to which sleep, specifically NREM sleep, is essential for the replenishment of cerebral glycogen stores that are depleted during waking. Indeed, when the brain is strongly active and the metabolic demand is high, ATP production, starting from cerebral glycogen, causes the continuous accumulation of extracellular adenosine, which acts as a signal of energy depletion and promotes sleep onset[21]. Nevertheless, a recent review[22] rejected the central involvement of glycogen metabolism in sleep regulation in favor of more complex cellular

mechanisms, while not denying the evident role of sleep in brain energy balance and homeostasis[2,23].

Furthermore, a lot of studies corroborate the **macromolecules synthesis theory**, according to which sleep exerts a restorative function by promoting the synthesis of proteins, peptides, or lipids necessary for normal waking function[2,24] and by actively changing intracellular dynamics[25]. For instance, NREM sleep fosters the synthesis of proteins[26,27] and RNA[28,29] in the brain of various animal models (rats, macaques, rabbits)[2]. Notably, this positive correlation between sleep and macromolecule synthesis was found for some synaptic proteins and neurotrophins, which are involved in memory consolidation and synaptic plasticity[30–33], and for some genes involved in cholesterol synthesis, protection from oxidative stress, energy regulation, lipid transport, membrane trafficking, neuronal transmission, and vesicle maintenance and transport[2,24,30,34,35].

In addition, sleep may be also involved in the elimination of something accumulated above a desirable level[2]. Indeed, the **glymphatic clearance hypothesis** focuses on the role of sleep in the elimination of waste products of metabolism[36]. This cleaning function is realized in both mice[37,38] and humans[39,40] by the glymphatic system, which is a highly organized series of cerebral lymph vessels that drive the exchange of interstitial fluid (ISF) with cerebrospinal fluid (CSF)[41]. Particularly, CSF flows from the subarachnoid space into the brain through a barrier constituted by the end-feet of the astrocytes lining the blood vessels, which are equipped with aquaporins and allow water and small molecular solutes to enter the ISF of the brain parenchyma. Then, ISF leaves the parenchyma through perivascular spaces around the venules and veins to return excess metabolic wastes and toxins to the general circulation[2,42,43]. Interestingly, the connection between the glymphatic system and sleep comes from the evidence that the interstitial space expands highly during sleep, consequently causing a dramatic increase in the exchange of substances between CSF and ISF[36]. In turn, these convective fluxes increase the clearance rate during sleep, enhancing the removal of potentially neurotoxic waste products[36], such as the lactate produced by neural activation during wakefulness[41] and the soluble β-amyloid[37].

Finally, the emerging use of simple animal models in the field of the genetics of sleep paved the way for new and intriguing findings and, consequently, a great number of modern theories about sleep function. However, these theories need cautious interpretation. Indeed, these advanced technologies have allowed the discovery of several genetic components related to sleep that are conserved across different species[5]. Nevertheless, while some of them are involved in circadian rhythm regulation (e.g., SIK3 promotes sleep in mice, fruit flies, and roundworms)[44], most of the identified molecular pathways are not explicitly

connected to sleep but to a variety of different and unspecific cellular events (e.g., Epidermal Growth Factor, protein kinase G, cyclic adenosine monophosphate, dopamine, histamine, and N-methyl-D-aspartate)[5].

1.3 CLASSIFICATION OF SLEEP STAGES

The traditional approach to study sleep began with the measurement of brain electrical activity through electroencephalography (EEG)[1], which was first introduced by Hans Berger in 1924[45] and then applied in the field of sleep study by Alfred Loomis in 1937[46]. This technique was later improved with the introduction of the electrooculogram (EOG) by Aserinsky and Kleitman[47] and of the electromyogram (EMG) thanks to the studies of Jouvet in cats[48]. Nowadays, the objective study of sleep physiology and disorders requires the use of polysomnography, which involves recording multiple physiological parameters relevant to sleep, such as EEG from central and occipital derivations, EOG activity from the right and the left eye, chin EMG, respiratory effort from thorax and abdomen, nasal and oral airflow, snoring, electrocardiography (ECG), blood oxygen saturation, and body position[1,49–51].

SLEEP IN HUMANS

The human sleep stage classification system[52,53] relies on EEG, EOG, and submental EMG activity in conventional time domains of 30 seconds[1]. According to the *American Academy of Sleep Medicine Manual for the Scoring of Sleep and Associated Events*, revised in February 2023, we can identify three main behavioral states: wakefulness (W), NREM sleep, and rapid-eye-movements (REM) sleep.

W is characterized by low-voltage EEG, predominantly localized in the alpha range (8-13 Hz) mixed with beta activity (13-30 Hz) when the eyes are closed. However, opening the eyes or performing a cognitive task such as counting leads to the reduction or inhibition of alpha activity in favor of beta waves (stopping reaction). In addition, strong muscle activity together with either rapid or slow eye movements is present during W[1,51].

NREM sleep onset is identified when the alpha waves occupy less than 50% of an epoch, or when delta activity (0.5-4 Hz) or peculiar wave patterns of sleep occur (e.g., vertex waves, K-complexes, sleep spindles)[1,51]. This sleep stage can be further divided into three sub-stages[1,51]:

- **N1** corresponds to the sleep onset and is identified by a low-voltage mixed-frequency EEG in the absence of K-complexes or spindles, with slow eye movements and preserved muscle activity.
- **N2** is characterized by an EEG activity at relatively low voltage and mixed frequency with high amplitude delta waves that occupy less than 20% of the epoch. Additionally, sleep spindles (i.e., symmetric bursts at 12-14 Hz) and K-complexes (i.e., high amplitude and symmetric waveforms with a sharp negative start followed by a slow positive phase) are present. The muscle tone is reduced, while eye movements are absent.
- **N3** represents the deepest stage of sleep and is defined by the predominance of a high-amplitude activity in the delta range (slow waves) which occupies more than 20% of the epoch with no eye movements.

REM sleep is characterized by a low-voltage mixed-frequency EEG activity with "saw-tooth" theta waves (4-7 Hz), muscle atonia with episodic tonic twitches, and rapid eye movements, which occur isolated or in bursts[1,51].

SLEEP IN MICE

Mice sleep can be classified into three stages (W, NREM sleep, and REM sleep) according to criteria derived from the standard human classification of sleep stages[52–54]. Similarly to humans, mouse W is characterized by desynchronized EEG patterns accompanied by high muscle tone. NREM sleep, whose different phases are not easily distinguishable in mice[55], is identified by synchronized EEG activity, primarily composed of delta waves, and decreased muscle tone. REM sleep is associated with skeletal muscles atonia and predominant EEG activity in the theta range[56–58].

However, despite the numerous similarities in genomic sequence, EEG pattern, and brain circuitry[55], some marked differences between humans and mice must be considered.

The first difference is represented by the percentage of time spent in each sleep stage over the total sleep time. Indeed, a healthy adult usually spends approximately 70-75% of sleep time in NREM sleep, with a prevalence in N2, and the remaining 20-25% in REM sleep, with negligible differences between men and women[1,51]. Conversely, in mice, NREM and REM sleep occupy 85-90% and 10-15%, respectively[59].

Second, the circadian distribution of sleep is normally monophasic in humans, as sleep is usually taken in one session during a 24-hour period, while mouse sleep is polyphasic[55]. In fact, humans show a regular pattern of reoccurrence of sleep cycles during the nighttime:

individuals first enter the N1 stage of NREM sleep for a few minutes, which is followed by 10-25 minutes of N2 (or interrupted by W), then by 20-40 minutes of N3, and finally by 4-8 minutes of REM sleep. Moreover, although NREM and REM sleep continue to alternate throughout the night in a cyclical fashion for 7-8 hours, NREM sleep episodes are more abundant in the first hours of sleep, becoming rare or absent near the morning awakening, while REM sleep episodes tend to increase in duration in the last sleep cycles[1,51]. On the other hand, even if mice are preponderantly awake during the dark (active) phase and asleep during the light (resting) phase, being nocturnal animals, they show a significant quote of NREM and REM sleep episodes distributed also during their active period[55,60,61]. Consequently, due to the intrinsic nature of the sleep cyclic pattern, sleep episodes in mice appear to be shorter (2-4 minutes) and more fragmented when compared with human beings, even under normal conditions[55,59].

Finally, other differences can be found in the duration of wake-sleep transitions. Humans spend from 10 seconds to a few minutes to pass from W to sleep, while mice need only a few seconds or less because of the rapid stabilization of the NREM sleep state[56,62,63].

1.4 REGULATION OF SLEEP

The coordination between sleep and wake is governed by a range of internal and external drivers which maintain the autonomic nervous system in a dynamic balance. The alternation of wake and sleep is entrusted to complex systems distributed throughout the brain, which can be outlined as two main mechanisms that synergically operate: the homeostatic sleep drive (or process S) and circadian rhythms (or process C)[1,64,65].

Homeostatic processes represent sleep debt, which exponentially increases along daily W and subsequently diminishes during sleep. This time trend strongly correlates with the EEG slow-wave activity (SWA) measured during NREM sleep, a well-characterized marker of sleep homeostasis[64]. Indeed, SWA increases in the presence of longer W episodes and progressively declines during a sleep episode in different species[66,67], revealing a possible downscaling of synaptic strength, which is important for neural function[20]. On the other hand, circadian mechanisms regulate the propensity for sleep throughout the entire day independently of prior W episodes[68]. Strong evidence suggests that the principal mammalian timekeeping structure, from which the circadian process arises, is the suprachiasmatic nucleus (SCN) of the anterior hypothalamus[69], that receives a major retinal input via the retinohypothalamic tract[64,70].

NEURAL CIRCUITS OF WAKE

Normal W is driven by a specific pathway which that originates from the rostral brainstem and, ascending through the paramedian region of the midbrain, it divides into two branches: the dorsal one leads to the thalamus, while the ventral one innervates the hypothalamus, the basal forebrain (BF), and the cortex[58].

This wake-promoting pathway involves many different neuronal regions which likely synergically work and share many anatomic interconnections and targets (Figure 1)[58]:

- The *locus coeruleus* (LC) is a norepinephrine-producing forebrain nucleus which receives arousal inputs from the brainstem and the prefrontal cortex[71] and projects to several nuclei throughout the central nervous system[72]. Therefore, due to its extensive interconnectivity, LC works as a broadcast system and is essential in the response to stress and stimuli related to reward or threat[73].
- The *dorsal raphe* (DR) and *median raphe* (MR) are serotonin-producing forebrain nuclei which regulate not only the wake/sleep cycle but also mood, reward, and patience since they innervate and receive reciprocal inputs from the amygdala, the insula, and the prefrontal cortex[74].
- Dopamine-releasing neurons of the *ventral tegmental area* (VTA) promote wake under conditions of high motivation[75], even if they lack the typical firing pattern of other monoamine neurons[76].
- The hypothalamic *tuberomammillary nucleus* (TMN) promotes cortical activation and generalized wake arousal, probably in synergy with the neurotransmitter gamma-aminobutyric acid (GABA)[77].
- The *BF* is a wide brain region consisting of numerous populations of neurons producing acetylcholine, GABA, or glutamate, which innervate both the cortex and local BF nuclei to promote wake[78–80], and the amygdala and the dorsal hippocampus to drive theta activity[79,81].
- Glutamatergic neurons of the *parabrachial nucleus* (PB) promote arousal in response to a variety of interoceptive stimuli, such as an increase in blood carbon dioxide (CO_2)[82].
- The *lateral hypothalamus* (LH) contains a neuronal population that produces orexins, fundamental neurotransmitters for maintaining long periods of wake[83,84] and for regulating the wake/sleep cycle[85,86]. These neurons diffusely project throughout the entire neuroaxis[87,88] and excite all the above-mentioned wake-promoting brain regions, the thalamus, and the cortex[89]. Additionally, orexins signaling also

influences the maintenance of arousal in response to stress, reward, and defense against homeostatic challenges, such as food deprivation[90–92].

To conclude, further studies are still required to discover the effective function of other presumptive wake-promoting areas. Among them, it is worthy to mention the dopaminergic neurons of the ventral periaqueductal gray[93], the cholinergic, GABAergic, and glutamatergic neurons of the pedunculopontine and laterodorsal tegmental nuclei[94], and the GABAergic neurons in the LH[95,96].

Figure 1

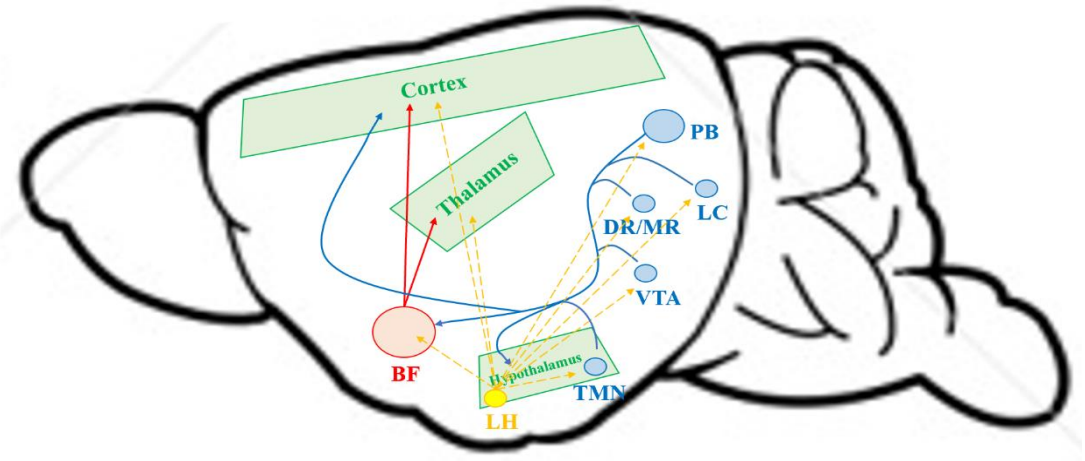

Figure 1. Schematic representation of wake-promoting brain regions.
Basal forebrain (BF), locus coeruleus (LC), dorsal and median raphe (DR/MR), ventral tegmental area (VTA), tuberomammillary nucleus (TMN), Parabrachial Nucleus (PB), and lateral hypothalamus (LH).

NEURAL CIRCUITS OF NREM SLEEP

NREM sleep regulation is mediated by specific promoting substances called somnogenes, which increase during W and act as paracrine mediators to promote sleep[58]; for instance, they include adenosine, prostaglandin D_2, interleukin-1, and tumor necrosis factor-α[97].
Among them, adenosine is certainly the most understood and studied. We know that this neurotransmitter, predominantly released by astrocytes in the extracellular environment[98,99], increases during prolonged periods of W and declines during sleep[99,100]. Particularly, it promotes sleep by directly inhibiting wake-promoting brain areas and activating sleep-promoting neurons[101].

Neuronal circuits for the promotion of NREM sleep include several brain regions (Figure 2):

- The *preoptic area* (POA), located in the anterior hypothalamus[102,103], contains neurons selectively active during NREM and REM sleep[104]. Notably, the ventrolateral preoptic area (VLPO) and median preoptic nucleus (MnPO) contain

GABA- and galanin-producing neurons essential for promoting NREM sleep[105,106] and for mediating the homeostatic response to sleep deprivation[58], as they inhibit arousal-promoting brain regions (i.e., BF, orexin neurons, TMN, DR/MR, PB, and LC)[107–109].

- The *BF* includes some GABAergic neuronal populations which are active during NREM sleep[110] to directly inhibit cortical neurons[111] and, possibly, the neighboring wake-promoting neurons via somatostatin[79,112].
- The *parafacial zone* (PZ), located in the caudal brainstem[113], encompasses GABAergic/glycinergic neurons whose activation induces sustained periods of NREM sleep with high EEG delta power by the direct inhibition of PB[114].

Nevertheless, even though the function of POA, BF, and PZ is clearly established in the regulation of NREM sleep, their role in the generation of the transition from W to NREM sleep and in the sustainment of NREM sleep episodes still needs extensive studies. In addition, further research will also clarify the role of cortical neuronal nitric oxide synthase (nNOS)-expressing neurons, which are active during NREM sleep[115,116] and are thought to synchronize slow cortical rhythms[58].

Figure 2

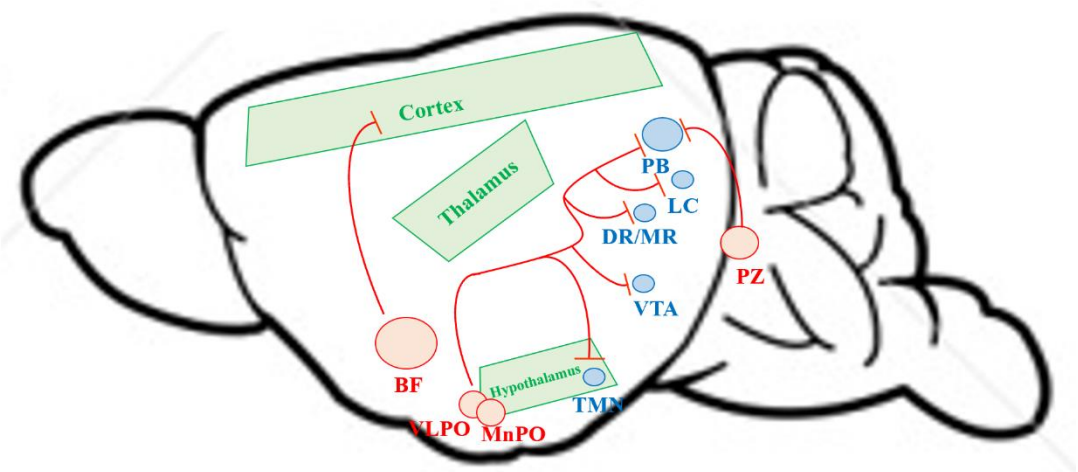

Figure 2. Schematic representation of non-rapid-eye-movement (NREM) sleep-promoting brain regions.

Basal forebrain (BF), Ventrolateral Preoptic Area (VLPO), Median Preoptic nucleus (MnPO), Parafacial Zone (PZ), Locus coeruleus (LC), Dorsal and Median Raphe (DR/MR), Ventral Tegmental Area (VTA), Tuberomammillary Nucleus (TMN), and Parabrachial Nucleus (PB).

NEURAL CIRCUITS FOR REM SLEEP

The principal brain regions involved in the neural circuits required for the regulation of REM sleep are mainly located in the pons[58] (Figure 3):

- *Pedunculopontine and laterodorsal tegmental nuclei* (PPT/LDT) include a cholinergic population of neurons which, although they have long been considered the key generator of REM sleep[117], are now seen as modulators probably promoting transitions from NREM to REM sleep[118].
- The *sublaterodorsal nucleus* (SLD) contains glutamatergic neurons essential for the generation of muscle atonia[119], even though its mechanisms are still debated[58]. Particularly, one model proposes that the SLD excites neurons in the ventromedial medulla (VMM) that, in turn, inhibit spinal motoneurons[120–122], while another hypothesizes that SLD neurons directly innervate spinal interneurons to inhibit motoneurons[123].
- *LC* and *DR* contain specific monoaminergic neurons thought to abolish REM sleep during W since they project to the SLD[124] and to PPT/LDT[125,126] to suppress the activity of REM sleep-active neurons.
- The *ventrolateral periaqueductal gray matter* and the *lateral pontine tegmentum* (vlPAG/LPT) inhibit REM sleep via GABAergic projections to the SLD[123,127–129].
- *Dorsal paragigantocellular reticular* (DPGi) and *lateral paragigantocellular* (LPGi) *nuclei* may promote REM sleep by inhibiting pontine REM sleep-suppressing neurons (i.e., LC, DR and vlPAG/LPT)[129,130].

Finally, the hypothalamus has been recently identified as a brain region which helps to generate and regulate REM sleep (Figure 3). Notably, VLPO[131], melanin-concentrating hormone (MCH)-producing neurons of LH and posterior hypothalamus (PH)[132–134], and orexinergic neurons of LH[84,135–137] promote REM sleep by inhibiting REM sleep-suppressing neurons of the brainstem. Additionally, MCH-producing neurons also innervate the SLD[138], directly promoting the entrance into REM sleep.

Figure 3

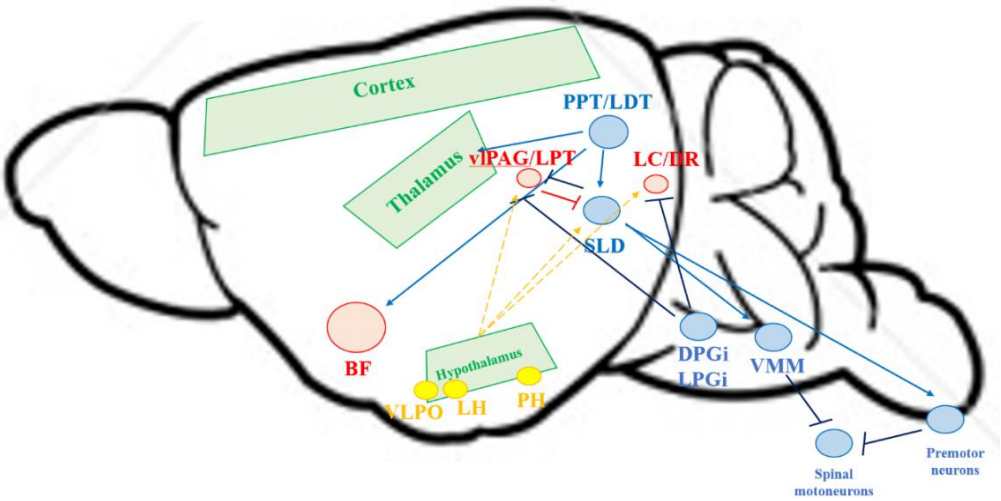

Figure 3. **Schematic representation of rapid-eye-movement (REM) sleep-promoting brain regions.** Basal forebrain (BF), Pedunculopontine and Laterodorsal Tegmental Nuclei (PPT/LDT), Sublaterodorsal Nucleus (SLD), Ventromedial Medulla (VMM), Locus coeruleus and Dorsal Raphe (LC/ DR), Ventrolateral Periaqueductal Grey matter and the Lateral Pontine Tegmentum (vlPAG/LPT), Dorsal Paragigantocellular reticular nucleus (DPGi), Lateral Paragigantocellular nucleus (LPGi), Ventrolateral Preoptic Area (VLPO), and lateral and posterior hypothalamus (LH and PH, respectively).

However, notwithstanding the extensive studies on REM sleep, a complete model that can explain its regulation is still missing. Therefore, future research is further required to determine whether the pons, medulla, or both together mainly drive REM sleep, to investigate whether glutamatergic and GABAergic neurons in the PPT/LDT regulate REM sleep, and to establish the relative contributions of all the different neuronal pathways involved in the control of REM sleep atonia.

Table 1 resumes the brain centers involved in the wake-sleep cycle regulation.

Table 1

State	Brain center	Neurotransmitters
Wakefulness	LC	Norepinephrine
	DR/MR	Serotonin
	VTA	Dopamine
	TMN	Histamine
	BF	Acetylcholine, GABA, or Glutamate
	PB	Glutamate
	LH	Orexins
NREM sleep	POA	GABA and Galanin
	BF	GABA and Somatostatin
	PZ	GABA and Glycine
REM sleep	PPT/LDT	Acetylcholine
	SLD	Glutamate
	LC	Monoamines
	DR	Monoamines
	vlPAG/LPT	GABA

Table 1. **Brain centers involved in the wake-sleep cycle regulation.**

Brain regions involved in wakefulness regulation: Locus coeruleus (LC), Dorsal and Median Raphe (DR/MR), Ventral Tegmental Area (VTA), Tuberomammillary Nucleus (TMN), Basal forebrain (BF), Parabrachial Nucleus (PB), and lateral hypothalamus (LH).

Brain regions involved in non-rapid-eye-movements (NREM) sleep regulation: Preoptic Area (POA), Basal forebrain (BF), and Parafacial Zone (PZ).

Brain regions involved in rapid-eye-movements (REM) sleep regulation: Pedunculopontine and Laterodorsal Tegmental Nuclei (PPT/LDT), Sublaterodorsal Nucleus (SLD), Locus coeruleus (LC), Dorsal Raphe (DR), and Ventrolateral Periaqueductal Grey matter and the Lateral Pontine Tegmentum (vlPAG/LPT).

CIRCADIAN REGULATION OF SLEEP

The SCN, the master circadian pacemaker, consists of heterogeneous neuronal populations capable of self-sustaining and producing circadian oscillations of both neuronal activity and gene expression to regulate sleep[139,140]. Notably, the autoregulatory ability of this network relies on the strong interconnection that characterizes its different neurons[141] and on the interaction between both positive and negative pathways involving specific patterns of transcription-translation and post-translational modifications[142]. Among them, it is worthy to mention the transcription factors Clock and its analogues which drive the transcription of numerous clock-controlled genes, such as *Period* and *Cryptochrome* genes, that, in turn, disinhibit Clock activity in a cyclic fashion every 24 hours[143–145].

Moreover, other evidence of the crucial role of the SCN in the circadian regulation of the wake/sleep cycle can be found in its anatomical connections. Indeed, this nucleus heavily innervates other hypothalamic areas (such as the subparaventricular zone and the dorsomedial nucleus)[70,146], suggesting its involvement in the promotion of arousal during the active period and of sleep during the rest period, as well as in the sustainment of circadian rhythms of heart rate, blood pressure, body temperature, locomotor activity, feeding, and daily melatonin secretion[58].

2. RESPIRATION

The respiratory system consists of specific organs and structures, extending from the nares and mouth to the lungs, allowing breathing. This vital body function is essential for gas exchange with the environment and is characterized by the continuous alteration between an inspiratory phase, enabling air to enter the lungs, and an expiratory phase to expel the air[147].

2.1 ELEMENTS OF RESPIRATORY ANATOMY AND PHYSIOLOGY

The upper airway commences with the nares and the mouth, serving as entry points for air into the body and to filter, heat, and humidify it. The path then extends through the pharynx and larynx, with the epiglottis permitting air passage while preventing food from entering the airway. This portion also permits some other non-breathing activities, such as talking and swallowing. Interestingly, due to the lack of bony or cartilaginous support (with the sole exception of the posterior vertebral column), this region is highly deformable and vulnerable to collapse during sleep, when a diffuse reduction in the respiratory muscles activity occurs[148–151].

The lower airway starts from the larynx and continues through the trachea, which splits into two primary bronchi, both fortified with cartilaginous rings to maintain their patency. These structures enter the lungs, which are situated within the thoracic cavity and enveloped by the visceral pleura, while the chest wall is lined by the parietal pleura. The thoracic cage, which serves as a protective housing for the lungs, is composed of the ribs and various respiratory muscles that allow the cyclic alternation of inspirations and expirations, including the diaphragm, intercostal muscles, abdominal muscles, and accessory muscles like the sternocleidomastoid and scalene muscles[148–151].

Inside the lungs, the bronchi further divide into a hierarchical network of smaller bronchial segments, giving rise to the non-cartilaginous bronchioles, which play dual roles in air conduction and gas exchange with the blood circulation. Beyond the bronchioles, there are the alveoli, which are sac-like structures connected to the bronchioles through alveolar ducts. It is within the alveoli that gas exchange occurs through diffusion, enabling oxygen to pass into the lung capillaries while CO_2 is released from the blood into the lungs[148–151].

Inspiration is made possible by the expansion of the rib cage caused by the contraction of specific muscles, the most prominent of which are represented by the diaphragm and external intercostal muscles[152]. However, there are other muscles that contribute to the expansion of the chest, such as the parasternal intercostal, sternocleidomastoid, and scalene muscles[153–155]. In addition, other groups of muscles help regulate the airflow by adjusting the resistance of the upper airways during inspiration. For instance, the dilator naris anterior muscle and the alar part of the nasal muscle help open the naris[156–158], while the muscles of the tongue reduce the collapsibility of the pharynx[159,160], and jaw movements[161] aid in this process as well[152]. Finally, larynx muscles also dilate to allow airflow into the lungs[162–165].

Expiration does not require muscle effort in resting breathing. However, in case of high energetic demand, abdominal and internal intercostal muscles can be engaged[155,166], facilitating air outflow to optimize breathing efficiency and enhance oxygen supply to the blood and brain (active expiration)[167,168]. Active expiration occurs in the case of exercise, high altitude, or during apneas, when the cessation of breathing generates low levels of oxygen and high levels of CO_2 in the blood[169,170]. Additionally, the muscles of the face, the tongue, and the larynx contract to regulate airway patency and reduce the flow of air, prolonging the duration of gas exchange[163,164,171–174].

2.2 CONTROL OF BREATHING RHYTHM

The regular pattern of breathing is governed by groups of neurons called central pattern generators (CPG) and located in the brainstem. Specifically, the preBötzinger Complex (preBötC) is responsible for inspiration and coordinating the different stages of the respiratory cycle[175–178], the lateral portion of the parafacial respiratory group (pFL) generates active expiration during periods of increased metabolic demand[178,179], and the post-inspiratory Complex (PiCo) is hypothesized to generate the post-inspiratory phase together with the Kölliker-Fuse nucleus (KFn)[174,180].

These three CPGs orchestrate the sequential contractions in the inspiratory and expiratory muscles to optimize the flow of air by adapting to the biomechanics of the body[181–186]. Specifically, they maintain the equilibrium of respiratory and blood gases, with a particular focus on arterial CO_2 ($PaCO_2$), ensuring that its level remains within a relatively narrow and stable range (35–45 mmHg)[150,187].

PREBÖTZINGER COMPLEX

The preBötC plays a crucial role in activating the muscles involved in the inspiration[147,175,188,189]. It accomplishes this by directly projecting to multiple respiratory motor nuclei, however, indirect projections are more commonly observed[152]. Specifically, preBötC influences the contraction of the diaphragm by sending activating signals through the phrenic nerve, originating from the phenic nucleus, via the rostral ventral respiratory group (rVRG)[190]. It also controls the musculature of the tongue through the hypoglossal nerve and nucleus via the parahypoglossal region of the reticular formation[189,191,192]. The preBötC also influences the facial muscles innervated by the facial nerve (VII) through the intermediate reticular formation[189,193,194].

In addition, preBötC is strongly connected with other brain regions involved in respiratory control[152]. Specifically, it influences and receives information from other CPGs (Bötzinger complex, PiCo, and pFL), areas involved in the modulation of breathing (KFn, lateral and medial PB, and PAG), in the chemosensitivity (the retrotrapezoid nucleus – RTN – and the LC), in the integration of cardiorespiratory stimuli (the nucleus tractus solitarii, NTS), and the limbic system (LH and PH)[189,192,193,195–197]. It also presents strong projections to the contralateral preBötC to promote their synchronization[190] and receives inputs from various areas of the neocortex, which are believed to be involved in the voluntary regulation of breathing[198,199].

KÖLLIKER-FUSE NUCLEUS

KFn is prominently involved in the switch from inspiration to expiration[173,200]. Indeed, most of its neurons are active during inspiration and cease firing at its end, signaling the transition from inspiration to expiration[173,201,202]. However, KFn is not the sole nucleus responsible for terminating inspiration, as when the activity in the KFn is bilaterally blocked, the termination of inspiratory activity is not completely abolished[173].

The KFn exhibits robust connections with the other CPGs (preBötC, Bötzinger complex, PiCo, and pFL), with central chemoreceptor areas (NTS and RTN), and with areas implicated in modulating breathing (lateral and medial PB, and PAG)[152,189,192,195,196,198,203–213]. The KFn also forms connections with premotor neurons responsible for controlling the respiratory muscles (rostral – rVRG – and caudal ventral respiratory group – cVRG –), hypoglossal and facial nuclei, to facilitate the contraction of valve muscles, thus helping regulate the outflow of air during expiration[152,180,212–223].

POST-INSPIRATORY COMPLEX

PiCo is located in the ventral part of the intermediate reticular formation and has been identified as a potential contributor to respiratory control[174,210,224]. Indeed, the PiCo exhibits rhythmic activity peaking during the post-inspiratory phase[174,225] and its optogenetic stimulation has been shown to extend the duration of post-inspiration[210]. This suggests that the PiCo likely plays a role in regulating respiration, possibly as part of an integrated network rather than being a primary pattern generator[174,225]. However, further investigation is required to fully understand its function[226,227].

The PiCo receives strong inputs from the KFn and PAG, from the NTS and the paraventricular nucleus of the hypothalamus[210]. Additionally, the preBötC projects to the PiCo, indicating a link between these two respiratory regions[189]. Although there is a current lack of comprehensive studies on the efferent connections of the PiCo, there have been demonstrations of projections to the preBötC and the RTN[198,228].

LATERAL PARAFACIAL NUCLEUS

The pFL plays a crucial role in initiating active expiration by engaging expiratory abdominal muscles via the cVRG and muscles controlling upper airways[168,178,179,229–233]. In embryonic and newborn rodents, pFL exhibits rhythmic activity during periods of rest[234,235], but this activity gradually diminishes during early development[236,237]. Conversely, in adult anesthetized rats, pFL is silent during normal ventilation and rhythmically active in case of increased respiratory demand (exercise, high levels of CO_2 and low levels of oxygen)[167,168,179]. Additionally, active expiration has been recently observed during sleep in both rats[238,239] and humans[240]. Specifically, it predominantly occurs following episodes of apnea or irregular breathing and is associated with the stabilization and regularization of the respiratory rhythm, as well as an increase in the volume of air inhaled.

pFL is activated by excitatory input originating from the NTS and the RTN, which carries chemosensitive signals from the carotid bodies, in the presence of elevated blood levels of CO_2[195,241–243]. Moreover, pFL receives input from various other sources, including the preBötC, Bötzinger complex, RTN, rVRG, KFn, reticular formation, caudal raphe, lateral and medial PB, and PAG[195].

Figure 4 summarizes the location of the brain regions involved in the control of breathing.

Figure 4

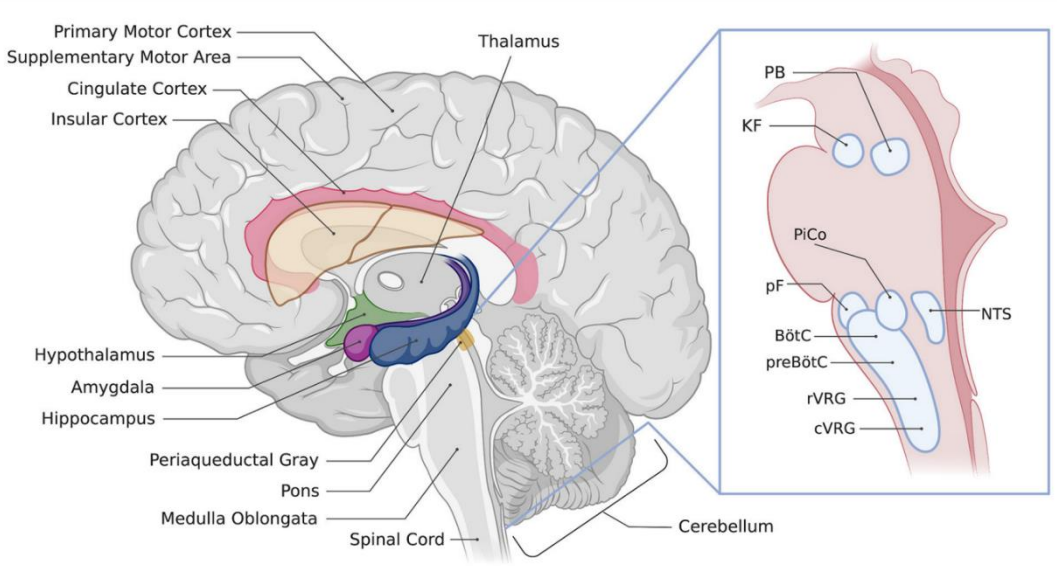

Figure 4. **Illustration of the brain regions involved in the control of breathing.**
Periaqueductal gray (PAG), parabrachial nuclei (PB), Kölliker-Fuse nucleus (KF), post-inspiratory complex (PiCo), parafacial respiratory groups (pF), the nucleus tractus solitarii (NTS), Bötzinger complex (BötC), preBötzinger complex (preBötC), rostral ventral respiratory group (rVRG), and caudal ventral respiratory group (cVRG). Image from *Schottelkotte and Crone, 2022*[186].

2.3 CONTROL OF VENTILATORY STABILITY

During W, the determination of the amount of air inhaled and exhaled in a breathing cycle (i.e., tidal volume, V_T), required to maintain stable levels of oxygen and CO_2 in the body, relies on both conscious control and metabolic pathways. However, as sleep begins, the wakefulness-related stimuli diminish, thus leaving the sole metabolic demand as the primary determinant of minute ventilation (i.e., the air volume inhaled or exhaled from the lungs per minute, V_E). Therefore, the onset of sleep, bringing a significant decrease in the activation of compensatory mechanisms that are responsible for maintaining proper ventilation, promotes hypoventilation and the development of sleep-related breathing disorders in predisposed individuals[150].

FACTORS AFFECTING BREATHING STABILITY

Ventilatory control mechanisms respond to chemical, mechanical, and behavioral information to adjust the depth of ventilation based on the body's metabolic demands and to

allow flexibility in breathing patterns to accommodate different activities, such as speech, swallowing, and other tasks[150,187,244,245].

Chemical information is received from the central chemoreceptors in the ventral medulla and peripheral chemoreceptors located in the carotid body and in the aortic body[150,187,244]. Specifically, the arterial concentration of oxygen (PaO_2) is sensed by glomus cells of the carotid and aortic bodies, which transmit signals via the glossopharyngeal and vagus nerves to the NTS and trigger an increase in ventilation when the PaO_2 falls below 60 mmHg. At the same time, both the carotid body and the central chemoreceptors are sensitive to the $PaCO_2$.

Mechanical information comes from receptors in the lung and chest wall in response to irritation, stretching, or changes in position and is conveyed to either the NTS through vagal afferent pathways or the cortex. When these receptors are stimulated, a rapid, shallow breathing pattern occurs to provide a feedback loop, known as the Herring-Breuer reflex, which helps maintain the lungs' optimal inflation and ensures that they do not become overly distended during the breathing process[150,187,244].

Finally, in addition to chemical and mechanical factors, the depth of ventilation is also influenced by behavioral information originating from higher cortical centers in the brain to allow many non-breathing functions (e.g., singing, laughing, talking, eating, crying, and speaking). In these cases, the efferent pathways responsible for executing these activities may bypass the traditional respiratory centers located in the medulla. As a result, the body prioritizes the performance of specific actions over maintaining strict control of ventilation solely based on metabolic needs[150,187,244].

RESPIRATORY LOOP GAIN

The mechanism controlling the stability of ventilation can be approximated to a loop circuit. Each loop circuit consists of a plant, which represents the system characteristics to be controlled, and of a controller, which is a unit that generates signals to reduce the deviation of the actual value from the desired value to almost zero or the lowest possible value. When a perturbation occurs in the plant (plant gain), the controller tends to modify the system (controller gain) to restore the initial situation. So, the loop gain of the system is represented by the ratio of the disturbance and the consequent response[150,244]. Specifically, in the respiratory system, the plant is the level of CO_2 present in the lungs, body tissues, and blood, the controller is the CPGs, and the respiratory loop gain is the ratio of the ventilatory response for a given ventilatory disturbance.

When $PaCO_2$ changes for a given change in ventilation, the signal arrives to the brain with a circulatory delay due to the transit time from the pulmonary capillaries to the central and peripheral chemoreceptors. At this point, CPGs provide a transient modification in the ventilatory drive, which is translated into a transient modification of ventilation, to restore the previous level of $PaCO_2$[150,244]. Particularly, a high loop gain indicates an unstable system susceptible to frequent oscillations, making it challenging to achieve a steady state; conversely, a low loop gain is characteristic of a stable respiratory system[150,246,247].

The key components of the controller gain to maintain chemical homeostasis in the respiratory loop gain model are represented by the hypoxic (HOVR) and hypercapnic (HCVR) ventilatory responses. These correspond to an increase in ventilation in reaction to reductions in PaO_2 or rises in $PaCO_2$, respectively.

2.4 EFFECTS OF SLEEP ON VENTILATION

Sleep can be considered a vulnerable state due to the diminished efficiency of breathing, resulting in inadequate oxygen intake and the removal of CO_2 from the body. These factors contribute to respiratory failure and insufficient gas exchange and homeostasis[248].

First, at sleep onset, there is a significant reduction in the activity of the upper airway muscles and the respiratory pump[151,248–251], due to the diminished tonic drive to respiratory motoneurons with the transition from W to NREM sleep, which is further reduced in REM sleep[248,252,253]. This leads to decreased compliance and lumen size in the upper airway and reduced muscle tonicity, thus making the airway more flexible, facilitating the tongue to fall backward, and creating a higher resistance to the passage of the air flow[187,251,254]. Additionally, at sleep onset, a sustained hypoventilation occurs causing an increase in $PaCO_2$ (2-4 mmHg) and a reduction in PaO_2 (3-9 mmHg)[150,151,249,255–259]. This is due, not only to the muscular hypotonicity, but also to the decreased metabolic rate of sleep[187,260,261]. Second, the functional residual capacity (FCR, the air volume remaining in the lungs after a normal, passive exhalation) is also reduced[151,248,262,263]. This decrease may be attributed to altered respiratory timing from the CPGs, a decreased compliance of the chest wall and lungs, an accumulation of blood in the thoracic region, and relative weakening of the diaphragm[264]. Third, V_T and V_E experience a reduction during NREM sleep, which is even higher during REM sleep (25% and 84% for V_T and V_E, respectively)[151,265–268].

Moreover, during sleep, the regulation of breathing relies predominantly on the metabolic control system, with the ventilation closely connected to the input received from chemoreceptors and pulmonary mechanoceptors[244]. Existing data indicates that HOVR and

HCVR are reduced during NREM sleep and fall further during REM sleep[187,269–272]. However, the exact mechanisms or reasons for this decline are still debated even if leading studies suggest it may result from a reduction in chemosensitivity or an increase in upper airway resistance during sleep[150,187,273]. To further destabilize ventilation during sleep, the critical level of $PaCO_2$ under which central respiratory drive ceases and an apnea occurs (known as "apnea threshold") is reduced by about 1-2 mmHg during sleep respect to W. Finally, during REM sleep, the mean inspiratory flow is reduced, consistent with shallow breathing patterns[150].

Therefore, taken together, these changes during sleep can contribute to alterations in respiratory parameters and gas exchange, potentially impacting overall respiratory function and contributing to the development of sleep-related breathing disorders.

3. SLEEP-RELATED BREATHING DISORDERS

Sleep-related breathing disorders (SBD) represent a wide range of pathologies encompassing impaired ventilation during sleep[54] and are extremely common in both children[274] and adults[275]. Indeed, it has been estimated that 0.7-33% of children and 14-67% of adults suffer from a form of breathing problem during sleep[274–278]. In addition, these numbers are expected to rise due to the increasing prevalence of obesity and obesity-related conditions in industrialized countries[54,279].

According to the Third Edition of the International Classification of Sleep Disorders (ICSD-3), SBDs can be divided into four sections: central sleep apnea (CSA), obstructive sleep apnea (OSA), sleep-related hypoventilation disorders, and sleep-related hypoxemia disorder[169].

Sleep apneas are defined as pauses from breathing of at least 10 seconds sufficient to disrupt sleep and to frequently cause hemoglobin desaturation and increased CO_2 levels[54,280]. Their diagnosis requires the presence of at least 5 apneic events per hour of sleep during a polysomnography[281]. Notably, according to their origin, they can be classified as CSA or OSA in case of the presence of an impairment in the transmission of the signal for inspiration from the brain to inspiratory muscles or of an obstruction of the airways, respectively[169,170,280]. On the other hand, sleep-related hypoventilation disorders are associated with increased $PaCO_2$, while the sleep-related hypoxemia disorder is characterized by sustained drops in arterial oxygen saturation (less than 88% for at least 5 minutes) without CO_2 measurement.

Among all the SBDs, the most frequent and dangerous are represented by sleep apneas of both central and obstructive origin[278,282,283]. Moreover, both of them produce a series of short- and long-term life-threatening cardiovascular, metabolic, and neurocognitive dysfunctions[54,254,275,284,285]. Indeed, frequent apneic events give rise to repetitive cycles of reduced oxygen levels in the blood, elevated CO_2 levels, and subsequent re-oxygenation, which are accompanied by frequent arousals, causing fragmented sleep pattern, changes in the intrathoracic pressure and tissue damages[286].

In the next chapters, I will examine the classification, epidemiology, pathophysiology, and treatment of sleep apneas. Particularly, for the purposes of this thesis, I will focus on three different diseases characterized by the presence of variable SBDs: Down Syndrome (DS), CDKL5 deficiency disorder (CDD), and Pierre Robin sequence (PRS).

3.1 CENTRAL SLEEP APNEA

CSA syndromes encompass conditions characterized by an intermittent or cyclical reduction or absence of respiratory effort due to dysfunctions in the central nervous system[287]. Specifically, CSA occurs when the brainstem network responsible for generating respiratory rhythm and driving breathing experiences a transient decrease in activity usually caused by a reduction in the partial pressure of CO_2 below the apneic threshold[280].

CSA is relatively uncommon in the general population, but it is more prevalent in individuals with heart failure, stroke, neurodegenerative disorders, and those receiving opioid treatment[288–291].

Primary CSA is a condition of uncertain origin that can manifest in adulthood, infancy, or even premature infants, while other forms of CSA are typically linked to underlying pathologies or environmental factors[54,281,287].

The Cheyne-Stokes breathing pattern is a prevalent occurrence during NREM sleep in individuals affected by heart failure, cerebrovascular disorders, and renal failure. It is characterized by recurrent apneas alternating with prolonged episodes of hyperpnea in which V_T rhythmically increases and decreases in a crescendo–decrescendo pattern[287,292,293]. CSA due to high-altitude periodic breathing is a disorder usually occurring at altitudes exceeding 7600 meters where the sleep is disrupted by repetitive cycles of apnea[287,291,294,295], while CSA due to long-term opioid use causes a respiratory depression by affecting the mu receptors of the ventral medulla[287,291,296,297].

Finally, although increasing evidence suggests that CSA could potentially trigger OSA[291], their health implications continue to be a topic of ongoing discussion[283,289].

3.2 OBSTRUCTIVE SLEEP APNEA

OSA syndromes involve repetitive events characterized by either complete or partial obstruction of the airways, leading to increased inspiratory effort and compromised ventilation[170,287]. OSA is highly prevalent in the general population, affecting 1.2-5.7% of children, between 6% and 17% of adults and reaching up to 49% in the elderly with a higher prevalence in the male sex (34% of men and 17% of women)[275,287,298].

The diagnosis of OSA varies based on the age group being considered. In adults, the criteria for diagnosis entail the presence of at least 5 episodes of airway obstruction per hour of sleep during a polysomnographic recording. On the other hand, in children, the diagnosis requires the recognition of just one OSA event per hour of sleep in association with daytime

excessive sleepiness, hyperactivity, behavioral problems, or learning problems[281,287,298]. Despite these diagnostic guidelines, it appears that OSA remains significantly underdiagnosed[275]

Obesity is strongly linked to OSA as deposits of fat within the upper airway and reduction in lung volume cause the loss of caudal traction on the upper airway[299]. However, 20-40% of OSA patients are not obese, indicating the potential role of other factors, such as muscle hypotonia, altered chemoreflex sensitivity, and low arousal threshold (i.e., waking up from sleep prematurely), in its pathophysiology[280]. Also the fluid around the upper airway may represent a risk factor since it may accumulate in the pharyngeal area and near the lungs in the supine position facilitating the collapse of airways or even potentiating CSA[280,300,301]. Furthermore, in neonates and children, OSA is strongly linked to the hypertrophy of adenoids or tonsils and to the reduced or abnormal development of the facial bone structures, which can be genetically predisposed or due to the changes in the reciprocal position of the tongue, the mandible, and pharynx[284,302–305]. This diversity suggests the existence of different OSA phenotypes that may require distinct treatment approaches[280].

OSA is considered the most common and dangerous form of SBD in Western countries as it poses an elevated risk of cardiovascular morbidity, mortality, as well as metabolic and neurocognitive impairment[280,285,299,302]. Indeed, numerous studies assessed that OSA leads to repetitive cycles of arterial hypoxia, hypercapnia, and re-oxygenation (intermittent hypoxia), and to frequent sleep arousals[281,287]. Thus, these stimuli cause excessive daytime sleepiness, systemic inflammation, oxidative stress, sympathetic nervous system activation, and hypercortisolemia, hypertension, stroke, myocardial ischemia and infarction, heart failure, atrial fibrillation, and coronary heart disease, pulmonary hypertension, and sudden death[280,283,300,302,306–309].

REM SLEEP-RELATED OBSTRUCTIVE SLEEP APNEA

A peculiar subtype of OSA is represented by the REM sleep-related OSA, which is characterized by airway obstruction that predominantly or exclusively occurs during REM sleep[310,311]. This happens because of the loss of tone in several skeletal muscles, including the genioglossus, that can facilitate the collapse of the upper airways[312]. Interestingly, REM sleep-related OSA constitutes 14–36% of all OSA cases and is more prevalent in females than in males[313–316]. In addition, the duration and magnitude of oxygen desaturation are reported to be more pronounced in REM sleep-related OSA than OSA occurring during NREM sleep[317]. Scientific literature also suggests that OSAs during REM sleep may have

more adverse cardiometabolic and neurocognitive outcomes compared to those during NREM sleep[285,313,318].

3.3 DOWN SYNDROME AND RELATED BREATHING DISORDERS

DS is a genetic disease caused by the partial or complete triplication of chromosome 21 (Hsa21)[319] due to errors in maternal meiosis or mitosis, translocations, or mosaicisms[320–327]. This pathology was first described in 1866 by the British physician John Langdon Haydon Down[328] and, nowadays, represents one of the most common chromosomal abnormalities with a prevalence estimated between 8.27 and 12.6 live-born babies with DS per 10,000 births[329,330].

DS is characterized by a wide collection of medical manifestations that impact on the entire organism, especially affecting the musculoskeletal (short stature, craniofacial abnormalities, muscle hypotonia), neurological (neurodevelopmental delay, language and memory impairments), and cardiovascular systems (congenital heart defects)[331–335]. Moreover, although the most invalidating aspect of this condition is represented by the intellectual disability, DS patients are also more likely to develop certain health conditions that may result in detrimental consequences, including hypothyroidism, type 2 diabetes, autoimmune diseases, OSA, epilepsy, hearing and vision problems, hematological disorders, gastrointestinal defects, recurrent infections, anxiety disorders and early-onset Alzheimer disease[334–346]. Additionally, it is worth to mention that, among them, OSA syndrome assumes a predominant role. Indeed, its prevalence has been estimated at 45-66% in children diagnosed with DS[347–350] and increases up to more than 90% in adulthood[351–354]. This finding is in line with previous studies reporting a series of risk factors that may facilitate the collapse of the upper airway during sleep in DS patients, including hypotonia, obesity, craniofacial anatomy (e.g., narrowed nasopharynx, mandibular hypoplasia, and macroglossia) and hypertrophy of adenoids and tonsils[303,349,355–357].

3.4 CDKL5 DEFICIENCY DISORDER AND RELATED BREATHING DISORDERS

CDD is an ultra-rare severe developmental epileptic encephalopathy, with an incidence of 2.36 per 100,000 livebirths[358], which is caused by mutations in the *CDKL5* gene, that is located on the short arm of the X chromosome[359]. This gene encodes for the cyclin-

dependent kinase-like 5 (CDKL5), a serine/threonine kinase involved in the regulation of axon outgrowth, dendritic morphogenesis, and synapse formation in early postnatal life, and in maintaining synaptic function in the adult brain[360]. However, even if predominantly expressed at the brain level as can be deduced from its main functions, the *CDKL5* gene is widely expressed among different tissues, including testis, lung, spleen, prostate, uterus, and placenta, whereas it is virtually absent in the heart, kidney, liver, and skeletal muscle[361].

The origin of CDD can be traced back to a relatively recent period. In 2003, a group of scientists from the Max-Planck-Institute for Molecular Genetics identified a balanced translocation, resulting in the disruption of *CDKL5* gene (at that time called STK9, serine-threonine kinase 9), in two unrelated female patients affected by severe developmental delay, mental retardation, and early-onset infantile spasms[362,363]. Meanwhile, the same mutation was found at the University of Western Australia[364] and at the University of Siena[365] in female children previously diagnosed with the Hanefeld variant of Rett Syndrome, characterized by early-onset seizure[366]. Then, as the number of patients carrying mutations in the *CDKL5* gene rose (up to 2013, 141 individuals were identified), a clearer clinical presentation and physical appearance of patients was established and, thus, a distinct diagnosis for the CDD was proposed[367]. However, despite many clinical centers have extensively examined this condition and contributed to understand the role and function of the CDKL5 protein since the foundation of the International CDKL5 Disorder Database in 2012[368], the term CDD emerged in the medical literature much later, specifically only in 2018[369].

Due to its chromosomal localization, CDD affects females four times more often than males, suggesting that pathogenic variants and loss of function of CDKL5 protein are mostly lethal for males during fetal life[368,370]. However, independently of the gender, the key feature of CDD is represented by epilepsy which is mostly drug-refractory, generally starts within the first three months of life[370–372], and is characterized by a variable morphology (e.g., partial, myoclonic, tonic seizures, and limb spasms)[368,373]. In addition, almost all patients also present retardation of psychomotor development and intellectual disability, generalized hypotonia, and cortical vision disorders[367,368,372,374]. Finally, to complicate the clinical picture, CDD is associated with an extremely variable phenotype, not only between boys and girls, but also among different *CDKL5* mutations, as demonstrated by a wide series of accompanying symptoms differently distributed in patients. Particularly, it is worth mentioning autism spectrum disorders (poor social interactions, poor eye contact, repetitive hand movements), bruxism, respiratory disorders (apnea or hyperventilation), arrhythmias, gastrointestinal impairments (constipation, gastroesophageal reflux, and aerophagia), orthopedic complaints (difficulty at walking, standing up or sitting), sleep disorders

(problems with falling asleep or waking up, SBD, and drowsiness), and dysmorphic facial features (e.g., deep set eyes, straight eyebrows, slightly short upturned nose, large ears, high forehead, or prominent lips)[367,368,370–372,374–377].

3.5 PIERRE ROBIN SEQUENCE AND RELATED BREATHING DISORDERS

PRS is a multifactorial disorder of the neonatal period with an estimated prevalence of 1-9 per 10,000 livebirths[378,379] that was first described in 1923 by Pierre Robin[380]. This condition is characterized by a reduced mandibular size in the sagittal direction (micrognathia) and the retroposition tendency of the mandible during infancy (retrognathia), which can lead to the displacement of the tongue into the hypopharynx (glossoptosis), thus resulting in frequent airway obstructions at the tongue base with consequent repeated oxygen desaturations and cyanosis[303,381,382]. Moreover, patients with PRS often present cleft lip and U-shaped cleft palate, difficulties to feed, gastroesophageal reflux, and long-term complications including cerebral impairment, pulmonary hypertension, and failure to thrive[381,383,384].

PRS can be widely found as isolated findings (40% of cases), usually together with mutations of *SOX9* or *KCNJ2* gene on chromosome 17[381,385], but also as part of an underlying syndrome (60% of cases). For instance, it is most commonly found in the Stickler Syndrome with mutations in *COL2A1*, *COL9A1*, *COL11A1*, and *COL11A2*, in the velocardiofacial syndrome with a microdeletion of chromosome 22q11.2 or mutation of *TBX1* gene, and in the Treacher Collins Syndrome with mutation in *TCOF1*, *POLR1C*, and *POLR1D* genes[303,381,384].

3.6 AVAILABLE THERAPIES FOR SLEEP APNEAS

The most effective therapy for OSA and CSA is the continuous positive airway pressure (CPAP)[280,299,386]. It employs an air compressor to supply pressurized air either in a single or bi-level mode (inspiratory and expiratory pressures) through a nasal mask to provide a pneumatic stent preventing upper airway obstruction[303].

CPAP significantly improves pulmonary hypertension and cardiac function, reduces blood pressure, especially in patients with resistant hypertension, the risk of cerebral events, the frequency of premature ventricular beats during sleep, and the recurrence rate of atrial fibrillation. In addition, CPAP enhances the need for revascularization, incident coronary heart disease, and survival[280,291,387–402]. In addition, the combination of exercise and weight loss with CPAP can boost its effectiveness[280]. Indeed, physical activity reduces the severity

and occurrence of OSA and ameliorates sleep quality by decreasing the redistribution of fluid in the neck region stabilizing the chemoreceptor sensitivity, and decreasing the incremental blood pressure[280,300,301,403–405].

However, CPAP is the treatment of choice only for adults, as its suitability for the pediatric population is limited. First, children do not fully understand the advantages of undergoing CPAP treatment, which can hinder their cooperation and adherence to the therapy. Second, ensuring a proper fit of nasal or oronasal masks can be more challenging in children due to their smaller facial structures, potentially leading to discomfort and inadequate treatment delivery. Third, some children may experience feelings of claustrophobia or discomfort when using CPAP masks. Therefore, these factors can significantly reduce adherence to the therapy compromising its effectiveness[280,298,394,406,407].

THERAPIES FOR SLEEP APNEAS IN CHILDREN

Apneas of prematurity are treated with the oral administration of caffeine, while CSAs occurring after the age of 37 weeks are treated with acetazolamide, a carbonic anhydrase inhibitor that enhances the respiratory drive by adjusting the threshold of partial pressure of CO_2[298].

OSA can be also treated with the application of a nasopharyngeal tube, that is inserted through the naris and extends to the oropharynx to act as a supportive structure for the upper airway, effectively preventing its collapse[298,303,408,409]. In addition, some oral devices that work in different ways applying pressure to the jaw to prevent retroglossal collapse are available, such as the mandibular advancement device which repositions the tongue and/or mandible to increase the size of the airway lumen[298,410].

Moreover, in specific clinical conditions peculiar treatment may attenuate the symptomatology linked to persistent or severe OSA[298,303]. For example, if OSA is limited to the supine position, sleeping on the side or prone could improve the condition at least once the infant is capable of rolling over, as it enables gravity to draw the tongue forward[303,384,411]. In children with adenotonsillar hypertrophy, the first-line treatment is represented by adenotonsillectomy or by the nasal administration of corticosteroids to reduce the tissue inflammation and swelling, while children with macroglossia can take benefits from tongue reduction surgery[298,303,412]. Finally, in case of extremely severe OSA, children (especially those with craniofacial abnormalities) may undergo tracheostomy to completely bypass the site of obstruction. However, although highly effective, this treatment requires an extensive training and a constant monitoring[303,384].

Furthermore, patients with PRS can undergo mandibular distraction osteogenesis, which is a surgical procedure which consists in the fracture of the mandible to affix a device that permits gradual moving forward of the mandible (about 1 mm/day) and allows new bone to form[303,384,413]. In addition, PRS patients can take benefits from the tongue-lip adhesion, which is a surgical intervention where the tongue is carefully fastened to the mucosa and muscle of the lower lip to correct glossoptosis and help to alleviate breathing difficulties[303,384,414,415].

Finally, another alternative experimental therapy for OSA, that still needs further investigation to obtain definitive data, is the hypoglossal nerve stimulation. This procedure encompasses the application of an electrical pulse at low voltage to the hypoglossal nerve during the inspiration phase to activate the muscles that move the tongue forward, thus alleviating airway obstruction due to tongue malposition[298,416,417].

4. STUDY OF SLEEP-RELATED BREATHING DISORDERS IN MICE

Animal models are essential tools in biomedical research due to the complex multilevel interactions between molecules, cells, organs, and systems that characterize evolved living systems and cannot be appreciated by exclusively looking at the single components[54]. Among them, mice have emerged as the species of choice thanks to the numerous advantages they offer. First, mice are relatively cost-effective to acquire and maintain, have a small size, are easy to handle, and have a short lifespan and a rapid reproductive rate. Second, mouse DNA organization and gene expression show a high degree of homology with those of humans, and it is estimated that these two species share approximately 99% of genes[418]. Third, since the complete sequencing of the mouse DNA in 2002[418], several inbred and genetically modified mouse strains have been developed and utilized under controlled laboratory conditions to expedite the acquisition of knowledge in various pathologies and to reduce the influence of genetic, behavioral, and environmental confounders[61]. Finally, several studies demonstrated the numerous similarities in genomic sequence, EEG pattern, and brain circuitry between mice and humans and the good conservation of neural mechanisms related to sleep and respiration throughout evolution[55,152,419].

Therefore, mice have proven to be valuable in advancing our understanding of fundamental physiological aspects, especially in the investigation of sleep disorders and SBDs, to expand our knowledge about sleep and respiratory neurophysiology, neuroanatomy, and regulation, and to facilitate the development of new therapies and to assess their safety and efficacy[54,55,59,61,170].

4.1 ANIMAL MODELS OF SLEEP-RELATED BREATHING DISORDERS

Despite SBDs constituting a subject of considerable interest due to the high prevalence of sleep apneas of both central and obstructive origin in the general population, most of the studies in recent decades have concentrated on exploring the pathological correlates of SBDs rather than on the development and validation of mouse models of SBDs[54]. This situation could potentially be linked to the fact that mice have long been considered unsuitable models for investigating sleep apneas and to the presence of technical challenges in accurately characterizing sleep apneas in such small animals[54]. Additionally, the report of several

differences in the anatomy of upper airways between mice and humans[420], although repetitively rejected thanks to the recent discovery of several similarities in upper airways and hypoglossal nerve functions between these two species[421,422], might also contribute to this scenario[54].

Nonetheless, a range of genetically engineered mouse strains has been proposed as potential models for studying sleep apnea for distinct reasons. For instance, mice lacking orexins[423–427], CDKL5 kinase[428,429], heme oxygenase-2 enzyme[430], the transcription factor Phox2b[431,432], and monoamine oxidase A enzyme[433] are regarded as viable models for CSA, whereas mice affected by obesity[434–437] are recognized as the only available model for OSA[54].

For the purposes of the thesis, the subsequent paragraphs will provide comprehensive descriptions solely for the SBD animal models employed in the current experiments.

MODEL OF DOWN SYNDROME: TS65DN MICE

Ts65Dn mouse (TS)[438] is the most largely used animal model of DS and carries a reciprocal translocation that leads to the partial triplication of the distal part of chromosome 16, which is homologous to Hsa21. Unlike mice with full trisomy of chromosome 16 which die in utero[439,440], TS mice live until adulthood (up to 36 months of age) and show a full genetic homology to the long arm of Hsa21[441]. However, it should be noted that this murine model also has three copies of 19 genes usually located on mouse chromosome 17 (and not orthologues of genes on Hsa21), and thus some aspects of the phenotype in this strain might not be related to human DS[442].

Despite that, TS mice recapitulate many clinical manifestations similar to those of humans, such as reduced birth weight, postnatal developmental delay, spontaneous locomotor hyperactivity, deficit in spatial learning and memory, muscular trembling, male sterility, brain abnormalities, and skeletal malformations directly corresponding to the craniofacial dysmorphogenesis in DS[323,443,444]. In addition, more recent studies also highlighted an increased propensity for obesity, primarily due to an augmented fat mass and energy intake and an impaired glucose homeostasis[445], the increment in the incidence of hypoxemia which occurs early in life and chronically[446], and the presence of sleep impairments[447].

Therefore, considering the widespread range of symptoms of DS common to both humans and mice, we expect that TS mice may exhibit obstructive events during sleep as human patients do. If this will be confirmed by our experiment, TS mice may represent a promising candidate to study the pathophysiological aspects of OSA and to accelerate the development of specific therapeutic approaches in line with the principle of promoting and conducting research tailored to individual patients.

MODEL OF *CDKL5* DEFICIENCY DISORDER: *CDKL5*-KNOCKOUT MICE

Since the majority of the CDKL5 coding region is orthologous and well-conserved between humans and mice[448], different CDKL5-knockout mice have been developed for understanding how this protein dysfunction can lead to the wide range of defects present in human CDD. Indeed, although animal models cannot fully replicate human pathologies, they serve as a valuable resource for investigating the molecular and pathophysiological mechanisms involved in the development and advancement of a disease and they also offer a means of identifying potential therapeutic strategies.

In line with this principle, the loss-of-function mutation of CDKL5 was mimicked by using the site-specific recombinase technology of Cre-lox recombination targeting different exons: exons 6[449–451], exon 4[428], and exon 2[452].

For the purposes of the present study, we will focus on the CDD mouse model used in the current work: the one created by Amendola and colleagues in 2014[428]. Notably, this peculiar kind of CDKL5-knockout (CDKL5-KO) mice was originally obtained by inserting loxP sites flanking the exon 4 of the CDKL5 gene into a plasmid which was transfected by electroporation and selected into ES cells (with a 129/Sv×C57BL/6N genetic background). Then, founder mice were generated by injecting the cells carrying the mutation into host embryos with a C57BL/6N genetic background, which were further crossed to C57BL/6J congenic FLP-deleter mice[453] to remove the selection cassette and to C57BL/6J congenic Cre-deleter mice[454] to generate the CDKL5 null allele[428].

CDKL5-KO mice by Amendola and colleagues recapitulate the core aspects of human CDD. For instance, they show motor disturbances (abnormal clasping of hind limbs, decreased locomotion in the familiar home-cage setting, and impaired motor coordination) and hippocampus-dependent learning and memory impairments[428], but not the early-onset seizures, found in the CDD model obtained by Wang and colleagues[449]. Interestingly, all neurological symptoms found in CDKL5-KO are consistent with the presence of defects in neuronal maturation, spine density, and synaptic connectivity present in primary hippocampal cultures from CDKL5-KO mice[455], and with cellular phenotypes of neurons derived from induced pluripotent stem cells reprogrammed from patients' fibroblasts[456]. In addition, CDKL5-KO mice also show severe dendritic hypotrophy[428], impaired neurogenesis at the hippocampal level[457,458], an augmented neuroinflammation associated with alterations of microglia[459], and an increased number of apneas during sleep[429].

Notwithstanding the existing differences between boys and girls[368,370], most of the research conducted on animal models has focused on male hemizygous CDKL5-KO mice in order to eliminate any potential confounding factors resulting from mosaic CDKL5 protein expression caused by random X-inactivation occurring in females[360]. However, recent studies concentrated at discovering potential gender and age-related differences. Indeed, it has been highlighted that female mice with heterozygous for the CDKL5-KO mutation exhibit several characteristics of CDD, including autism-like behaviors, motor coordination and memory performance impairments, as well as abnormalities in breathing patterns[460]. Moreover, another work found an age-dependent decline in motor, cognitive, respiratory, hypnic, and social behaviors in CDKL5-KO mice, without a worsening of neuroanatomical alterations[461].

MODEL OF PIERRE ROBIN SEQUENCE: BMP7-KNOCKOUT MICE

Bone morphogenetic proteins (BMPs) consist of a wide range of dimeric glycoproteins that fall under the transforming growth factor-β (TGF-β) family. These proteins mainly govern the growth, formation, and regeneration of bones and cartilages, as well as the development of the skeletal structure[462–466]. However, most of these family members exhibit a pleiotropic effect, as they participate in several different physiological processes, such as cardiac development, ovarian functionality, embryonic patterning, and cardiac and neural organogenesis[467–471].

BMP7 represents one of the most extensively researched BMPs. This protein primarily contributes to cartilage and bone morphogenesis and to kidney formation[464,472–474] and its mutations give rise to the abnormal formation of the secondary palate during the embryonic formation in humans, thus resulting in the occurrence of a cleft palate[475,476].

For a more comprehensive understanding of BMP7's role in maintaining equilibrium and facilitating the repair of various adult tissues, a full BMP7-knockout mouse model was created by strategically flanking the first coding exon of *BMP7* gene with loxP sites and using Cre-mediated recombination to remove it[477]. However, the complete absence of BMP7 in mice resulted in cleft palate and high *in utero* mortality[478], which, regrettably, impeded the subsequent evaluation of craniofacial growth after birth. Successively, a conditional mutant mouse model was generated by deleting the *BMP7* gene exclusively within the neural crest, a transient pluripotent stem cell-like population of the embryos that give rise to a broad spectrum of cell and tissue types, including craniofacial skeleton, teeth, connective tissue, pharyngeal arch muscles, and carotid body glomus cells[479–481]. Specifically, these mice were obtained by mating mice carrying loxP sites flanking the first coding exon of *BMP7* gene

(BMP7$^{fl/fl}$ or BMP7-WT) with Wnt1-Cre transgenic mice[482] to obtain a Cre-mediated recombination for the removal of exon 1 and the consequent creation of mice with a neural crest-specific deletion of BMP7 (BMP7$^{fl/fl}$:Wnt1-Cre or BMP7-KO)[477].

BMP7-KO mice manage to survive beyond the initial postnatal period and recapitulate the fundamental aspects of PRS. Indeed, they display a variety of orofacial malformations, including micrognathia, midfacial hypoplasia, cleft palate, shorter and more acutely angled cranial base, diminished nasal bone length, nasal septum deviation and turbinate swelling[483,484]. Moreover, these mice encounter disturbances in the attachment sites and the morphology of the genioglossus muscle, responsible for mediating tongue movements and protrusion in the initial stages of embryonic growth[483]. All these features together predispose mice to potential blockages in nasal airflow during the postnatal period, a scenario paralleling human conditions[303]. Indeed, at the age of 4 weeks, when all the craniofacial abnormalities have been firmly established, BMP7-KO mice commence developing a series of respiratory disturbances, including an increased duration of respiratory events, a greater number of spontaneous apneas and a greater frequency of irregular breathing following a sigh[484]. However, despite that these breathing disorders are likely associated with OSA, no definitive confirmation of a heightened prevalence of this specific type of apneic events has been established, although the field of pediatric sleep medicine could greatly gain insights from the availability of a rodent model of nasal airway obstruction[484].

4.2 METHODS FOR STUDYING SLEEP APNEA IN ANIMAL MODELS

Over the last few decades, there has been a notable surge in interest in the field of SBD, particularly for sleep apnea, as confirmed by the remarkable and rapid rise in the number of research papers centered around sleep apnea in mouse models[54]. However, it is crucial that investigations concerning rodents' breathing patterns are conducted in tandem with the concurrent classification of sleep states to optimize the potential translational applicability of the data to human conditions[54].

WHOLE-BODY PLETHYSMOGRAPHY

The gold standard technique for the investigation of the breathing characteristics in humans and animal models is represented by whole-body plethysmography (WBP).

This non-invasive and precise method relies on the pressure modifications which occur inside a non-compliant and airtight chamber in response to the cyclical breathing rhythm of

the subject[54,485]. Specifically, when the mouse is positioned inside the apparatus supplied with a constant inflow and outflow of air and the chamber is hermetically sealed, the air inside the chamber is drawn into the lungs during inspiration, saturated with water vapor, warmed, and then exhaled. These modifications, together with the movements of the animal's rib cage which expands and contracts alternatively, induce modifications in the volume, humidity, and temperature of the air inside the chamber. As a direct result, these physical alterations influence the pressure within the chamber[54,485,486]. Consequently, the degree of each pressure fluctuation is related to the amount of inspired/expired air and to physical gas modifications occurring during each breath. Finally, thanks to the application of dedicated equations it becomes possible to get information on various respiratory parameters[54,487,488].

WBP exhibits several advantages: the non-invasiveness, the high levels of precision and reliability, and the ability to be consistently replicated. Secondly, the plethysmographic recordings can be easily repeated on the same subject, facilitating longitudinal investigations for tracking the progression of pathologies or testing novel therapeutic interventions. Third, this technique does not require the use of anesthesia or physical restraint when introducing the mouse into the WBP chamber, thereby diminishing the stress experienced by the animal and the variability between studies[54,461,488]. Finally, the remarkable versatility of this method enables the contemporary examination of respiratory variables alongside the investigation of the wake-sleep cycle. Specifically, the analysis of sleep pattern encompasses the surgical implantation of specific electrodes capable of recording the EEG and the electromyogram of neck muscles (EMG) and the subsequent evaluation of the recorded biological signals to categorize the animal's behavioral states into W, NREM sleep, and REM sleep according to criteria extrapolated from the established human standards for sleep stage classification[53,54,57].

However, despite its significant contributions to define the neuronal network responsible for regulating respiratory rhythm[489], to examine several SBDs[429,461,490] or the role of inflammation in breathing control[491], some limitations must be acknowledged. First, the alterations occurring inside the sealed, non-compliant chamber are typically of small magnitude and susceptible to distortion and corruption[487], thus limiting the measurements of ventilation to periods of sleep or minimal activity. Furthermore, to attain accurate data about air volumes, chamber pressure data must be recorded together with barometric pressure and chamber temperature and humidity[485]. However, the introduction of a calibration procedure at the end of each recording session (essentially consisting of a series of injections of known volumes of air) can avoid the need for precise knowledge regarding chamber volumes and the characteristics of the animal's respiratory system[54,492,493].

DETECTION OF CENTRAL AND OBSTRUCTIVE SLEEP APNEAS

Despite the evident clinical significance, the investigation of the underlying mechanisms of CSA and OSA in rodents, particularly in mice, remains exceedingly limited. This scarcity of research is due not only to the technical challenges of recording and characterizing sleep apneas in such small animals but also to the longstanding misconception that only CSAs are physiologically present in mice[494]. However, recent research has challenged this notion, shedding light on the presence of spontaneous occurrences of OSA in wild-type mice[435,495].

Various strategies have been employed to differentiate between CSA and OSA in adult mice. For instance, Vsevolod Polotsky and co-workers utilized a non-invasive technique to record the respiratory effort. Specifically, they equipped the WBP chamber with two air bladders (one acting as a sensor and the other as a reference) to detect the mechanical changes to the internal pressure caused by the mouse's breathing and to eliminate the contaminating noise fluctuations[421,422,435,496]. On the other hand, a more invasive approach (employed in the current thesis) involves the monitoring of the activity of respiratory muscles thanks to an electrode inserted into the abdominal cavity and in contact with the lower surface of the diaphragm[495].

However, achieving a comprehensive interpretation of the data regarding hypnic and breathing parameters, along with apneas, remains intricate and complex and continues to pose challenges due to several methodological limitations[54]. First, the lack of oximeters that can provide data about hemoglobin desaturation during sleep apneas. Second, the adoption of divergent criteria for delineating sleep apnea: some studies defined apneas as breathing pauses lasting twice than a standard breath, whereas others three times longer than a standard breath. Third, the variability in the ambient temperature at which mice are recorded inside the WBP chamber, which can significantly affect the occurrence rate of sleep apneas. Finally, particular attention must be given to the choice of the animal strain since the genetic background can modulate breathing pattern and sleep apnea frequency[54,490,497–501].

AIM

Sleep apnea of central (CSA) and obstructive (OSA) origin represents the most common and dangerous sleep-related breathing disorder (SBD)[278,282,283]. They are due, respectively, to an impairment in the transmission of the signal for inspiration from the brain to inspiratory muscles or to a physical obstruction of the airways[169,170,280]. Despite their potential to lead to a range of short- and long-term cardiovascular, metabolic, and neurocognitive lethal complications[54,254,275,284–286], there is still limited understanding of the pathophysiology and the genetic factors contributing to CSA and, particularly, to OSA. In addition, currently available therapies (CPAP, pharmaceutical interventions, and surgical procedures) do not consistently achieve full effectiveness or personalized treatment for patients[280,298,299,303,384,386,394,406,407,412–415]. This challenge is especially notable for individuals with craniofacial abnormalities, as seen in conditions like Down Syndrome (DS), CDKL5 deficiency disorder (CDD), or Pierre Robin sequence (PRS).

Therefore, the primary objective of this thesis is to assess whether the genetic mouse models of DS (TS mice), CDD (CDKL5-KO mice), and PRS (BMP7-KO mice) can replicate the respiratory disturbances observed in human patients. Specifically, we aim to categorize, for the first time, apneas occurring during sleep as either CSA or OSA. To address these questions, we investigated the hypnic and respiratory phenotype using whole-body plethysmography (WBP) in conjunction with the implantation of specific electrodes for sleep stage discrimination and diaphragmatic activity detection[57,493,495,497].

The following exposition is structured in two main sections, one describing the experiments performed at the University of Bologna (Italy) on TS mice and CDKL5-KO mice, while the other describing the experiments conducted at the University of Alberta (Canada) on BMP7-KO mice. Since all experiments were conducted using an almost overlapping methodology, these two sections are preceded by a description of the common experimental approach.

EXPERIMENTAL APPROACH

5. CRAFTING OF ELECTRODES

Mice were implanted with homemade electrodes[57,495] to perform a differential bipolar recording of electroencephalographic (EEG), nuchal electromyographic (EMG), and diaphragm electromyographic (DIA) signals.

It is important to mention that the dimensions of the DIA electrode were adapted to the different animals' size. Particularly, in the experiments conducted at the University of Bologna, where adult mice were used, the DIA electrode was made starting from a 12-cm long wire. On the other hand, in the experiments performed at the University of Alberta, in which 1-month-old mice were employed, the DIA electrode was made starting from an 8-cm long wire.

5.1 EEG ELECTRODES

EEG electrodes (Figure 5)[57,502] were created by cutting a pair of 1.2 cm long multi-stranded stainless-steel wires coated with a PFA-insulating sheath (KF Technology srl, Rome, Italy or A-M Systems, WA, USA) and soldering each one to a stainless-steel screw (length 2.4 mm and diameter 1.19 mm, 00-96x3/32; Plastics One, Roanoke, VA, USA) after removing 2-3 mm of the coating from both ends. Then, the uninsulated wires were soldered to a connector equipped with two terminal pins (0.5 cm wide and 0.3 cm high; 701-9925, RS Components International, Cinisello Balsamo, Milan, Italy, or TX, USA).

5.2 EMG ELECTRODES

EMG electrodes (Figure 5)[57,502] were crafted by cutting a pair of 4 cm long multi-stranded stainless-steel wires coated with a PFA-insulating sheath (KF Technology srl, Rome, Italy or A-M Systems, WA, USA) and removing 2-3 mm of coating both from one end and at 1.5 cm from it to allow electrical contact with nuchal muscles after implantation. Then, the uninsulated ends were soldered to a connector equipped with two terminal pins (0.5 cm wide and 0.3 cm high; 701-9925, RS Components International, Cinisello Balsamo, Milan, Italy, or TX, USA).

5.3 DIA ELECTRODES

DIA electrodes (Figure 5)[495] consisted of two 12 or 8 cm long (according to animal size) multi-stranded stainless-steel wires coated with a PFA insulating sheath (KF Technology srl, Rome, Italy or A-M Systems, WA, USA), each of which was bent into a hairpin-like shape and twisted on itself to form a circular end. As a result, the final length of the electrode was 6 cm for the experiments conducted at the University of Bologna on adult mice and 4 cm for the experiments performed at the University of Alberta on juvenile mice. Then, 2-3 mm of the coating was removed from the free end and from the circular tip to allow the passage of electricity, and the coating along the wire was gently melted by means of a hot air flux to maintain the shape of the electrode. Finally, the uninsulated ends were soldered to a connector equipped with two terminal pins (0.5 cm wide and 0.3 cm high; 701-9925, RS Components International, Cinisello Balsamo, Milan, Italy, or TX, USA).

Figure 5

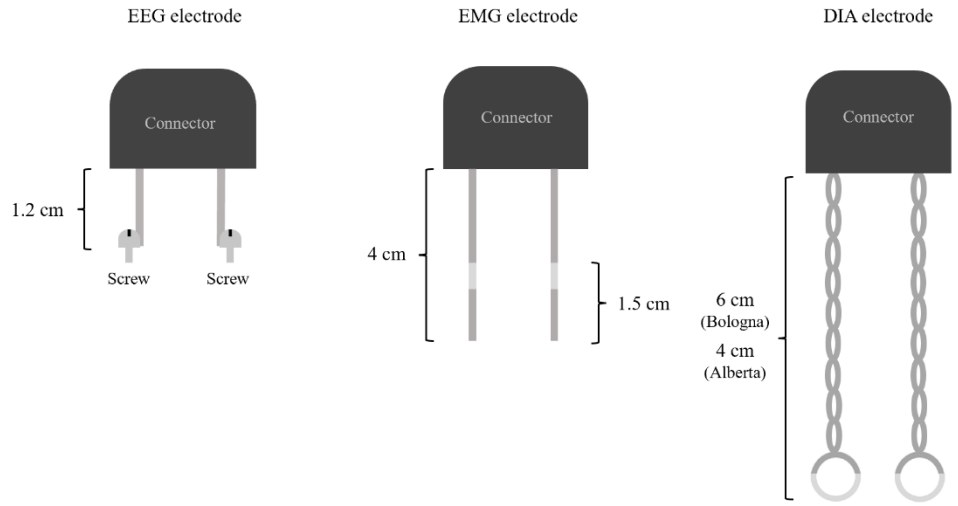

Figure 5. Representation of the electrodes used for the electroencephalographic (EEG), nuchal electromyographic (EMG) and diaphragm electromyographic (DIA) signals recording.

6. SURGERY

The surgery[495], consisting of the implantation of the electrodes for EEG, EMG, and DIA signals recording, was performed under aseptic conditions. Although the surgical procedure is almost the same in the experiments conducted at the University of Bologna and at the University of Alberta, some differences in materials used, sterilization procedures and usage and dosage of drugs must be considered. In addition, at the University of Alberta, mice were also implanted with a temperature probe (APT12 PIT Tag; BioMark, ID, USA) inside the peritoneum.

6.1 SURGERY PREPARATION AND STERILIZATION PROCEDURE

At the University of Bologna, surgical instruments were sterilized by an autoclave cycle at 121°C for 15 minutes or with a specific disinfectant (benzalkonium chloride 0.30 g and ethyl alcohol 71%; LH Benzalcol Ferri, Lombarda H srl, Albairate, Milan, Italy), while suture threads, screws, cotton swabs, gauzes, and electrodes were placed under a UV lamp for at least 20 minutes.

Similarly, at the University of Alberta, surgical instruments were sterilized by an autoclave cycle at 121°C for 15 minutes, while the instrumentation not compatible with high-temperature exposure (i.e., suture threads, screws, cotton swabs, gauzes, and electrodes) were sterilized by means of an at least 20-minutes cycle under a UV lamp.

6.2 ANESTHESIA, DRUG ADMINISTRATION AND SURGICAL AREAS DISINFECTION

At the University of Bologna, surgical procedures were performed under general anesthesia with isoflurane (1.8-2.4% in pure oxygen, inhalation route) on a thermoregulated heating pad (Homeothermic blanket Control Unit, Harvard Apparatus, MA, USA) set at 37°C to maintain the physiological body temperature and to avoid its decreasing during anesthesia due to the minimized thermoregulatory capacity of mice. Furthermore, the anesthetic level was continuously monitored during the entire procedure looking at changes in the breathing rate.

Once anesthetized, mice were injected with a pain killer drug (0.1 mg of Rimadyl®, Carprofen 50 mg/mL, Zoetis, Rome, Italy; subcutaneous injection of 200 µL of a solution of 10 µL of Rimadyl® dissolved in 1 mL of saline) and a cortisone ointment (Cortison Chemicetina, Abbott, IL, USA; hydrocortisone acetate 2.5 g and chloramphenicol 2 g) was applied directly on the animal's eyes to avoid dehydration. Then, surgical fields (i.e., the left subcostal area and the skin above the head) were shaved and disinfected with an iodine solution.

Furthermore, after surgery, to prevent infections and to rehydrate the animal, an antibiotic (Strong Rubrocillin®, Intervet Productions srl, MSD Animal Health srl, Segrate, Milan, Italy) was administered subcutaneously. The wide-spectrum antibiotic was composed of benzathine benzylpenicillin (250'000 I.U./mL) and dihydrostreptomycin sulfate (100 mg/mL), so 15 µL of Strong Rubrocillin® dissolved in 800 µL of saline were injected (3'750 I.U./mouse of benzathine benzylpenicillin and 1.5 mg/mouse of dihydrostreptomycin sulfate).

Similarly, at the University of Alberta, surgical procedures were performed under general anesthesia with isoflurane (1.8-2.4% in room air, inhalation route), modulating the anesthetic level by monitoring changes in the breathing rate, thanks to an anesthesia delivery system (SomnoSuite®, Kent Scientific Corporation, Torrington, CT, USA), which used a precision syringe pump and a digital vaporizer. In addition, this machine was also equipped with a warming pad and a rectal probe for the real-time monitoring and maintenance of the animal's temperature (RightTemp® module, Kent Scientific Corporation, Torrington, CT, USA).

Before the anesthesia induction, mice were treated by oral gavage with a pain killer drug (1.5 mg/kg of Metacam®, oral suspension of Meloxicam 1.5 mg/mL, Boehringer Ingelheim Pharma KG; Germany) and the anti-pain therapy was continued for 48 hours after surgery with administrations every 24 hours. Then, once anesthetized, mice were shaved in the left subcostal area and the skin above the head, which were disinfected twice with 70% ethanol and an iodine solution.

6.3 DIA ELECTRODE IMPLANTATION

DIA electrode implantation[495] was performed by placing the mouse on an inclined plane to obtain a better exposure of the surgical field and to avoid damaging the peritoneal cavity internal structures.

The surgeon made a 0.5 cm incision in the skin of the flank under the last left rib and another one on the head between the ears, then, a subcutaneous tunnel was created in the lateral portion of the trunk using surgical scissors with a curved tip. Maintaining aseptic conditions, the DIA electrode was passed into previously described incisions, leaving the connector near the animal's head.

With the help of a surgical microscope (Carl Zeiss, Germany), peritoneal wall muscles under the last left rib were cut by means of microsurgical scissors to insert the electrode's wires into the abdominal cavity. Then, both circular uninsulated ends were sutured to the internal surface of peritoneal muscles in correspondence of the eighth intercostal space by passing a silk thread (5-0 or 6-0, respectively, for adult and young mice) through them to place and keep them in contact with the abdominal surface of the diaphragmatic muscle (Figure 6).

Figure 6

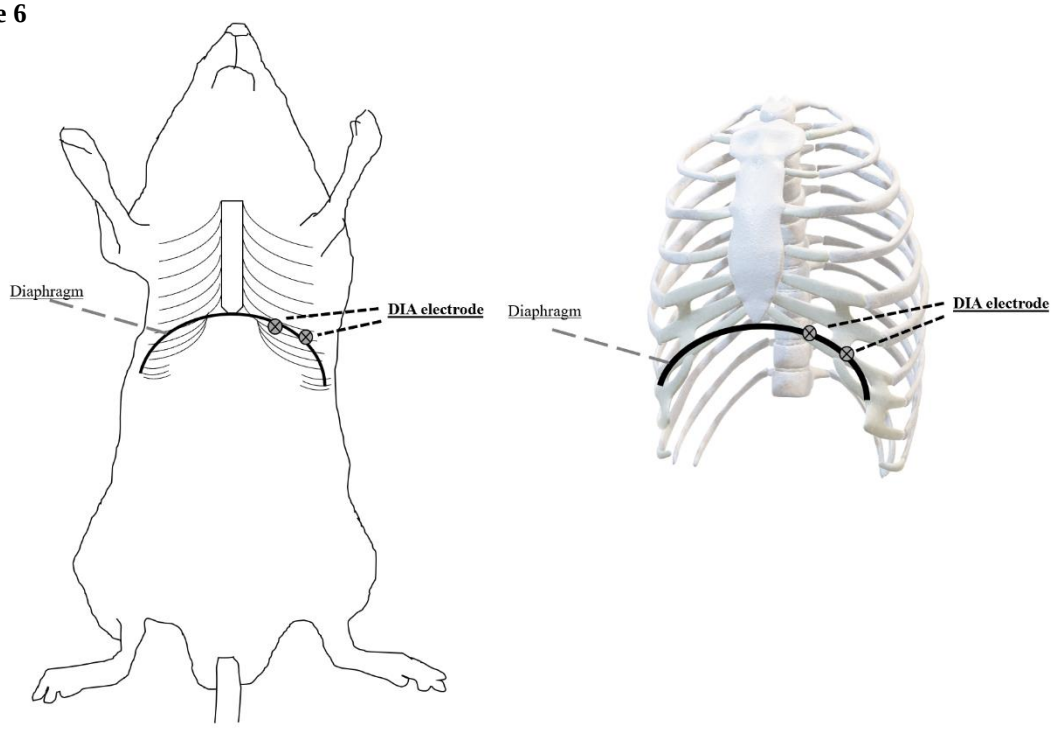

Figure 6. Schematic representation of the diaphragmatic (DIA) electrode positioning.
Circular uninsulated DIA electrode's ends were sutured to the muscles of the peritoneal cavity in the eighth intercostal space to be kept in contact with the abdominal surface of the diaphragm.

Exclusively for the experiments conducted at the University of Alberta, before suturing the wounds in the peritoneal wall and on the subcostal skin with stitches, a temperature probe (APT12 PIT Tag; BioMark, ID, USA) was inserted into the peritoneal cavity and fixed to the internal surface of the wall muscles with a 6-0 silk thread.

Later, wounds in these areas were sutured with stitches; particularly, the peritoneal wall muscles were sutured with a 5-0 silk or a 4-0 absorbable thread, while the skin was sutured with a 3-0 non-absorbable thread (polyester or nylon), following the veterinary guidelines of the two different universities in which the experiments were performed.

6.4 EEG AND EMG ELECTRODES IMPLANTATION

For the correct positioning of the EEG and EMG electrodes, the mouse was placed on the stereotaxic apparatus (51600 Lab Standard™ Stereotaxic Instruments, Stoelting Co., IL USA or Model 900 Small Animal Stereotaxic Instrument, Kopf Instruments, Tujunga, CA) to immobilize the skull[57,502,503].

First, passing through the previously made incision between the animal's ears, the periosteum was removed from the skull and a drop of hydrogen peroxide (3% H_2O_2) was locally applied to better highlight the cranial sutures and anterior and posterior crossing points, respectively called bregma and lambda. Using a surgical drill and taking these cranial points as a reference, four holes were made 1 mm anterior and 1 mm lateral on both sides of bregma and lambda, respectively, on the frontal and parietal bones. Second, the two screws of the EEG electrode were inserted in the holes on the right side in contact with the *dura mater*, without trespassing it. Then, two free stainless-steel anchor screws (length 2.4 mm and diameter 1.19 mm, 00-96x3/32; Plastics One, Roanoke, VA, USA) were placed in the left holes (Figure 7) and the entire structure was fixed to the skull bone by cement for dental use (3M™ ESPE™ RelyX™ Unicem, 3M, Segrate, Milan, Italy or Ontario, Canada).

After that, to obtain a differential electromyographic signal, EMG electrode wires were inserted bilaterally in the nuchal muscles using a curved needle and blocked with a knot. Finally, the EEG, EMG and DIA electrodes' connectors were incorporated in a biocompatible acrylic paste for dental use (DuraLay, Reliance Dental Manufacturing LLC, IL, USA) on the mouse's skull.

It is notable that this acrylic structure was light enough (about 1 g) not to affect the animal's posture.

Figure 7

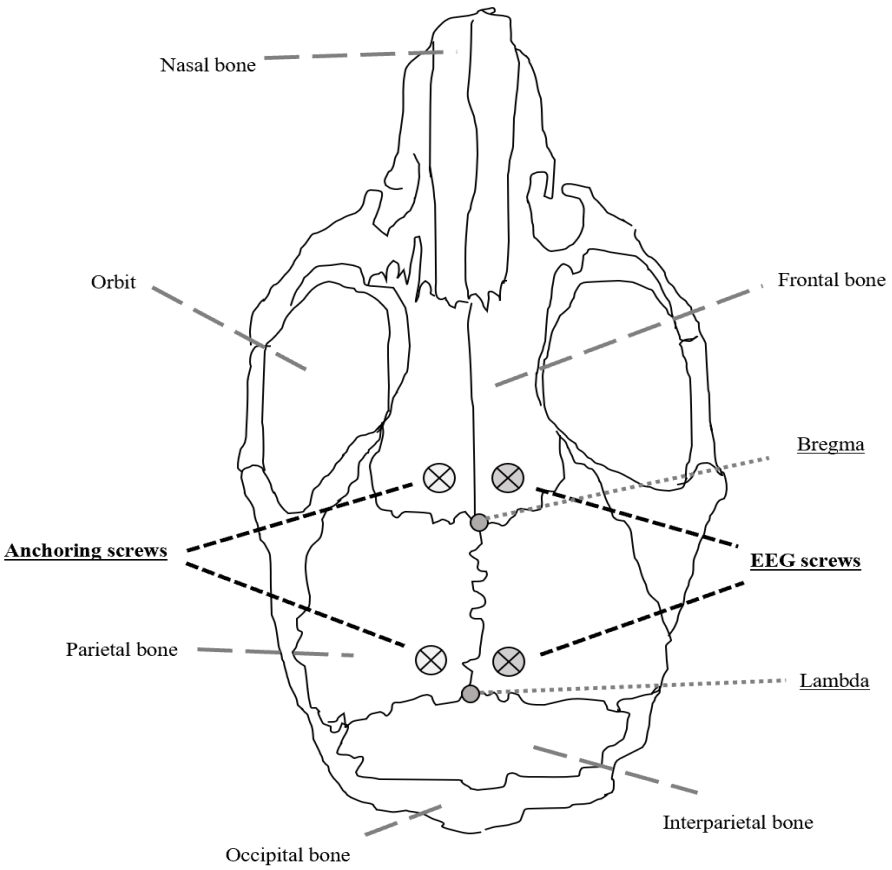

Figure 7. Schematic representation of the mouse's head and screws positioning.
The four holes were made 1 mm anterior and 1 mm lateral on both sides to bregma and lambda, respectively, on the frontal and parietal bones. Electroencephalographic (EEG) electrode screws were inserted in the right holes, while the anchoring screws in the left holes.

7. EXPERIMENTAL PROTOCOL

After surgery, mice were individually housed for a post-operative recovery of at least 5 days within a soundproof room under a 12:12-hour light-dark cycle (lights on at 9 a.m. at the University of Bologna and at 7 a.m. at the University of Alberta) with the ambient temperature set at 25 ± 1 °C and free access to water and food.

The experimental schedule (Figure 8) dictated that each mouse underwent two 8-hour recording sessions inside a WBP chamber, spaced by 24 hours of recovery, to simultaneously record ventilation, behavioral states, and diaphragmatic activity.

Before each recording, animals were slightly anesthetized (1–2 minutes under 1-2% isoflurane anesthesia) to plug a lightweight cable for the acquisition of EEG, EMG, and DIA

signals and then inserted in the WBP chamber. No restraint, except for the cable, was used, so mice were able to physiologically behave (exploring the plethysmograph, grooming, eating, and sleeping).

Figure 8

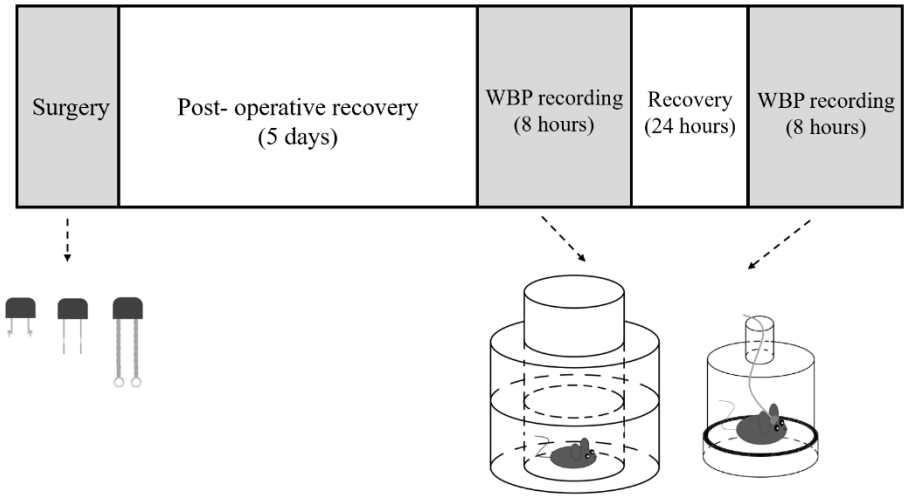

Figure 8. **Scheme of the experimental protocol.**

After 5 days of post-operatory recovery, each mouse underwent two 8-hour recording sessions inside a whole-body plethysmography chamber (WBP), spaced by 24 hours of recovery, for the simultaneous recording of ventilation, behavioral states, and diaphragmatic activity.

UNIVERSITY OF BOLOGNA (ITALY): STUDY OF TS65DN AND CDKL5-KO MICE

Characterization of sleep apneas in a mouse model of Down syndrome and in a mouse model of CDKL5 deficiency disorder

Part of these data was published in *Bartolucci et al., 2021*[495]

8. METHODS

8.1 ETHICAL APPROVAL

The study protocol complied with the European Directive 2010/63/EU for animal experiments and with Italian law (authorization n. 779/2017-PR, n. 205/2019-PR and n. 535/2022-PR).
Experiments were performed according to the guidelines of the Animal Welfare Committee of the University of Bologna, Italy (Legislative Decree 26 of 2014). All efforts were made to minimize the number of animals and their suffering.

8.2 MICE

Experiments were performed using 12 TS and 14 euploid (EU) control male mice for the study of the DS, and 14 CDKL5-KO mice and 10 wild-type (CDKL5-WT) male mice for the study of the CDD.

Mice were housed under a 12:12-hour light-dark cycle with ambient temperature set at 23 ± 1 °C and free access to water and food (diet 4RF21; Mucedola, Settimo Milanese, Milan, Italy) in the facilities of the Department of Biomedical and Neuromotor Sciences, University of Bologna, Italy.

8.3 BREEDING AND GENOTYPING OF DOWN SYNDROME MODEL MICE

TS and EU mice were obtained by mating B6EiC3Sn a/A-Ts(1716)65Dn/J females, which are carriers of the reciprocal translocation, with B6EiC3SnF1/J males, which are commonly used as a background for some deleterious mutations, since trisomic males generally do not breed[504]. The mouse colony was expanded at the Department of Biomedical and Neuromotor Sciences of the University of Bologna, Italy, starting from founder mice purchased from Jackson Laboratories (Bar Harbor, ME, USA).

Genotypes were assessed at 4 weeks of age by extracting DNA from bioptic tissue taken during the ear punching procedure performed under general anesthesia, as previously described[505]. Briefly, DNA was amplified by polymerase chain reaction (PCR) using two primers covering the translocation breakpoint, leading to the amplification of a 275 bp

product, and two control primers, which amplify a sequence of 600 bp from the Rosa locus. Then, PCR products were resolved by electrophoresis on a 1.5% agarose gel.

Table 2

Breakpoint primers:	PCR cycling:
5′GTGGCAAGAGACTCAAATTCAAC-3′	2 minutes at 94°C 45 seconds at 94°C 45 seconds at 55°C 1 minute at 72°C — for 40 cycles
5′TGGCTTATTATTATCAGGGCATTT-3′	7 minutes at 72°C - Extension
Control primers:	
5′AAAGTCGCTCTGAGTTGTTAT-3′	
5′GGAGCGGGAGAAATGGATATG-3′	

Table 2. **Primers sequences and polymerase chain reaction (PCR) conditions.**

8.4 BREEDING AND GENOTYPING OF CDKL5 DEFICIENCY DISORDER MODEL MICE

CDKL5-KO and CDKL5-WT mice derive from the CDKL5 null strain in the C57BL/6N background developed by Amendola and colleagues[428]. They were obtained at the Department of Biomedical and Neuromotor Sciences of the University of Bologna, Italy by crossing heterozygous CDKL5 females with CDKL5-KO or CDKL5-WT male mice after backcrossing in C57BL/6J for three generations.

Animals were karyotyped by PCR on genomic DNA using the following primers: 5′-ACGATAGAAATAGAGGATCAACCC-3′, 5′-CCCAAGTATACCCCTTTCCA-3′, and 5′-CTGTGACTAGGGGCTAGAGA-3′, as previously described[428].

8.5 WHOLE-BODY PLETHYSMOGRAPHY

The WBP (PLY4223, Buxco, Wilmington, NC, USA) consisted of two chambers (Figure 9): one used as reference, while the second one used to accommodate the mouse[493,503].

The mouse chamber was modified by inserting a solid, machined 10-cm diameter Plexiglas block to reduce its internal volume to 0.97 L and was equipped with a probe capable of

measuring the temperature and the humidity of the chamber (PC52–4-SX-T3 sensor, Rense Instruments, Rowley, MA, USA). In addition, it was also equipped with a rotating electrical swivel (SL6C/SB, Plastics One, Roanoke, VA, USA) to prevent twisting of the mouse wire tether during the recordings. The reference chamber was located above the mouse chamber, surrounding the tower above the animal's head.

Figure 9

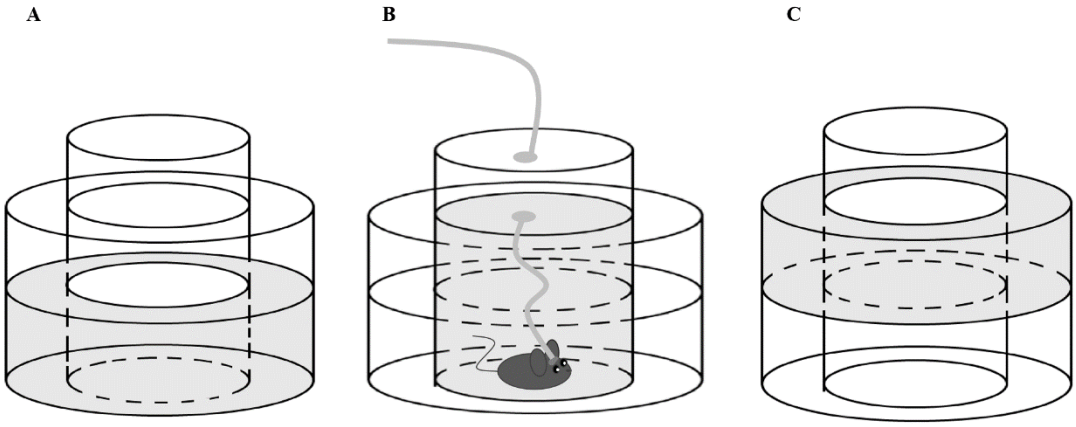

Figure 9. **Schematic representation of the modified 2-chamber whole-body plethysmograph (WBP).**

The figure shows the Plexiglas block used to reduce the animal chamber internal volume (A), the mouse chamber with the tower equipped with the rotating electrical swivel (B), and the reference chamber (C).

During the recording sessions, both chambers were continuously purged with air (breathable air cylinder; 78% N_2, 21% O_2, 1% Ar; Fluido Tecnica sas, Campi Bisenzio, Florence, Italy) at a relatively high flow rate (1.5 L/min) to prevent CO_2 build-up. The animal respiratory signal was measured as the differential pressure between the chamber containing the animal and the reference chamber by means of a high-precision differential pressure transducer (DP103–06+ CD223 digital transducer indicator; Validyne Engineering, Northridge, CA, USA).

At the end of each recording, the system was calibrated dynamically with a 100 µL micro-syringe (Hamilton, Reno, NV, USA) by performing a series of air jets at increasing known volumes (10, 20, 30, 40, and 50 µL) which reproduced the animal's breaths.

8.6 DATA RECORDING

During each 8-hour session, the EEG, EMG, DIA, and respiratory signals were continuously recorded together with the WBP's animal chamber humidity and temperature.

The EEG, EMG, and DIA signals were acquired via a lightweight electrical cable connected to a rotating electrical swivel, by amplifying and filtering them with 'pass band' filters (EEG: 0.3–100 Hz; EMG and DIA: 100–1000 Hz) using 7P511J amplifiers (Grass, West Warwick, RI, USA). Data were digitized, together with the mouse respiratory signal, using a PCI6224 board (National Instruments, Austin, TX, USA) operated by a software written in the laboratory using LabVIEW (National Instruments, Austin, TX, USA).

The EEG signal was stored at 256 Hz, while the EMG and DIA signals at 2048 Hz; the WBP differential pressure, which corresponded to the respiratory signal, was stored at 1024 Hz while WBP temperature and humidity were sampled at 4 Hz and stored together with all the above-mentioned signals. Then, all signals were synchronized and down-sampled (EEG, EMG, and WBP signals at 128 Hz, DIA signal at 1024 Hz).

As stated above, since each mouse underwent two 8-hour recording sessions spaced by 24 hours of recovery, all the variables computed during each recording session were then averaged for each mouse.

8.7 DATA ANALYSIS

DISCRIMINATION OF THE WAKE-SLEEP STATES

The discrimination of the wake-sleep states was performed by visual analysis of raw EEG and EMG traces on 4-second epochs, using a validated semi-automatic algorithm (SCOPRISM) developed in MATLAB (The MathWorks Inc., Natick, MA, USA)[57]. Briefly, the sleep scoring algorithm considered the ratio between the EEG spectral power in the θ (6–9 Hz) and δ (0.5–4 Hz) frequency ranges and the root mean square of the EMG signal of each 4-second epoch, and the results of the scoring in adjacent epochs to discriminate among the different behavioral states. Epochs with high EMG root mean square values were scored as W, while epochs with a low EMG root mean square were defined as NREM sleep if the ratio between θ and δ was lower than 0.75 or as REM sleep when it was higher than 1.25. In addition, epochs with a low EMG root mean square and θ/δ ratio between 0.75 and 1.25 were scored as indeterminate.

After that, results of automatic discrimination on all consecutive 4-seconds epochs were displayed together with the raw EEG and EMG signals and were, eventually, confirmed or corrected by trained operators, according to validated guidelines[57,502,506]. W was assigned when the EMG tone was high and variable and the EEG was at a low voltage with possible θ and δ frequency components, NREM sleep was scored when the EMG tone was lower than in W and the EEG was at a high voltage with prominent δ frequency components, and REM sleep was defined in presence of muscle atonia with occasional muscle twitches and of an EEG at a low voltage with predominant θ activity. Epochs with signals that were on a borderline between two different states were scored as "indeterminate".

An example of raw EEG and EMG traces is shown in Figure 10.

Figure 10

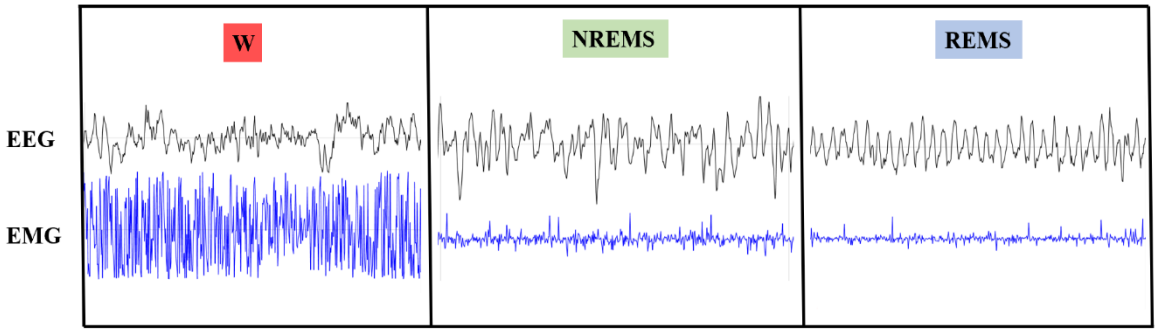

Figure 10. Discrimination of the wake-sleep states.

Example of raw electroencephalographic (EEG) and nuchal electromyographic (EMG) data obtained during wakefulness (W), non-rapid-eye-movements sleep (NREMS) and rapid-eye-movements sleep (REMS).

ANALYSIS OF RESPIRATORY VARIABLES

The analysis of respiratory variables was confined to stable periods of NREM and REM sleep lasting at least 12 seconds, therefore excluding periods of transition between wake-sleep states. In addition, W episodes were excluded since they showed a high prevalence of breath-obscuring artifacts due to mouse movements[495,503,507].

Single breaths were automatically identified from the upward (positive) WBP pressure deflection peak; errors in breath detection (i.e., repeated or stereotyped negative deflections) and pressure artifacts due to opening and closing of the room door were manually excluded from the analyses.

Respiratory variables were calculated starting from raw WBP traces using a script developed in MATLAB (The MathWorks Inc., Natick, MA, USA)[493,495].

Tidal volume (V_T), which is the amount of air moved in or out of the lungs during each respiratory cycle, was calculated with a specific equation[508], as follows:

$$V_T = \frac{V_K}{P_K} * P_T * \frac{T_B * (P_B - P_{Ch})}{T_A * (P_B - P_{Ch}) - T_{Ch} * (P_B - P_A)}$$

where V_K is the volume of air injected during the calibration of the system, P_K is the pressure deflection associated with the calibration volume, P_T is the pressure deflection associated with the breath of interest, P_B is the barometric pressure, P_{Ch} and P_A are the water vapor pressures respectively associated with the animal chamber and with the animal's temperature, and T_A and T_{Ch} are the temperatures respectively associated with the animal's body and with the chamber.

For practical purposes, P_B was approximated to the average atmospheric pressure at mean sea level (i.e., 760 mmHg), T_A was assumed to be the average mouse core temperature (i.e., 37°C)[509], T_{Ch} was calculated as the average chamber temperature measured by the probe during the time interval of interest, and P_{Ch} and P_A were calculated with the Antoine equation[510,511], as follows:

$$P = 10^{A - \frac{B}{T+C}} * \frac{h}{100}$$

where P is the water vapor pressure associated with a specific temperature, T is the temperature of interest, and h is the relative humidity of the system (for the chamber it is estimated as the average chamber humidity measured by the probe in the time interval of interest, while for the mouse is approximated at 100%). Instead, A, B, and C are constants depending on the nature of the substance (in the case of water in a temperature range between 1 and 100°C, they are equal to 8.07131, 1730.63, and 233.426, respectively) (Saturated Vapor Pressure Tool available at www.ddbst.com by DDBST Dortmund Data Bank Software & Separation Technology GmbH).

Ventilatory period or total breath duration (T_{TOT}), that is the duration of each breath, was calculated as the time interval included between two successive peaks of inspiration. Minute ventilation (V_E, that is the air volume inhaled or exhaled from lungs per minute) was calculated as the ratio between the average V_T and the average T_{TOT}. Then, volumes and flows were normalized by expressing them per gram of body weight[493,495].

Sighs, which are augmented breaths that almost exclusively occur during NREM sleep in mice[497], were detected as breaths with a V_T at least three times higher than the average V_T for each mouse in NREM sleep. Similarly, apneas, that are breathing pauses, were designated as breaths with a T_{TOT} at least three times longer than the average T_{TOT} for each mouse in each

sleep state. Then, the automatic identification of sighs and apneas, performed by the algorithm written in MATLAB (The MathWorks Inc., Natick, MA, USA), was manually checked by visual inspecting the raw traces for each event and to exclude eventual artifacts. The sigh and sleep apnea occurrence rate were expressed as the number of events per hour of time spent in a specific sleep state.

Figure 11 shows a depictive example of V_T and T_{TOT} of a normal breath, of a sigh, and of an apnea.

Figure 11

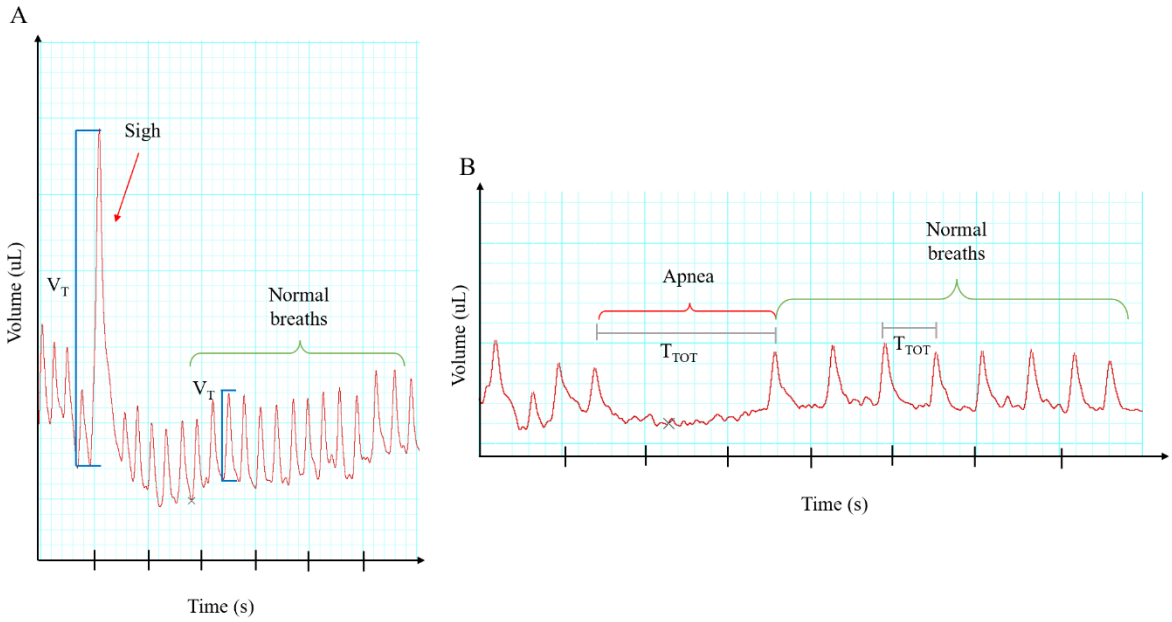

Figure 11. Example of different breathing events: normal breath, sigh, and apnea.
The figure shows a sigh (red arrow in panel A), an apnea (red parenthesis in panel B), and some normal breaths (green parenthesis in both panels) as comparison.
Blue lines identify the tidal volume (V_T) associated with the two different types of breathing events in panel A, while grey lines represent the ventilatory period (T_{TOT}) associated with the two different types of breathing events in panel B. In both graphs, the time scale is one second.

CLASSIFICATION OF APNEAS

Apneas were categorized following two different classifications: one based on the distance from a previous sigh and the other one based on the breathing pattern and the DIA activity.

The first classification, based on the distance from a previous sigh, allowed a discrimination between post-sigh apneas, when the apneic event started within 8 seconds from a sigh, and spontaneous apneas, when they started more than 8 seconds from the preceding sigh[495,497].

The second classification, based on the analysis of WBP and DIA signals, allowed the discrimination between CSA and OSA. CSA is characterized by the concomitant absence of activity in WBP and DIA signals, while OSA was identified by a clear activation of the DIA signal in the absence of WBP signal activity[495].

Moreover, it has been highlighted that the extent of airway obstruction in OSA events varied from complete to partial, leading to a further discrimination between OSA and sub-obstructive (sub-OSA) events. This latter kind of apnea was defined by a clearly distinct DIA activity concomitant with a slight positive deflection of the respiratory WBP signal that could not be automatically detected as an inspiration. Therefore, in accordance with the American Academy of Sleep Medicine airflow criterion for hypopnea detection in humans[512], the inspiratory airflow (i.e., the ratio between the V_T and the duration of the DIA activity) cut-off, needed to categorize an apneic event as sub-OSA, was identified as an at least 30% reduction compared with the baseline value estimated in the previous breathing event. Sub-OSAs were identified during the manual review of the raw tracings performed for each apnea event.

Representative examples of raw tracings corresponding to post-sigh and spontaneous apneas, CSA, OSA, and sub-OSA events are shown in Figure 12 and Figure 13.

Figure 12

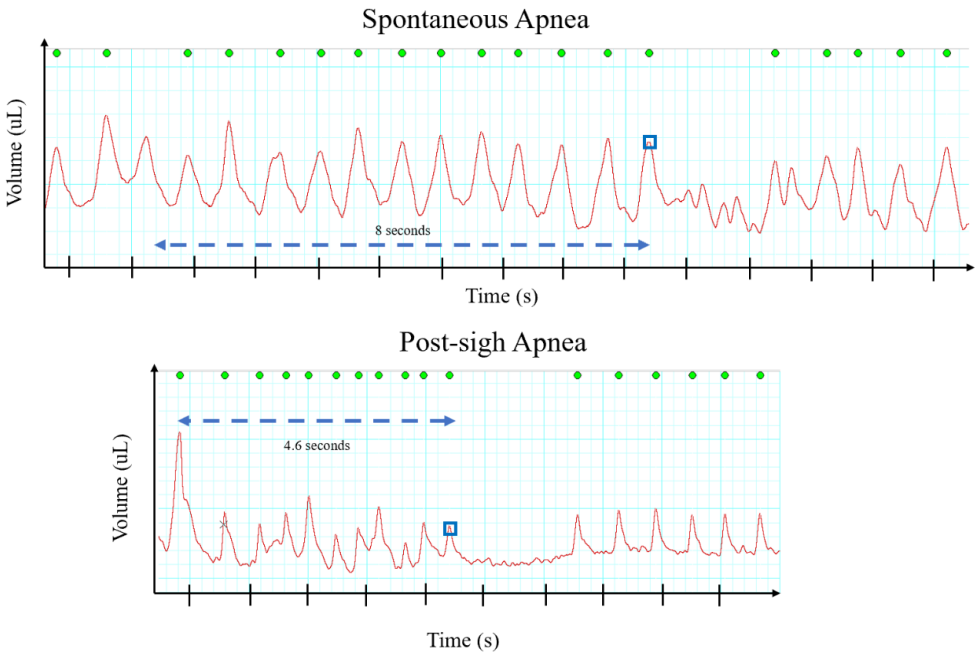

Figure 12. Different types of sleep apneas: spontaneous and post-sigh sleep apnea.

Representative examples of raw tracings corresponding to a spontaneous and a post-sigh sleep apnea.

Green dots indicate the peak of each inspiratory act while blue squares indicate the beginning of the apneic event. The blue dotted line corresponds to the period of 8 seconds chosen and validated as the threshold for the discrimination between post-sigh and spontaneous apneas (*Bastianini et al.*, 2019)[497] or the distance from the previous sigh.

Figure 13

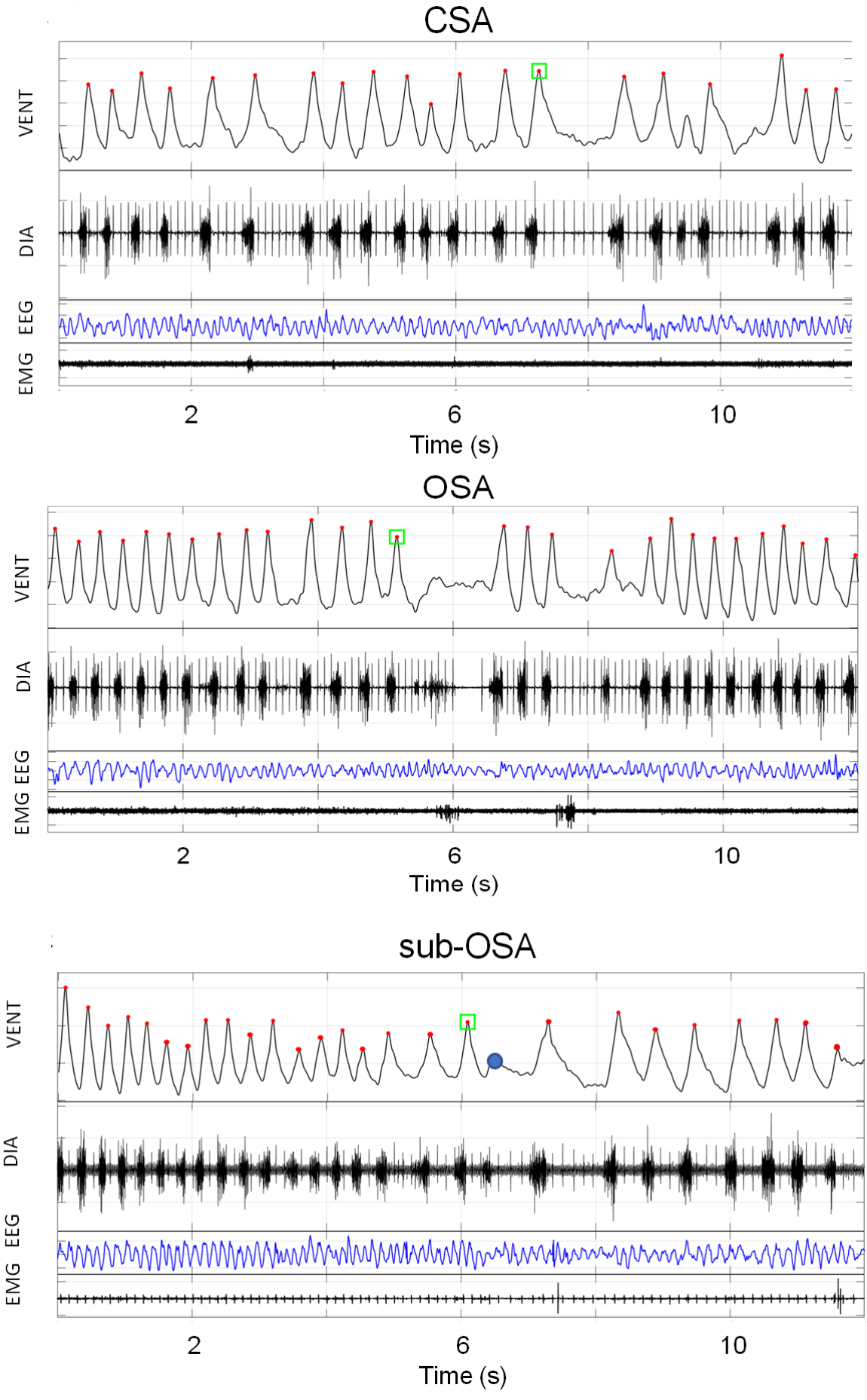
CSA
VENT
DIA
EEG
EMG
2
6
10
Time (s)
OSA
VENT
DIA
EMG EEG
2
6
10
Time (s)
sub-OSA
VENT
DIA
EMG EEG
2
6
10
Time (s)

Figure 13. **Different types of sleep apneas: central, obstructive, and sub-obstructive sleep apnea.**

Representative examples of raw tracings corresponding to a central sleep apnea (CSA), an obstructive sleep apnea (OSA), and a sub-obstructive sleep apnea (sub-OSA).

Each panel shows the ventilatory (VENT, which is the differential pressure recorded into the whole-body plethysmograph corresponding to mouse respiratory pattern), the diaphragm electromyographic (DIA), the electroencephalographic (EEG) and the nuchal electromyographic (EMG) signals.

On the VENT signal, red dots indicate the peak of each inspiratory act while green squares indicate the beginning of the apneic event. The blue dot in panel corresponding to sub-OSA indicates a reduction of >30% in estimated airflow compared to baseline value (computed based on the last red dot before the green square) with concomitant DIA activity.

ANALYSIS OF AIRFLOW AND DIAPHRAGM STRENGTH

To study the eventual changes in airflow before and after the breathing pause, for all identified apneic events, the airflow of the first breath after the breathing pause was estimated as the ratio between V_T and the duration of the DIA activity and expressed as a percentage of the corresponding baseline value estimated during the last breath before the apneic event. For sub-OSA events, the reported airflow estimates correspond to those observed during the event.

In addition, to test the potential modification of the extent of diaphragm contraction during OSA and sub-OSA events, DIA activity was evaluated in terms of burst duration (in milliseconds) and amplitude, calculated as the root mean square of the DIA signal and expressed as percentage of the corresponding baseline values during the last breath before the event. Notably, the identification of sub-OSAs was performed only during REM sleep due to the almost total absence of obstructive events during NREM sleep.

ANALYSIS OF HEART PERIOD

The positioning of the DIA electrode in contact with the abdominal surface of the diaphragmatic muscle also allowed the simultaneous detection of the electrical activity of the heart, indeed R waves of the QRS complexes were clearly distinguishable on the background of the DIA signal (Figure 14).

To investigate the modulation of heart rhythm during the apneic events, the heart period (HP) was calculated as the RR interval (i.e., the period between successive R wave peaks).

For each apneic event, the difference (ΔHP) between the mean HP value during the apneic event and the mean HP value of the 10 heartbeats before the event was computed and analyzed. For graphical clarity, HP was substituted with its reciprocal, the heart rate (HR, HR = 1/HP), expressed in beats per minute.

Figure 14

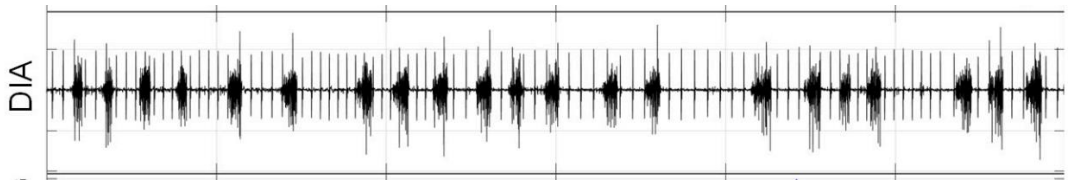

Figure 14. **Raw tracing of the diaphragmatic (DIA) signal.**
R waves of the QRS complexes of cardiac electrical activity are detectable on the background of the DIA signal.

8.8 STATISTICAL ANALYSIS

Statistical analysis was performed using SPSS software (SPSS Inc., Chicago, IL, USA). Results are shown as mean ± SEM (Standard Error of the Mean), with statistical significance set at $p < 0.05$. Data were analyzed with two-way ANOVAs, considering the following factors: mouse genotype (2 levels: TS vs. EU controls or CDKL5-KO vs. CDKL5-WT) and sleep state (2 levels: NREM sleep or REM sleep), or wake-sleep episode duration (4 temporal bins: < 12 seconds, between 12 and 60 seconds, between 60 and 120 seconds, > 120 seconds), or apnea subtypes (2 levels: either post-sigh vs. spontaneous sleep apnea or CSA vs. OSA).

In the case of significance of the two-way interaction, simple effects of the mouse genotype were assessed with independent-sample t-tests. Inflation of the family-wise type 1 error rate was controlled with the False Discovery Rate procedure[513].

The analysis of cardiac electrical activity was restricted to the mouse model of DS. Therefore, to evaluate whether OSAs impacted the modulation of heart rhythm in TS mice, the values of ΔHP during OSA events in experimental mice were analyzed with a one-sample t-test with a reference value of 0. This analysis was not performed in EU mice, as most of them did not show any OSA event.

9. RESULTS

9.1 TS65DN MICE

GENERAL INFORMATION

At surgery, TS mice exhibited a significant decrease in body weight compared to EU controls (25.6 ± 1.0 vs. 28.3 ± 0.6 g, respectively for TS and EU; t-test, p = 0.043), despite the absence of a significant variation in age between them (19.5 ± 0.8 vs. 19.8 ± 0.7 weeks, respectively for TS and EU; t-test, p = 0.829).

SLEEP

The analysis of the time spent in each wake-sleep state did not show any significant difference between TS and EU controls (Table 3).

Table 3

Experimental Group	W (%)	NREM sleep (%)	REM sleep (%)
TS (n=12)	22.6 ± 1.3	59.5 ± 2.6	13.2 ± 1.9
EU (n=14)	18.6 ± 1.9	64.8 ± 2.5	10.7 ± 1.9

Table 3. **Time spent in each wake-sleep state for the Down syndrome mouse model.**
The table shows the percentage of time spent in wakefulness (W), non-rapid-eye-movements (NREM) sleep or rapid-eye-movements (REM) sleep of Ts65Dn mice (TS), model of Down syndrome, and their euploid controls (EU) during an 8-hour recording session inside the whole-body plethysmography chamber.

Data are expressed as mean ± SEM and *n* represents the number of mice employed for each different experimental group.

However, a further analysis aimed at assessing the presence of wake-sleep fragmentation revealed a significant interaction between mouse genotype and bout duration during both W and NREM sleep, but not during REM sleep (two-way ANOVA, p = 0.008, p = 0.001, and p = 0.501, respectively) (Figure 15). Notably, TS mice showed a significantly higher number of short bouts of W lasting less than 12 seconds and of NREM sleep lasting less than 60

seconds (t-tests with false discovery rate correction, $p < 0.05$), compared to EU controls (Figure 15A and 15B).

Figure 15

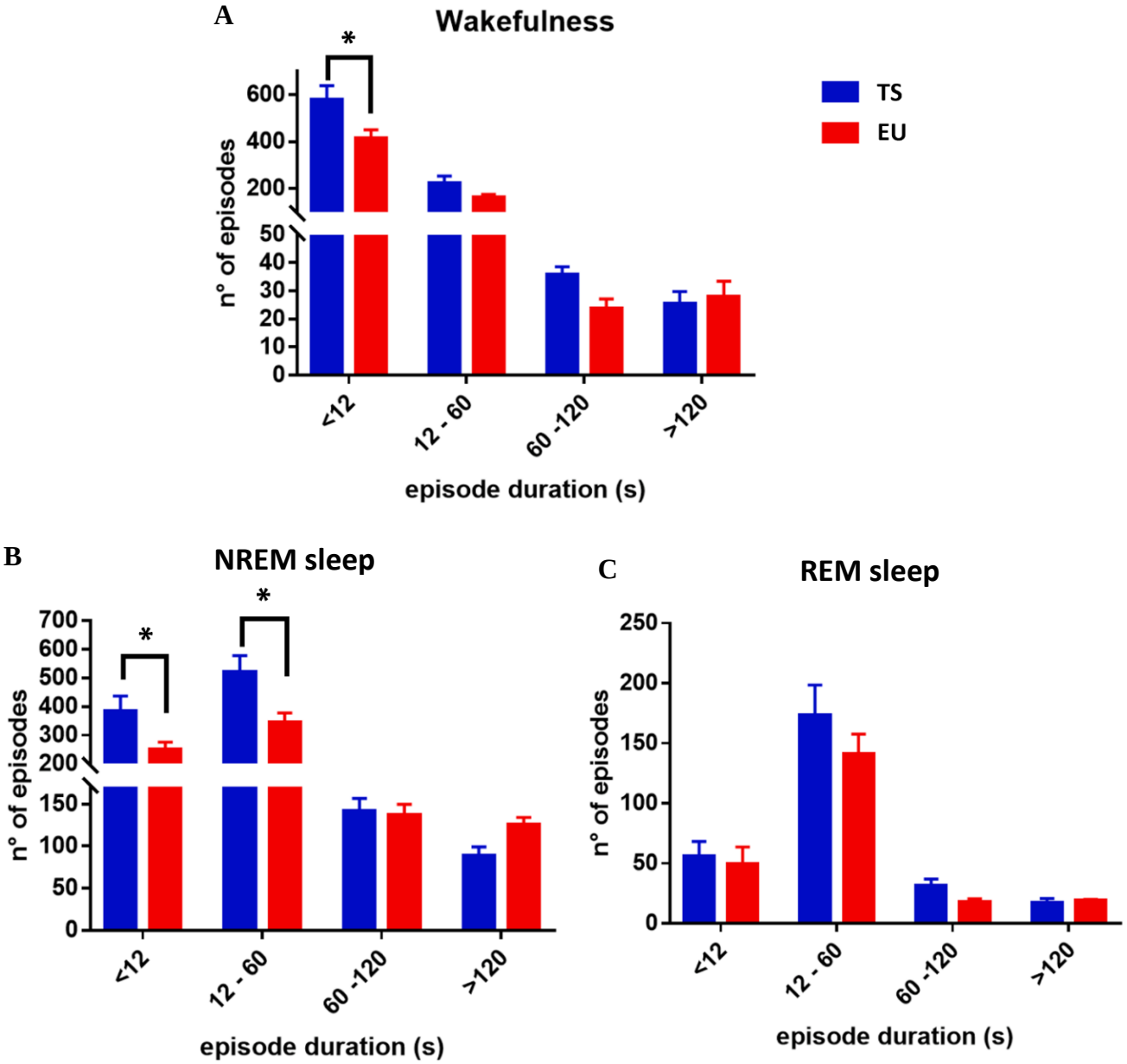

Figure 15. **Distribution of wake-sleep episodes for the Down syndrome mouse model.**
Wake and sleep episodes are distributed according to their duration in four temporal bins (<12 seconds, between 12 and 60 seconds, between 60 and 120 seconds, and > 120 seconds). Each panel compares the condition found in Ts65Dn mice (TS, model of Down syndrome) with their euploid counterparts (EU) into a different behavioral state (panel A is for wakefulness, panel B for the non-rapid-eye-movements sleep – NREM sleep – and panel C for the rapid-eye-movements sleep – REM sleep).

***** $p < 0.05$ TS vs. EU (t-test with false discovery rate correction).

RESPIRATION DURING SLEEP

The analysis of respiratory variables during sleep, conducted in TS and EU mice during the 8-hour WBP recording session during the light period, showed no statistically significant difference in the values of T_{TOT}, V_T, and total occurrence rate of sighs. Similarly, no significant difference was found for the total occurrence rate of apneas during NREM and REM sleep (two-way ANOVA, genotype main effect, p = 0.997; interaction between sleep state and mouse genotype, p = 0.073) (Table 4 and Figure 16).

Table 4

	NREM sleep		**REM sleep**	
	TS (n=12)	**EU** (n=14)	**TS** (n=12)	**EU** (n=14)
T_{TOT} (ms)	269 ± 44	255 ± 17	220 ± 37	206 ± 12
V_T (µl)	362 ± 25	376 ± 10	350 ± 20	356 ± 9
Sighs (events/h)	22.0 ± 1.6	15.7 ± 1.7	3.5 ± 1.4	1.4 ± 0.5
Apneas (events/h)	1.6 ± 0.2	3.1 ± 0.6	5.9 ± 1.2	4.3 ± 1.1

Table 4. Respiratory variables for the Down syndrome mouse model.
The table shows the values of ventilatory period (T_{TOT}, expressed in milliseconds), tidal volume (V_T, expressed in microliters), and the occurrence rate of sighs and apneas (expressed as events per hour of sleep) recorded during non-rapid-eye-movements (NREM) sleep or rapid-eye-movements (REM) sleep in Ts65Dn mice (TS), model of Down syndrome, and their euploid controls (EU) in an 8-hour recording session inside the whole-body plethysmography chamber.

Data are expressed as mean ± SEM and *n* represents the number of mice employed for each different experimental group.

Figure 16

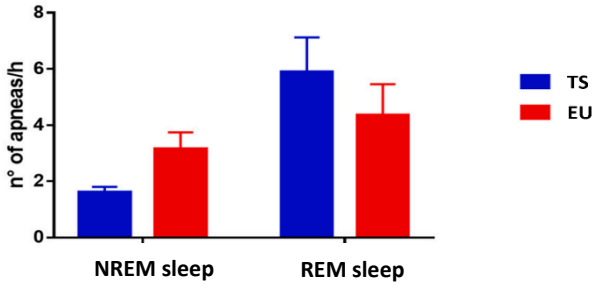

Figure 16. Total apnea occurrence during sleep for the Down syndrome mouse model.
Comparison of sleep apnea occurrence rate between Ts65Dn (TS) mice, model of Down syndrome, and euploid control (EU) mice. The graph shows no differences in total sleep apnea occurrence rate during both non-rapid-eye-movements (NREM) sleep or rapid-eye-movements (REM) sleep in an 8-hour recording session inside the whole-body plethysmography chamber.

POST-SIGH VS. SPONTANEOUS SLEEP APNEAS

Despite the absence of significant differences in the analysis of total sleep apnea occurrence rate during NREM and REM sleep (Table 5 and Figure 16), a significant interaction between mouse genotype and apnea subtype (two-way ANOVA, $p = 0.021$) was found by classifying apneas according to their proximity to a preceding sigh[497]. Particularly, independent t-tests revealed that TS mice exhibited a significantly lower occurrence rate of spontaneous sleep apneas during NREM sleep compared to EU controls (1.25 ± 0.20 vs. 2.83 ± 0.35 events/h, respectively, t-test, $p = 0.020$, Table 5), while no difference was found concerning post-sigh sleep apnea occurrence during NREM sleep (0.32 ± 0.17 and 0.25 ± 0.13 events/h, respectively for TS and EU, t-test, $p = 0.735$). Additionally, no differences were found for the occurrence rate of both spontaneous and post-sigh apneas during REM sleep in TS mice compared to EU controls (Table 5).

Table 5

	NREM sleep		**REM sleep**	
	TS (n=12)	**EU** (n=14)	**TS** (n=12)	**EU** (n=14)
Post-sigh apneas (events/h)	0.32 ± 0.17	0.25 ± 0.13	0.1 ± 0.1	0
Spontaneous apneas (events/h)	1.25 ± 0.20*****	2.83 ± 0.35	5.8 ± 1.3	4.3 ± 1.1

Table 5. **Post-sigh and spontaneous sleep apneas for the Down syndrome mouse model.**

The table shows the values of the occurrence rate of apneas (expressed as events per hour of sleep) classified as post-sigh or spontaneous according to the distance from a preceding sigh. These events were recorded during non-rapid-eye-movements (NREM) sleep or rapid-eye-movements (REM) sleep in Ts65Dn mice (TS), model of Down syndrome, and their euploid controls (EU) in an 8-hour recording session inside the whole-body plethysmography chamber.

Data are reported as mean ± SEM and *n* represents the number of mice employed for each different experimental group. ***** $p < 0.05$ TS vs. EU.

CENTRAL VS. OBSTRUCTIVE SLEEP APNEAS

The subsequent classification of apneic events into CSA and OSA was performed only in 9 TS and 11 EU mice because of signal artifacts interfering with DIA evaluation.

Our data indicated that almost all apneas during NREM sleep in both groups were identified as CSAs, accounting for 97.8 ± 2.2 % in TS mice and 100.0 ± 0.0 % in EU mice (Table 6 and Figure 17).

On the other hand, during REM sleep both CSA and OSA were present, although with a different rate considering the two experimental groups (Table 6 and Figure 17). Particularly, during REM sleep, TS showed a reduced percentage of CSA compared to EU controls (37.0 ± 8.4 % vs. 65.4 ± 15.1 %, respectively) in favor of an augmented percentage of events with an obstructive component (about 60% in TS vs. about 35% in EU). Indeed, 35.4 ± 9.7 % of events were classified as OSAs and 27.7 ± 7.9 as sub-OSAs in TS, while 27.9 ± 11.1 % of apneic events were categorized as OSAs and 6.7 ± 4.5 % as sub-OSAs in EU mice.

Table 6

	NREM sleep		**REM sleep**	
	TS	**EU**	**TS**	**EU**
CSA (%)	97.8 ± 2.2 (9)	100.0 ± 0.0 (11)	37.0 ± 8.4 (9)	65.4 ± 15.1 (8)
OSA (%)	2.2 ± 2.2 (7)	0 (11)	35.4 ± 9.7 (9)	27.9 ± 11.1 (8)
Sub-OSA (%)	/	/	27.7 ± 7.9 (9)	6.7 ± 4.5 (8)

Table 6. Central and obstructive sleep apneas for the Down syndrome mouse model.

The table shows the percentage of apneas classified as central (CSA), obstructive (OSA), or sub-obstructive (sub-OSA) according to the presence or not of a diaphragmatic effort in correspondence of a breathing pause. These events were recorded during non-rapid-eye-movements (NREM) sleep or rapid-eye-movements (REM) sleep in Ts65Dn mice (TS), model of Down syndrome, and their euploid controls (EU) in an 8-hour recording session inside the whole-body plethysmography chamber.

Data are reported as mean ± SEM and brackets contain the number of mice employed for each experimental group. Apneas with undetectable or artifactual diaphragm electromyographic signal were excluded from the analysis.

Figure 17

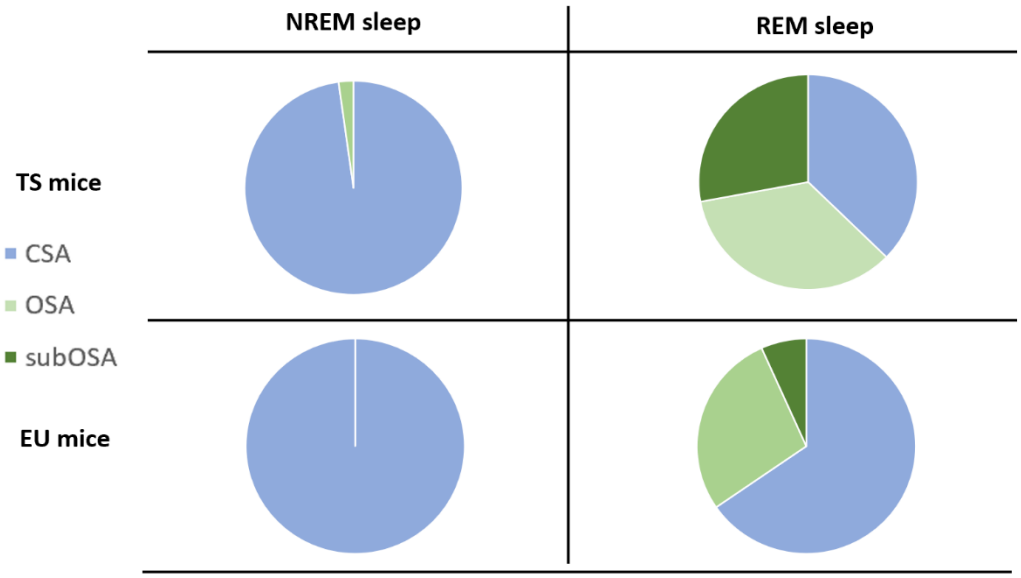

Figure 17. Percentage of central and obstructive apneas during sleep for the Down syndrome mouse model.

Comparison of the percentage of sleep apnea of central (CSA), obstructive (OSA) or sub-obstructive (sub-OSA) origin between Ts65Dn mice (TS), model of Down syndrome, and euploid control (EU) mice, recorded during the non-rapid-eye-movements (NREM) sleep and the rapid-eye-movements (REM) sleep.

Consistent with the previous data, the analysis confirmed that the occurrence rate of CSA during NREM sleep was significantly lower in TS mice than in EU controls (interaction between apnea type and genotype, two-way ANOVA, $p = 0.005$; t-test, $p = 0.006$), whereas no significant difference was observed for OSAs (Figure 18A).

Conversely, these data also demonstrated that TS mice had an increased number of apneas with an obstructive component (i.e., OSAs and sub-OSAs) during REM sleep, when compared to EU controls (interaction between apnea type – with vs. without an obstructive component – and mouse genotype, two-way ANOVA, $p = 0.049$; t-test, $p = 0.003$) (Figure 18B), while no difference was found concerning the occurrence rate of CSA (t-test, $p = 0.983$).

Figure 18

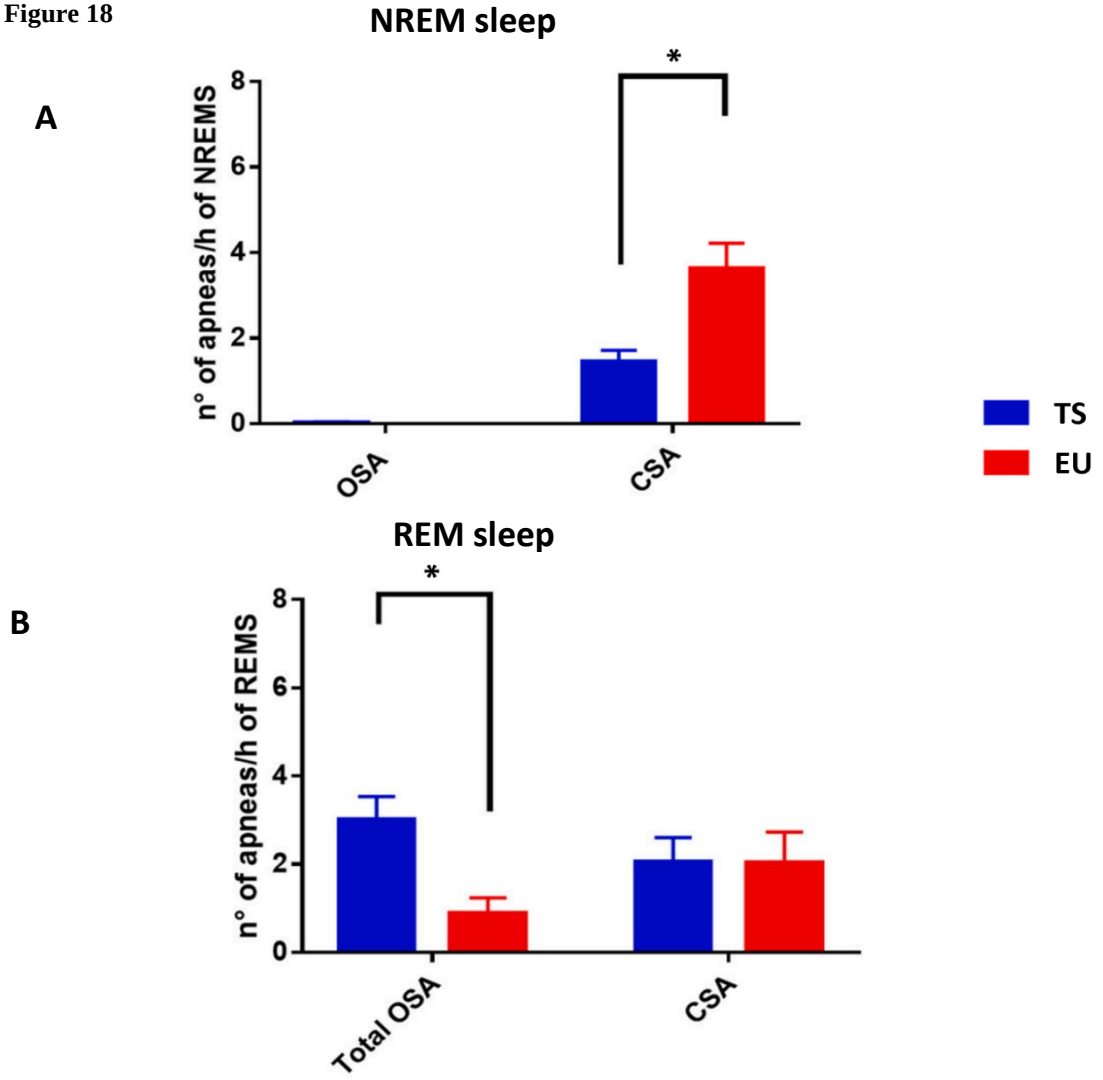

Figure 18. Central and obstructive apneas occurrence during sleep for the Down syndrome mouse model.

Comparison of the occurrence rate of sleep apnea of central (CSA) and obstructive (OSA) origin between TS, model of Down syndrome, and euploid control (EU) mice. The graphs show a reduced CSA occurrence rate during the non-rapid-eye-movements (NREM) sleep and an augmented frequency of apneas with an obstructive event during the rapid-eye-movements (REM) sleep in TS mice when compared to EU.

Total OSA includes both apneic events (OSAs) characterized by diaphragmatic contraction and concomitant absence of airflow and events (sub-OSAs) characterized by diaphragmatic contraction and concomitant reduction of at least 30% of estimated airflow compared to baseline value.

* $p < 0.05$ TS vs. EU (t-test).

AIRFLOW AND DIAPHRAGM STRENGTH

The analysis of the airflow before and after the breathing pause and the ratios of DIA burst duration revealed no significant difference in any of the identified apneic events (i.e., CSAs, OSAs, and sub-OSAs) between the two experimental groups during REM sleep (t-tests, $p \geq 0.08$). Conversely, the ratios of DIA burst amplitude during both REM sleep OSAs and sub-OSAs were significantly higher in TS than in EU mice when compared to the baseline (t-test, $p = 0.002$ and $p = 0.028$, respectively).

Table 7

	CSA		**OSA**		**Sub-OSA**	
	TS (n=6)	**EU** (n=5)	**TS** (n=9)	**EU** (n=4)	**TS** (n=6)	**EU** (n=4)
Airflow (%)	99 ± 16	81 ± 6	116 ± 13	114 ± 25	53 ± 11	52 ± 10
DIA burst amplitude (%)	/	/	127 ± 17*****	52 ± 7	90 ± 11*****	45 ± 11
DIA burst duration (%)	/	/	72 ± 12	53 ± 12	94 ± 14	56 ± 9

Table 7. **Central and obstructive sleep apneas for the Down syndrome mouse model.**
The table displays the measurements of airflow, and of amplitude and duration of diaphragmatic activity (DIA) during sleep apneas of central (CSAs), obstructive (OSAs) and sub-obstructive (Sub-OSAs) nature, recorded during rapid-eye-movements (REM) sleep in a mouse model of Down syndrome (TS) and their euploid controls (EU).

Since CSA and OSA are both characterized by the complete absence of airflow activity, the airflow values refer to the post-apneic event, whereas, for sub-OSAs, these values pertain to the event demonstrating partial obstruction (>30% compared to baseline). Amplitude and duration of the diaphragmatic activity refer to the bursts that occurred during the obstructions (thus, they could not be computed for CSA). All these values are presented as percentage in comparison to the values of the event preceding the apnea.

Data are reported as mean ± SEM and *n* represents the number of mice employed for each experimental group. ***** $p < 0.05$ TS vs. EU.

HEART PERIOD MODULATION

All apneic events (including CSA, OSA, and sub-OSA), recorded during both NREM and REM sleep, were accompanied by a deceleration in heart rhythm in TS mice, as supported by a significant increase in the HP during the apneic event in comparison to the 10 preceding heartbeats (one-sample t-test on ΔHP with reference value of zero, p = 0.038) (Figure 19).

Figure 19

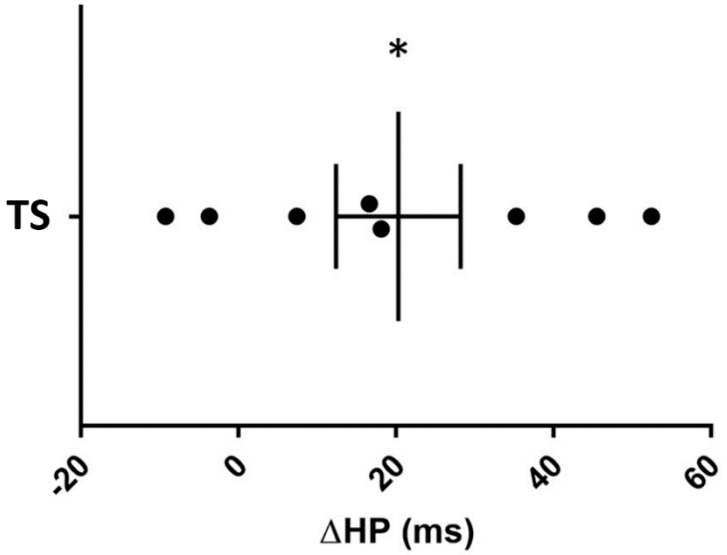

Figure 19. **Heart rhythm modulation during apneic event for the Down syndrome mouse model.**

The graph shows the difference in the heart period (ΔHP, expressed in milliseconds) between the apneic event and the 10 preceding heartbeats.

Each black dot represents a single TS mouse, model of Down syndrome, the middle line indicates the mean value of ΔHP, and the external lines indicate SEM.

Figure 20 contains visual representations of raw signals recorded during different apneic events in the TS mouse, model of DS.

Figure 20

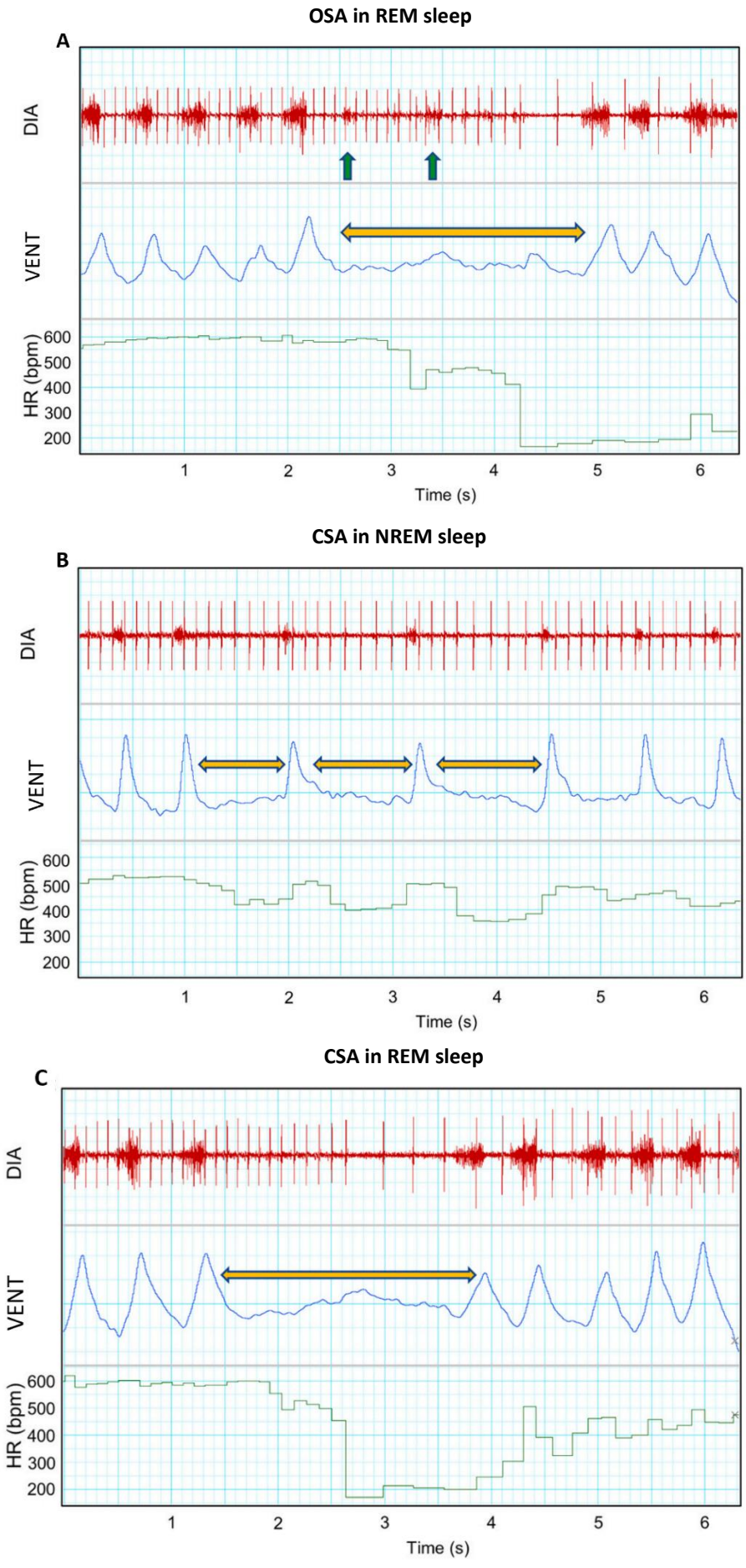
OSA in REM sleep
A
DIA
VENT
HR (bpm)
600
500
400
300
200
1
2
3
4
5
6
Time (s)
CSA in NREM sleep
B
DIA
VENT
HR (bpm)
600
500
400
300
200
1
2
3
4
5
6
Time (s)
CSA in REM sleep
C
DIA
VENT
HR (bpm)
600
500
400
300
200
1
2
3
4
5
6
Time (s)

Figure 20 – Continue

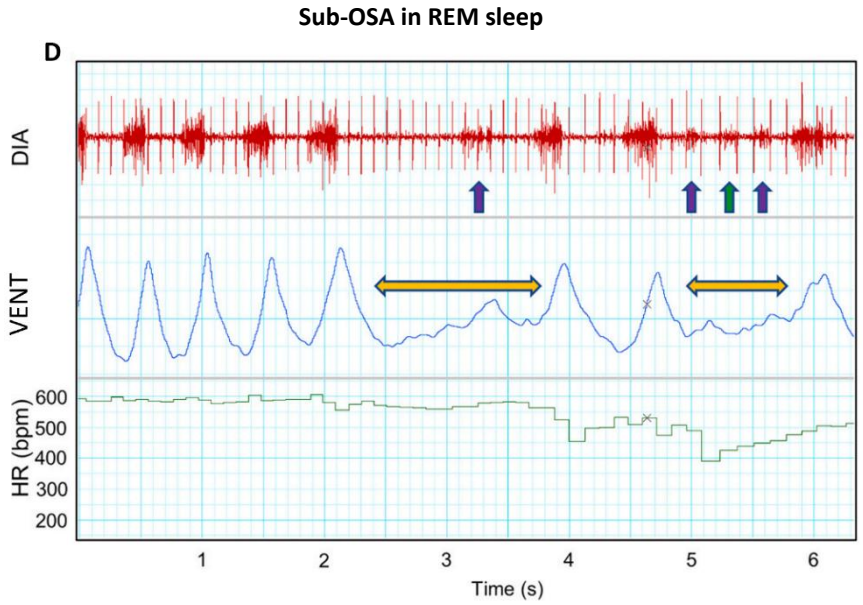

Figure 20. **Examples of raw tracings in a mouse model of Down syndrome.**
Each panel displays a representative example of cardiorespiratory variables and diaphragm contraction recorded during different apneic events in the TS mouse model of Down syndrome. Panel A refers to an obstructive sleep apnea (OSA) during rapid-eye-movements (REM) sleep, panel B to a central sleep apnea (CSA) during non-rapid-eye-movements (NREM) sleep, panel C to a CSA occurring in REM sleep, and panel D to a sub-obstructive sleep apnea (sub-OSA) in REM sleep.

Each panel shows the diaphragm electromyographic (DIA, in red) and the ventilatory (VENT, which is the differential pressure recorded into the whole-body plethysmograph corresponding to mouse respiratory pattern, in blue), signals together with the heart rate (HR, expressed in beats per minute, in green).

On the DIA signal, green arrows indicate OSA events, and the purple arrow indicates a sub-OSA event. On the VENT signal, orange arrows indicate apnea events.

9.2 CDKL5-KNOCKOUT MICE

GENERAL INFORMATION

At surgery, aged-matched CDKL5-KO and CDKL5-WT mice (49.4 ± 0.4 vs. 49.8 ± 0.4 weeks, respectively; t-test, p = 0.5731) did not exhibit significant differences in body weight (29.1 ± 0.9 vs. 31.0 ± 0.9 g, respectively; t-test, p = 0.1589).

SLEEP

The percentage of recording time spent in W, NREM sleep, or REM sleep did not differ significantly between CDKL5-KO and CDKL5-WT (two-way ANOVA, genotype main effect, p = 0.846; interaction between sleep state and mouse genotype, p = 0.300) (Table 8).

Table 8

Experimental Group	W (%)	NREM sleep (%)	REM sleep (%)
CDKL5- KO (n=14)	25.1 ± 3.5	64.5 ± 2.9	7.5 ± 0.5
CDKL5- WT (n=10)	22.2 ± 1.6	68.9 ± 1.4	7.1 ± 0.7

Table 8. Time spent in each wake-sleep for the CDKL5 deficiency disorder mouse model.

The table shows the percentage of time spent in wakefulness (W), non-rapid-eye-movements (NREM) sleep or rapid-eye-movements (REM) sleep of CDKL5-knockout mice (CDKL5-KO), model of CDKL5 deficiency disorder, and their wild-type controls (CDKL5-WT) during an 8-hour recording session inside the whole-body plethysmography chamber.

Data are expressed as mean ± SEM and *n* represents the number of mice employed for each different experimental group.

RESPIRATION DURING SLEEP

The analysis of respiratory variables during sleep, conducted in CDKL5-KO and CDKL5-WT mice during the 8-hour WBP recording session during the light period, showed no statistically significant differences in the values of T_{TOT} and V_T (Table 9).

Additionally, the two-way ANOVA revealed a significant interaction between genotype and sleep states on the occurrence rate of total apneas (two-way ANOVA, p = 0.013).

Specifically, independent t-tests confirmed that CDKL5-KO mice exhibit a higher occurrence rate of apneas during REM sleep (t-test, p =0.012), but not during NREM sleep (t-test, p = 0.930) (Table 9 and Figure 21A).

Finally, the two-way ANOVA also revealed a significant interaction between genotype and sleep states on the occurrence rate of sighs (two-way ANOVA, p = 0.031), which was further investigated only during NREM sleep, as sighs are almost exclusive of this sleep state[497]. Specifically, we found that CDKL5-KO mice had a lower frequency of sighs during NREM sleep compared to CDKL5-WT mice (t-test, p = 0.033) (Table 9 and Figure 21B).

Table 9

	NREM sleep		**REM sleep**	
	CDKL5-KO (n=10)	**CDKL5-WT** (n=14)	**CDKL5-KO** (n=10)	**CDKL5-WT** (n=14)
T_{TOT} (ms)	412 ± 8	427 ± 7	373 ± 10	386 ± 8
V_T (µl)	274 ± 9	239 ± 14	205 ± 7	190 ± 13
V_T (µl/g)	9.5 ± 0.4	7.6 ± 0.3	7.2 ± 0.4	6.1 ± 0.3
Apneas (events/h)	4.0 ± 0.7	3.9 ± 0.7	17.5 ± 2.5*	8.3 ± 1.7
Sighs (events/h)	13.6 ± 1.2*	19.0 ± 2.3	0	0.1 ± 0.1

Table 9. **Respiratory variables for the CDKL5 deficiency disorder mouse model.**
The table shows the values of ventilatory period (T_{TOT}, expressed in milliseconds), tidal volume (V_T, expressed in microliters or in microliters per gram of body weight), and the occurrence rate of apneas and sighs (expressed as events per hour of sleep) recorded during non-rapid-eye-movements (NREM) sleep or rapid-eye-movements (REM) sleep in CDKL5-knockout mice (CDKL5-KO), model of CDKL5 deficiency disorder, and their controls (CDKL5-WT) in an 8-hour recording session inside the whole-body plethysmography chamber.

Data are expressed as mean ± SEM and *n* represents the number of mice employed for each different experimental group. * p < 0.05 CDKL5-KO vs. CDKL5-WT.

Figure 21

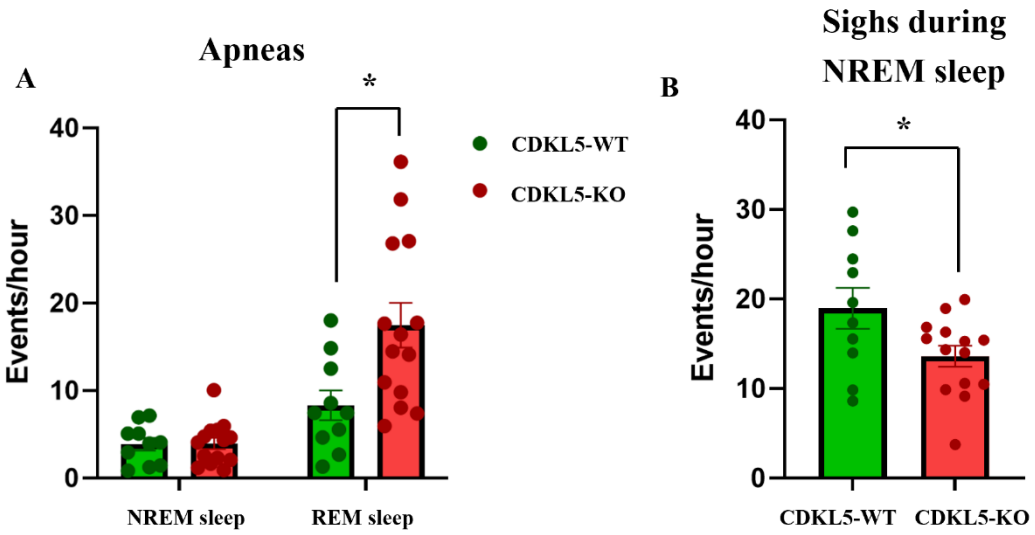

Figure 21. Total apnea and sigh occurrence during sleep for the CDKL5 deficiency disorder mouse model.

Comparison of sleep apnea and sigh occurrence rate between CDKL5-knockout (CDKL5-KO) mice, model of CDKL5 deficiency disorder, and wild-type (CDKL5-WT) mice, recorded for 8 hours during the light period inside the whole-body plethysmography chamber.

Panel A shows an increased total sleep apnea occurrence rate in CDKL5-KO during rapid-eye-movements (REM) sleep, but not during non-rapid-eye-movements (NREM) sleep. Whereas, panel B represents the sigh occurrence rate, which was decreased in CDKL5-KO compared to CDKL5-WT mice.

Data are expressed as mean ± SEM. * $p < 0.05$ CDKL5-KO vs. CDKL5-WT.

POST-SIGH VS. SPONTANEOUS SLEEP APNEAS

By classifying apneas based on their temporal relationship to preceding sighs[497], we found no significant interaction between mouse genotype and apnea subtype during NREM sleep (two-way ANOVA, $p = 0.638$) (Table 10). However, a similar analysis was not conducted for REM sleep, primarily because post-sigh apneas were entirely absent during this sleep state (Table 10).

Table 10

	NREM sleep		REM sleep	
	CDKL-KO (n=14)	**CDKL5-WT** (n=10)	**CDKL-KO** (n=14)	**CDKL5-WT** (n=10)
Post-sigh apneas (events/h)	1.5 ± 0.3	1.3 ± 0.4	0	0
Spontaneous apneas (events/h)	2.4 ± 0.6	2.6 ± 0.8	17.5 ± 2.5	8.3 ± 1.7

Table 10. **Post-sigh and spontaneous sleep apneas for the CDKL5 deficiency disorder mouse model.**

The table shows the values of the occurrence rate of apneas (expressed as events per hour of sleep) classified as post-sigh or spontaneous according to the distance from a preceding sigh. These events were recorded during non-rapid-eye-movements (NREM) sleep or rapid-eye-movements (REM) sleep in CDKL5-knockout mice (CDKL5-KO), model of CDKL5 deficiency disorder, and their wild-type controls (CDKL5-WT) in an 8-hour recording session inside the whole-body plethysmography chamber.

Data are reported as mean ± SEM and *n* represents the number of mice employed for each different experimental group.

CENTRAL VS. OBSTRUCTIVE SLEEP APNEAS

Since the significant change in apnea occurrence rate was observed exclusively during REM sleep (Figure 21), the subsequent categorization of apneic events into CSA and OSA was conducted only for this sleep stage. Particularly, it was performed on 13 CDKL5-KO and 10 CDKL5-WT mice because one CDKL5-KO mouse showed a high level of signal artifacts interfering with DIA evaluation.

Our findings revealed that, during REM sleep, both CSA and OSA were present, although varying for the rate between the two experimental groups (Table 11 and Figure 22). Specifically, the analysis demonstrated that the occurrence rate of apneas with an obstructive component (Total OSA, i.e., the sum of OSA and sub-OSA events) was significantly higher in CDKL5-KO mice compared to CDKL5-WT mice (interaction between apnea type and genotype, two-way ANOVA, $p = 0.032$; t-test, $p = 0.033$). In contrast, no significant difference was observed in the occurrence of CSAs (Mann Whitney test, $p = 0.965$) (Table 11 and Figure 22).

Table 11

	REM sleep	
	CDKL5-KO (n = 13)	**CDKL5-WT (n = 10)**
CSA (events/hour)	1.1 ± 0.4	1.2 ± 0.4
Total OSA (events/hour)	10.2 ± 1.6*	5.5 ± 1.0

Table 11. Central and obstructive sleep apneas for the CDKL5 deficiency disorder mouse model. The table shows the values of occurrence rate of apneas classified as central (CSA) or obstructive (Total OSA) according to the presence or not of a diaphragmatic effort in correspondence of a breathing pause. These events were recorded during rapid-eye-movements (REM) sleep in CDKL5-knockout (CDKL5-KO) mice, model of CDKL5 deficiency disorder, and wild-type (CDKL5-WT) mice in an 8-hour recording session inside the whole-body plethysmography chamber.

Data are reported as mean ± SEM and *n* represents the number of mice employed for each different experimental group. Apneas with undetectable or artefactual diaphragm electromyographic signal were excluded from the analysis. * $p < 0.05$ KO vs. WT.

Figure 22

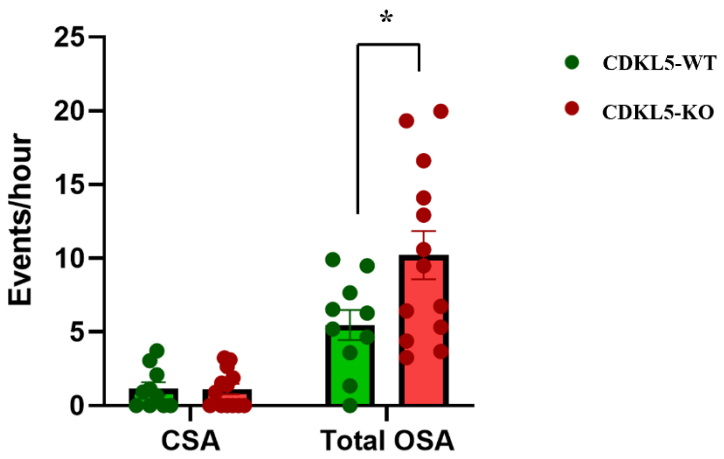

Figure 22. Central and obstructive apneas occurrence during REM sleep for the CDKL5 deficiency disorder mouse model.

Comparison of the occurrence rate of sleep apnea of central (CSA) and obstructive (Total OSA) origin between CDKL5-knockout (CDKL5-KO) mice, model of CDKL5 deficiency disorder, and wild-type (CDKL5-WT) mice. The graphs show an augmented frequency of apneas with an obstructive component during the rapid-eye-movements (REM) sleep in CDKL5-KO mice when compared to CDKL5-WT.

Total OSA includes both apneic events (OSAs) characterized by diaphragmatic contraction and concomitant absence of airflow and events (sub-OSAs) characterized by diaphragmatic contraction and concomitant reduction of at least 30% of estimated airflow compared to baseline value.

***** $p < 0.05$ CDKL5-KO vs. CDKL5-WT (t-test).

10. DISCUSSION

The aim of these experiments was to determine whether the respiratory disturbances observed in human DS and CDD patients are replicated in the genetic mouse models of these diseases (respectively, TS and CDKL5-KO mice). Our results demonstrated that:

a) Mice are valuable animal models for the study of SBDs, especially for OSAs.
b) The extent of airway obstruction in these events varies from complete to partial, leading to the discrimination between OSA and sub-OSA events.
c) The occurrence rate of apneas with an obstructive component (which include OSAs and sub-OSAs) is significantly increased during REM sleep in both animal models.

MICE AS MODEL OF OBSTRUCTIVE SLEEP APNEA

Mice have been extensively used as valuable models for studying SBDs, especially for sleep apneas[54]. These disorders carry significant socioeconomic implications beyond the impacts on patients' wellness[285,289,318]. Indeed, sleep apnea inevitably leads to sleep deprivation, sleep disturbances, and a diminished quality of life[514]. As sleep plays a pivotal role in enhancing cognitive function and productivity in occupational settings, the absence of adequate sleep is associated with increased risks of traffic and workplace incidents, medical mistakes, and reduced work efficiency, resulting in huge economic losses[514].

Even though the number of studies investigating sleep apnea in mice has risen in the last two decades, much of the research involving them has predominantly focused on exploring the impact of OSA on oxygen saturation levels, using intermittent hypoxia paradigms[54,515]. However, this methodological approach does not allow for investigating the pathogenesis or treatment of sleep apnea, thus only few studies addressed this task. This may relate to two possible explanations. First, mice have long been considered not suitable models to study sleep apnea because of the misbelief that only CSA can occur in mice[494] and the report of several differences in the anatomy of upper airways between mice and humans[420]. However, this concept was challenged by Polotsky's research team, who discovered the presence of inspiratory flow limitation employing a non-invasive technique (see chapter 4.2 “Methods for studying sleep apnea in animal models” or *Alvente et al., 2023*)[54] and who emphasized it as an indicator of airway obstruction during sleep in obese mice[54,435,516,517]. They also repetitively demonstrated that the functioning of the upper respiratory airways and of hypoglossal nerve function in mice closely mirrors that of humans[421,422]. Second, it is

technically challenging to make all the necessary measurements to properly characterize sleep apneas in such small animals[54].

In the current study, we demonstrated for the first time the physiological occurrence of OSAs in non-obese mice. Specifically, we found that OSA was highly prevalent during REM sleep in both TS and CDKL5-KO mice, although they did not show an increased body weight compared to their respective counterparts.

These data are in line with human studies which report that, although upper airway obstructions can occur in both NREM and REM sleep in humans, there is a heightened propensity for upper airways to collapse during REM sleep[285]. This phenomenon is likely due, at least in part, to a reduced upper airway muscles tone[518] caused by the activation of cholinergic muscarinic receptors, which, in turn, stimulate G-protein-coupled inwardly rectifying potassium channels on motoneurons[312]. Moreover, it has been shown that REM sleep-related OSA tends to be longer and involves more frequent and more pronounced drops in oxyhemoglobin saturation levels compared to those observed in NREM sleep[317]. Accordingly, clinical studies have shown a significant correlation between OSA occurrence rate and arterial hypertension during REM sleep[519].

We also demonstrated that, similarly to what happens in humans[280,520], the level of obstruction during apneic events in both DS and CDD mouse models is variable. Consequently, we included in the counting of total OSAs both events encompassing the complete absence of airflow with concomitant diaphragmatic contraction (i.e., complete OSA) and events with a partial reduction in airflow (i.e., sub-OSAs)[495,512].

TS65DN MICE

We applied a surgical and analytical approach to categorize between CSA and OSA in a mouse model of DS. Our aim was to investigate whether TS mice, carriers of the trisomic mutation, showed an augmented occurrence rate of OSA during sleep when compared to their control counterparts (EU mice), as it happens in humans[349,352,521].

Our investigation successfully revealed a significant increase in the frequency of apneas exhibiting an obstructive component during REM sleep, whereas no statistically significant differences were found during NREM sleep between the two experimental groups (Figure 18). This discovery is consistent with findings in human studies, where individuals with DS tend to experience a higher prevalence of OSA during REM sleep[522], leading to hypoxemia, cognitive deficits, arterial hypertension, and sleep fragmentation[523]. Interestingly, despite our study focuses on a limited time window for assessing the sleep phenotype (8 hours during

the light period), we detected signs of sleep fragmentation in TS mice (Figure 15), confirming prior research results[447]. Additionally, as further evidence of their physiological relevance, we observed the occurrence of bradycardia in TS mice during apneic events, regardless of their origin. This cardiac alteration mirrors the intricate modulation of the heart rhythm of humans, which may reflect the effectiveness of parasympathetic regulation of the heart during sleep[524,525].

Despite OSA represents a more severe condition in DS patients[521,526–528], CSA remains consistently present in this population. In humans, it predominantly manifests following sighs, reflecting an immature peripheral chemoreceptor reflex control, and its frequency increases with age[522]. Surprisingly, our data revealed a reduction in the occurrence rate of CSA during NREM sleep in TS mice compared to EU mice and, notably, that these events were largely unrelated to sigh appearance. However, this discrepancy may be attributed to animals' age or genetic background. Indeed, it is plausible that older TS mice might exhibit relatively more CSA events and genetic background is known to modulate breathing pattern and sleep apnea in both NREM and REM sleep[54,498–501].

Finally, it is worth to mention that these findings hold considerable significance, particularly in the context of patients affected by DS. In fact, the life expectancy of this kind of patients has more than doubled in the last forty years[329]. This emphasizes the need to deepen our understanding of the pathological correlates of DS (including OSA) and the critical importance of both past and forthcoming research in seeking to improve the overall quality of life of people.

CDKL5-KNOCKOUT MICE

The experimental protocol previously described was also applied to CDKL5-KO mice, model of CDD, in which an augmented occurrence rate of apneas during sleep was recently reported[429,460,461].

Our research effectively unveiled a significant rise in apnea frequency during REM sleep, while no statistically significant change was detected during NREM sleep between CDKL5-KO and CDKL5-WT mice (Figure 21). However, even though confirming again the presence of sleep apneas as a fundamental characteristic and a respiratory biomarker of CDD, this result does not perfectly align with prior research on this model. Specifically, studies conducted on young male CDKL5-KO mice (15 weeks), young homozygous and heterozygous females (14 weeks), and middle-aged male CDKL-KO mice (12-14 month-old) had reported an increased frequency of apneas exclusively during NREM sleep, and not during REM sleep[429,460,461]. This discrepancy may be attributed to the different experimental

protocol used to assess the respiratory phenotype in these various studies. Indeed, previous investigations employed the non-invasive WBP solely for identifying respiratory anomalies, whereas the current study combined WBP technology with the surgical implantation of electrodes for sleep stage discrimination (EEG and EMG) and detection of diaphragm contraction (DIA). More likely, this difference may reflect the high level of heterogeneity present in human pathology. Indeed, except for the three core symptoms (early onset and drug-resistant epilepsy, intellectual disability, and psychomotor delay) other symptoms exhibit varying degrees of penetrance in affected individuals[367,368,370–372,374–377].

In the present study, we also successfully categorize sleep apneas occurring during REM sleep into CSA and OSA. Specifically, we found that CDKL5-KO mice had more frequent apneas with an obstructive element during REM sleep compared to CDKL5-WT mice, while no difference was found for the occurrence of CSA (Figure 22). However, to the best of our knowledge, there is no documented evidence of OSA in individuals with CDD and a definitive connection between CDD and respiratory disturbances in humans has yet to be established. This can be mainly related to the scarcity of human studies and to the limited pool of CDD patients available for study. Indeed, between 2003 and 2019, only around 400 individuals received a CDD diagnosis, and among them, only four young female children underwent a comprehensive assessment of the hypnic and respiratory phenotype[372,529,530]. Therefore, since we cannot readily extend our findings to a translational hypothesis, we suggest that the CDKL5 kinase may play a role in the regulation of breathing pattern and rhythm, likely linked to the control of upper airway muscles. Nevertheless, our data reinforce the rationale for routinely assessing SBDs in CDD patients and emphasize the necessity for further research to investigate the potential presence of respiratory abnormalities during sleep in both children and adults affected by CDD.

LIMITATIONS OF THE STUDY

This study acknowledges some limitations, the first and most evident of which is the exclusive inclusion of male mice, which prevents the extension of the results to females. Indeed, clearly defined differences in respiratory behavior have been established between males and females, as well as during different life stages. For instance, these include the dimensions of respiratory system elements[531], the pulmonary kinematics (with males primarily exhibiting diaphragmatic breathing patterns and females tending toward intercostal breathing)[532], and the susceptibility to SBDs (three times more prevalent in men than women)[275,351,533]. These sex-specific characteristics may be partially explained by the diverse actions of sex hormones, which play specific roles in lung inflammation, breathing control

and response to diseases[152,531,533]. Moreover, the presence of sex hormone receptors in various parts of the brain, including central chemoreceptor areas[531,533] and certain respiratory motor neurons (hypoglossal and phrenic nuclei)[534], further supports the idea that sex hormones play a role in respiratory function. In line with this, progesterone levels have been linked to the genioglossus muscle tone, which affects upper airway rigidity and may mediate the occurrence of OSAs[152,535]. Finally, other sex-specific differences, albeit controversial, have been found for the ventilatory response to hypercapnia (HCVR) and hypoxia (HOVR). Indeed, women tend to preserve HCVR during NREM sleep[536] and are thought to have an intact HOVR during NREM sleep, as the decline in HOVR during NREM sleep is noted only in studies where men predominate[273,537].

A second limitation pertains to the technical difficulties of the implantation of DIA electrodes due to the invasiveness of the procedure and the required surgical skills. However, we were able to clearly distinguish diaphragmatic bursts associated with breaths from the background noise in the majority of mice in both studies. To provide a quantitative measure, we achieved an 86% success rate in categorizing apneas: 9 out of 12 TS mice, 11 out of 14 EU mice, 13 out of 14 CDKL5-KO mice, and all 10 CDKL5-WT mice.

Third, we could not directly derive the mean values of inspiratory airflow for breaths from the WBP signal. So, we had to rely on an indirect estimation method, involving the ratio between V_T and the duration of the DIA activity, and on a 30% threshold reduction, a criterion extrapolated from the definition of hypopnea in human subjects[512]. However, to standardize the whole procedure and ensure the validity of our results, the analysis of raw tracings was performed with the consensus of two different researchers. Additionally, we did not attempt to further categorize apneic events as mixed apneas and we did not employ oximeters for the continuous detection of hemoglobin desaturation.

A fourth limitation relies on the inability of our approach to evaluate muscle weakness due to the technical challenges involved in calibrating the recording electrodes, which exhibited variable impedance. Therefore, to give an estimation of the strength of the diaphragm, we measured the amplitude of the DIA burst as the root mean square of the DIA signal, which was compared to that of the last breath before the apneic event. With this method, we managed to show a significant increase in DIA burst amplitude during obstructive events in TS mice relative to EU control mice (Table 7). Therefore, in future research, it will be interesting to explore whether our results depend, at least in part, on diaphragm muscle weakness in TS mice and CDKL5-KO mice, since both DS and CDD patients showed an abnormal muscle tone[367,538].

Finally, we failed in detecting the presence of sleep impairments in these mice, even though these disturbances are well-known to exist in individuals affected by DS[334–346] and CDD[367,368,370–372,374–377]. This lack of detection may be attributed to the fact that the relatively small WBP chamber does not provide an optimal environment for conducting extended and uninterrupted sleep studies due to the accumulation of waste and the potential for added stress. Indeed, our recordings were performed only for 8 hours during the light (resting) period. However, future studies could aim to address this peculiar aspect by performing a complete assessment of sleep phenotype using the EEG-EMG signals for sleep stage discrimination or conducting WBP recordings lasting at least 24 hours.

UNIVERSITY OF ALBERTA

(CANADA): STUDY OF BMP7-KO

MICE

Preliminary study for the characterization

of sleep apneas in mice with neural crest-specific

deletion of Bone Morphogenetic Protein 7

11. METHODS

11.1 ETHICAL APPROVAL

Experiments were conducted in compliance with guidelines by the Canadian Council of Animal Care in Prof. Silvia Pagliardini's Laboratory at the University of Alberta (Edmonton, Alberta, Canada). The study protocol complied with the Research Ethics Office of the University of Alberta (Animal Use and Care Committee; protocol AUP461). All efforts were made to minimize the number of animals and their suffering.

11.2 MICE

Experiments were performed on 3 male mice BMP7-KO mice and 3 male BMP7-WT mice, used as controls.

Mice were housed under a 12:12-hour light-dark cycle with ambient temperature set at 23 ± 1 °C and *ad libitum* access to water and food in the Animal Facility of the University of Alberta (Health Sciences Laboratory Animals Services, University of Alberta, Edmonton, Canada), where the mouse colony was also expanded and kept on a C57Bl/6J background (more than 10 generations).

11.3 BREEDING AND GENOTYPING

Experimental mice were obtained by mating mice carrying loxP sites flanking the first coding exon of the BMP7 gene (BPM7-WT) with Wnt1-Cre transgenic mice[482] to obtain a Cre-mediated recombination allowing the removal of exon 1 and the consequent creation of mice with a neural crest-specific deletion of BMP7 (BMP7-KO)[477].

Genotypes were assessed by extracting DNA from bioptic tissue taken during the marking procedure with phalanges cutting, which was performed under general anesthesia before the 10th day from birth, as previously described[477,539]. Briefly, DNA was amplified by PCR using four different primers (Table 12): one common to all sequences, and the other three specific to the BMP7 gene not flanked by loxP sites, to WT or to BMP7-KO mice. Then, PCR products were resolved by electrophoresis on a 1.5% agarose gel, resulting in products of 407 bp (BMP7 gene not flanked by loxP sites), 491 bp (BMP7-WT) or 607 bp (BMP7-KO).

Table 12

Common primer:
5'- AAGCCAGCCTCGCTGATTG -3'
Primer specific to BMP7 gene not flanked by loxP sites:
5'- GCGTGAGGGTCAGAGCTTATG -3'
Primer specific to WT mice:
5'- GGTCAGCATGGCCTAGGAAG -3'
Primer specific to BMP7-KO mice:
5'- TTTAGCCCCTCAGACAGTCAC -3'

Table 12. **Primers sequences and polymerase chain reaction conditions.**

11.4 WHOLE-BODY PLETHYSMOGRAPHY

The WBP apparatus (Buxco® Small Animal Whole Body Plethysmography, Data Sciences International, NW, USA) comprised a 200 ml acrylic box (Figure 23), continuously supplied with room air at 300 ml/min and connected to a vacuum system which pulled the air out. This was done to prevent the accumulation of CO_2 and to eliminate any potential pressure variations between the internal and external environment. The chamber was modified by introducing an aperture in its roof through which a lightweight cable could pass. During recordings, this aperture was sealed using clay. Furthermore, the WBP was furnished with a high-precision differential pressure transducer (Validyne Engineering, Northridge, CA, USA), which gauged the pressure difference between the chamber housing the mouse and the surrounding environment (used as reference)[486,540].

At the beginning of each recording, the WBP system was calibrated with an automatic pump. This involved introducing subsequent 0.25 ml injections into the animal chamber at various frequencies to replicate the breathing pattern of a mouse. Subsequently, the mouse was slightly anesthetized to allow for the connection of a lightweight cable for the collection of electrical signals before being placed within the WBP chamber.

Figure 23

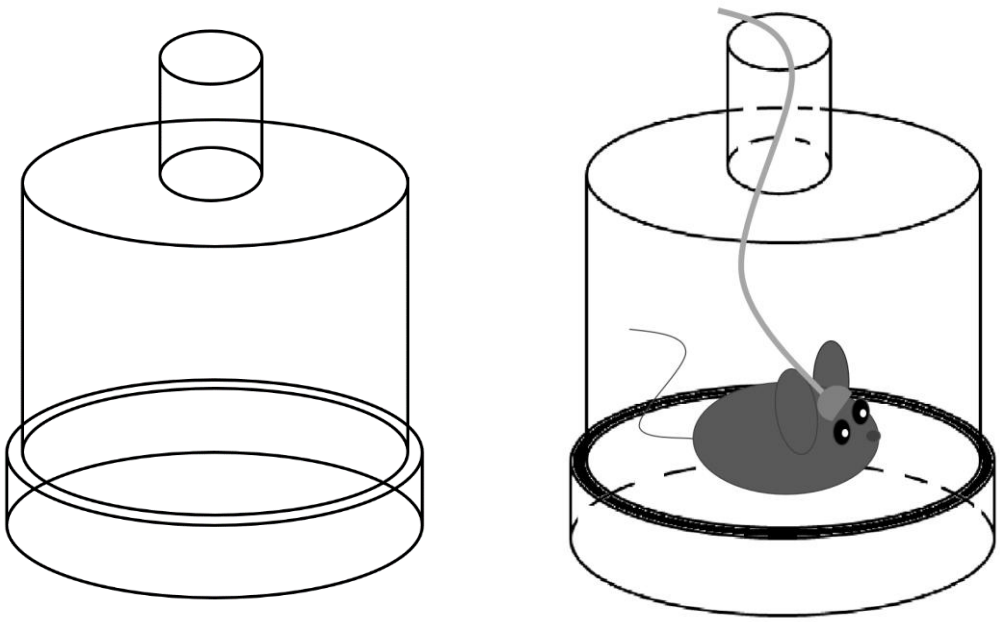

Figure 23. Schematic representation of the Buxco® Small Animal Whole Body Plethysmography.

The diagram offers a visual representation of the whole-body plethysmography (WBP) apparatus both in its empty state and with an animal situated within it.

11.5 DATA RECORDING

During each 8-hour session, EEG, EMG, DIA, and respiratory signals were continuously recorded.

Data were acquired, amplified, and digitized using PowerLab System (ADInstruments Inc., Colorado, USA) and sampled and analyzed using the data analysis software LabChart (version 8, ADInstruments Inc., Colorado, USA).

EEG, EMG, and DIA signals were acquired via the cable transmission. EEG and EMG were sampled at 200 Hz and filtered at 0.3–300 Hz and 100–1000 Hz, respectively, and the EEG signal was further filtered with a low-pass filter at 100 Hz in LabChart. DIA signal was sampled at 1000 Hz and filtered at 100–1000 Hz. The WBP differential pressure, which corresponds to the respiratory signal, was sampled at 200 Hz.

Chamber and animal temperature were measured every hour: the first one using a high precision thermometer, while the latter with a specific handheld reader (HPR Plus Handheld PIT Tag Reader; BioMark, Idaho USA).

Chamber humidity was assumed to be 100% since the WBP chamber was saturated in water steam by placing a layer of water under the animal.

As stated above, since each mouse underwent two 8-hour recording sessions spaced by 24 hours of recovery, all the variables computed during each recording session were then averaged for each mouse.

11.6 DATA ANALYSIS

DISCRIMINATION OF THE WAKE-SLEEP STATES

The discrimination of the wake-sleep states was performed by visual examination of raw EEG, EMG, and respiratory traces[57,493,502]. Briefly, W was identified by a high EMG tone, a low voltage EEG signal with δ (0.5-4 Hz) and θ (6-9 Hz) waves, and by a highly irregular breathing pattern with frequent artifacts due to animal movements. NREM sleep was scored in the presence of an EMG tone lower than in W, of a high voltage EEG signal with a prevalence of δ waves, and of extremely regular and stable breaths. REM sleep was defined when there was muscular atony with occasional muscle twitches, low voltage EEG signal with a prevalence of θ waves, and a breathing pattern characterized by breaths with irregular frequency and amplitude, concomitant with a stable baseline.

For an example of raw EEG and EMG, please refer to Figure 10 in the paragraph “8.7 Data analysis - Discrimination of the wake-sleep states”, whereas an illustrative representation of respiratory traces is shown in Figure 24.

Figure 24

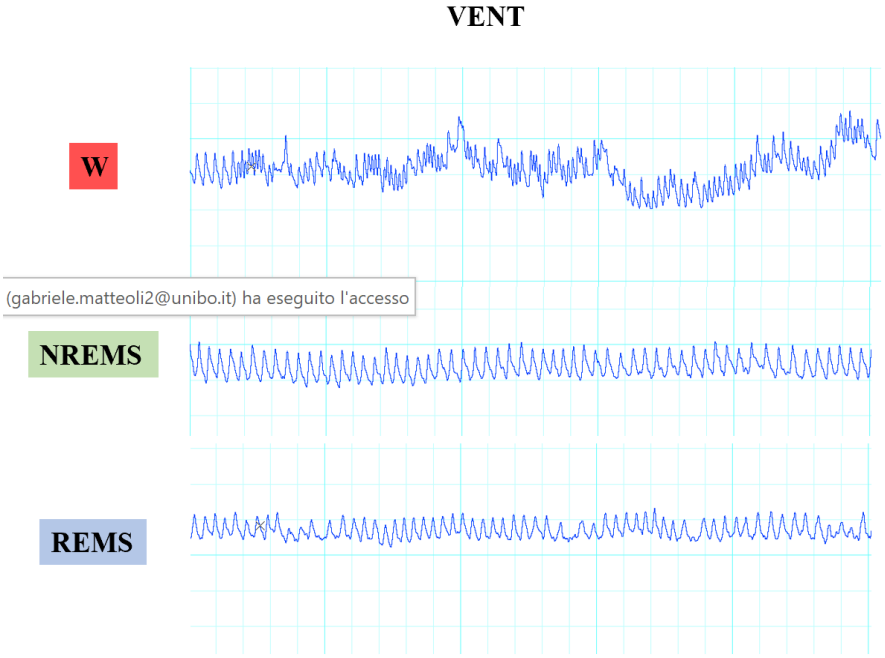

Figure 24. Discrimination of the wake-sleep states based on breathing pattern.
Example of respiratory (VENT) data obtained during Wakefulness (W), Non-Rapid-Eye Movement Sleep (NREMS) and Rapid-Eye Movement Sleep (REMS).

ANALYSIS OF RESPIRATORY VARIABLES

The analysis of respiratory variables was confined to stable periods of NREM and REM sleep lasting at least 12 seconds, excluding periods of transition between wake-sleep states. In addition, W episodes were excluded since they showed a high prevalence of breath-obscuring artifacts due to mouse movements[495,503,507].

Single breaths were automatically identified from the upward (positive) WBP pressure deflection peak. Any inaccuracies in breath detection, such as repeated or stereotypical negative deflections, as well as pressure anomalies arising from events like the opening and closing of the room door or measurements of the chamber temperature, were manually eliminated from the dataset before analysis.

V_T (i.e., air moved in or out of the lungs during each respiratory cycle), was calculated using an appropriate formula[508], as follows:

$$V_T = \frac{V_K}{P_K} * P_T * \frac{T_B * (P_B - P_{Ch})}{T_A * (P_B - P_{Ch}) - T_{Ch} * (P_B - P_A)}$$

where V_K is the volume of air injected during the calibration of the system, P_K is the pressure deflection associated with the calibration volume, P_T is the pressure deflection associated with the breath of interest, P_B is the barometric pressure, P_{Ch} and P_A are the water vapor pressures respectively associated with the animal chamber and with the animal's temperature, and T_A and T_{Ch} are the temperatures respectively associated with the animal's body and with the chamber. For practical purposes, P_B of the recording day was retrieved from the Edmonton Weather Station website (https://edmonton.weatherstats.ca/), T_A was calculated as the mean temperature of the mouse during sleep, T_{Ch} was calculated as the average chamber temperature gauged by the high-precision thermometer, and P_{Ch} and P_A were extrapolated from dedicated tables[541].

T_{TOT} (i.e., duration of each breath), breathing frequency (fR), and inspiratory time (Ti, i.e., duration of inspiration) were automatically calculated with the Blood Pressure Module for LabChart (version 8, ADInstruments Inc., Colorado, USA). Expiratory time (Te, i.e., duration of expiration) was determined by subtracting Ti from T_{TOT}, while V_E was computed as the ratio between the average V_T and the average T_{TOT}. Then, volumes and flows were normalized to body weight[493,495].

Sighs were detected as breaths with a V_T at least three times higher than the average V_T for each mouse in NREM sleep. Similarly, apneas were designated as breaths with a T_{TOT} at least three times longer than the average T_{TOT} for each mouse in each sleep state.

CLASSIFICATION OF APNEAS

Apneas were categorized following two different classifications: one based on the distance from a previous sigh and the other one based on the breathing pattern and the DIA activity. For a detailed description, please refer to the section "8.7 Data analysis – Classification of apneas".

12. RESULTS

GENERAL INFORMATION

Table 13 provides a summary of data pertaining to the age and body weight of mice of the two experimental groups at surgery.

Table 13

Experimental Group	Age (days)	Weight (g)
BMP7-KO	31	13
	32	15
	36	16
BMP7-WT	29	16
	32	19
	28	16

Table 13. **Overview of data for the Pierre Robin sequence mouse model.**
The table provides a comprehensive overview of essential information concerning the age and body weight of mice with a neural crest-specific deletion of BMP7 (BMP7-KO), model of Pierre Robin sequence, and their male control counterparts (BMP7-WT mice) at surgery.

SLEEP

Table 14 and Figure 25 summarize the data about the time spent in each wake-sleep state in BMP7-KO and BMP7-WT mice.

Table 14

Experimental Group	W (%)	NREM sleep (%)	REM sleep (%)
BMP7-KO (n=3)	35.5 ± 1.7	59.4 ± 1.9	4.5 ± 0.7
BMP7-WT (n=3)	40.3 ± 2.6	55.0 ± 1.8	4.4 ± 0.9

Table 14. Time spent in each wake-sleep state for the Pierre Robin sequence mouse model.

The table shows the percentage of time spent in wakefulness (W), non-rapid-eye-movements (NREM) sleep or rapid-eye-movements (REM) sleep of mice with a neural crest-specific deletion of BMP7 (BMP7-KO), model of Pierre Robin sequence, and their controls (BMP7-WT mice) during an 8-hour recording session inside the whole-body plethysmography chamber.

Figure 25

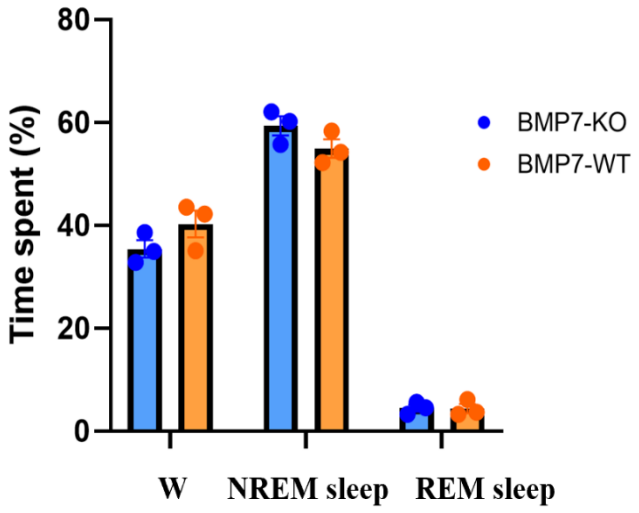

Figure 25. Time spent in each behavioral states in the Pierre Robin sequence mouse model.

The graph illustrates the percentage of time spent in wakefulness (W), non-rapid-eye-movements (NREM) sleep or rapid-eye-movements (REM) sleep of mice with a neural crest-specific deletion of BMP7 (BMP7-KO, n=3), model of Pierre Robin sequence, and their controls (BMP7-WT mice, n=3) during an 8-hour recording session inside the whole-body plethysmography chamber.

RESPIRATION DURING SLEEP

Table 15 and Figure 26 offer a concise presentation of data concerning the principal respiratory parameters (T_{TOT}, V_T, V_E, fR, Ti, and Te) in the two experimental groups.

Table 15

	NREM sleep		**REM sleep**	
	BMP7-KO (n=3)	**BMP7-WT** (n=3)	**BMP7-KO** (n=3)	**BMP7-WT** (n=3)
T_{TOT} (ms)	306 ± 23	361 ± 30	282 ± 27	292 ± 19
V_T (µl)	195 ± 12	226 ± 18	151 ± 11	156 ± 6
V_T (µl/g)	12.8 ± 1.1	13.3 ± 0.9	10.0 ± 1.2	9.2 ± 0.6
V_E (ml/min)	39.7 ± 2.9	38.7 ± 3.3	34.0 ± 3.0	33.4 ± 1.3
V_E (ml/min/g)	2.6 ± 0.1	2.3 ± 0.1	2.2 ± 0.2	2.0 ± 0.1
fR (breaths/min)	204 ± 14	174 ± 13	230 ± 22	220 ± 17
Ti (ms)	112 ± 9	128 ± 11	119 ± 12	122 ± 7
Te (ms)	194 ± 14	233 ± 19	163 ± 15	170 ± 11

Table 15. **Respiratory parameters for the Pierre Robin sequence mouse model.**
The table summarizes the principal respiratory parameters recorded during non-rapid-eye-movements (NREM) sleep or rapid-eye-movements (REM) sleep in mice with a neural crest-specific deletion of BMP7 (BMP7-KO), model of Pierre Robin sequence, and their controls (BMP7-WT mice) during an 8-hour recording session inside the whole-body plethysmography chamber. Specifically, this chart displays the values of ventilatory period (T_{TOT}, expressed in milliseconds), tidal volume (V_T, expressed in microliters or in microliters per gram of body weight), minute ventilation (V_E, expressed in milliliters per minute or in milliliters per minute per gram of body weight), breathing frequency (fR, expressed in breaths per minute), and inspiratory and expiratory times (Ti and Te, respectively, expressed in milliseconds).

Data are expressed as mean ± SEM and *n* represents the number of mice employed for each different experimental group.

Figure 26

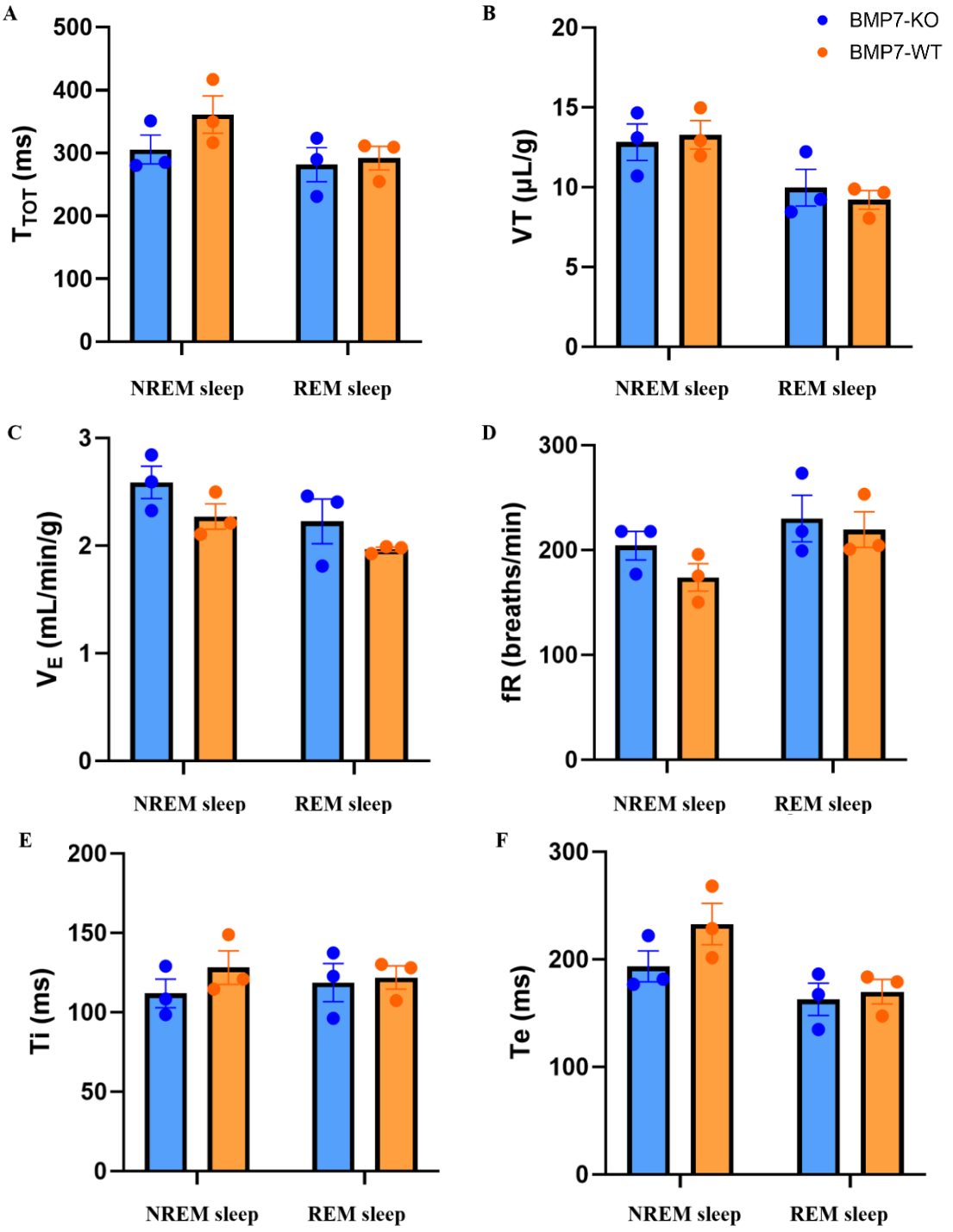

Figure 26. **Respiratory parameters for the Pierre Robin sequence mouse model.**

Graphs resumes the principal respiratory parameters recorded during non-rapid-eye-movements (NREM) sleep or rapid-eye-movements (REM) sleep in mice with a neural crest-specific deletion of BMP7 (BMP7-KO), model of Pierre Robin sequence, and their controls (BMP7-WT mice) during an 8-hour recording session inside the whole-body plethysmography chamber. Specifically, this figure compares the ventilatory period (T_{TOT}, expressed in milliseconds, panel A), the tidal volume (V_T, expressed in microliters per gram of body weight, panel B), the minute ventilation (V_E, expressed in milliliters per minute per gram of body weight, panel C), the breathing frequency (fR, expressed in breaths per minute, panel D), the inspiratory time (Ti, expressed in milliseconds, panel E), and the expiratory time (Te, expressed in milliseconds, panel F) between the two experimental groups.

SLEEP APNEAS

Table 16 and Figure 27 summarize data concerning the occurrence rate of both sigh and apneas (divided in both post-sigh and spontaneous apneas, and CSA and OSA) in the two experimental groups.

Table 16

	NREM sleep		**REM sleep**	
	BMP7-KO (n=3)	**BMP7-WT** (n=3)	**BMP7-KO** (n=3)	**BMP7-WT** (n=3)
Sighs (events/h)	17.0 ± 2.3	20.1 ± 3.1	0	0
Apneas (events/h)	13.3 ± 8.8	5.9 ± 3.4	12.1 ± 5.0	5.6 ± 3.8
Apnea duration (ms)	1337 ± 104	1335 ± 179	942 ± 83	1241 ± 226
Post-sigh apneas (events/h)	11.2 ± 7.5	5.7 ± 3.2	0	0
Spontaneous apneas (events/h)	2.2 ± 1.3	0.2 ± 0.2	12.2 ± 4.9	5.6 ± 3.8
CSA (events/h)	11.9 ± 8.5	5.4 ± 3.0	3.8 ± 2.6	0
OSA (events/h)	0.5 ± 0.5	0.4 ± 0.4	8.4 ± 4.6	5.6 ± 3.8

Table 16. **Sighs and apneas in the Pierre Robin sequence mouse model.**

The table summarizes the duration of apneas (expressed in milliseconds) and the occurrence rate (expressed as events per hour of sleep) of both sigh and apneas recorded during non-rapid-eye-movements (NREM) sleep or rapid-eye-movements (REM) sleep in mice with a neural crest-specific deletion of BMP7 (BMP7-KO), model of Pierre Robin sequence, and their controls (BMP7-WT mice) during an 8-hour recording session inside the whole-body plethysmography chamber.

Apneas were classified both as post-sigh or spontaneous according to the distance from a preceding sigh and as central (CSA) or obstructive (OSA) according to the presence or not of diaphragmatic effort in correspondence of a breathing pause.

Data are expressed as mean ± SEM and *n* represents the number of mice employed for each different experimental group.

Figure 27

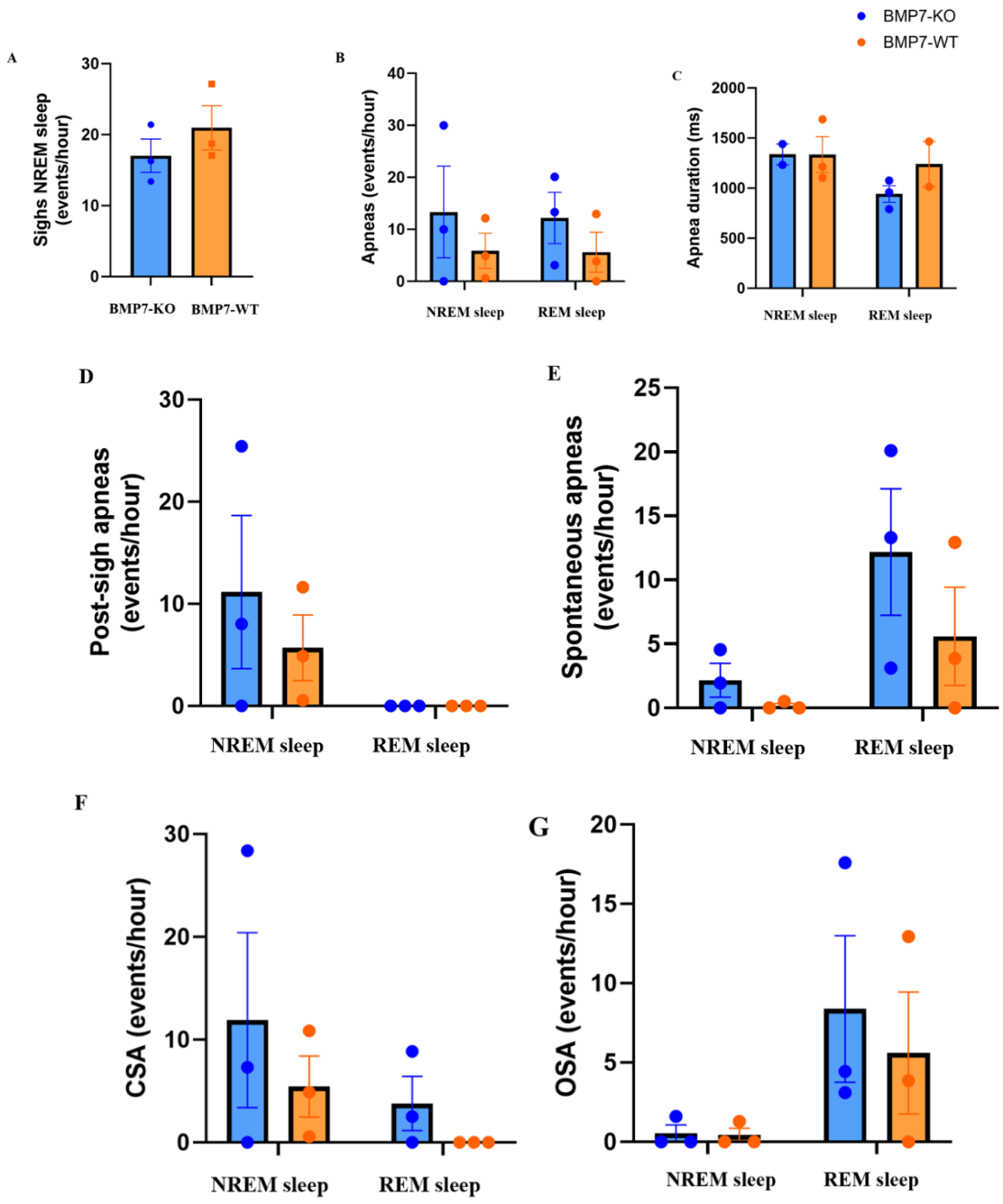

Figure 27. Sighs and apneas in the Pierre Robin sequence mouse model.

Graphs summarizes the principal respiratory parameters recorded during non-rapid-eye-movements (NREM) sleep or rapid-eye-movements (REM) sleep in mice with a neural crest-specific deletion of BMP7 (BMP7-KO), model of Pierre Robin sequence, and their controls (BMP7-WT mice) during an 8-hour recording session inside the whole-body plethysmography chamber. Specifically, this figure shows the comparison of the occurrence rate of sighs during NREM sleep (expressed in events per hour of NREM sleep, panel A), the frequency of apneas (expressed in events per hour, panel B), the duration of apneic events (expressed in milliseconds, panel C), and the occurrence rate (expressed in events per hour) of post-sigh (panel D), spontaneous (panel E), central (CSA, panel F), and obstructive sleep apneas (OSA, panel G).

13. DISCUSSION

Experiments described in this section were carried out at the University of Alberta (Edmonton, Alberta, Canada). The aim of this study was to evaluate whether the genetic mouse models of PRS (BMP7-KO mice) exhibit a predisposition to airway obstruction as human patients.

Our preliminary data suggest that, despite considerable variability among the subjects, BMP7-KO mice appear to show a higher incidence of apneic events during both NREM and REM sleep compared to BMP7-WT mice (Figure 27B). Furthermore, by categorizing these apneas based on their proximity to a sigh, we discovered that BMP7-KO mice exhibited an elevated frequency of post-sigh apneas during NREM sleep (as sighs are absent in REM sleep, as expected)[497] (Figure 27D). Additionally, a heightened occurrence of spontaneous apneas is also present in BMP7-KO mice during both NREM and REM sleep when compared to BMP7-WT mice (Figure 27E). It is noteworthy that this latter observation aligns with the findings of a recent study on BMP7-KO mice[484], where researchers noted an increased occurrence of spontaneous sleep apneas over a 150-minute recording period, albeit without considering sleep patterns.

In the aforementioned study[484], the authors also identified certain modifications in the respiratory patterns of BMP7-KO mice, which encompassed a reduced fR, elongated T_{TOT} and Ti, a tendency for a prolonged Te, and the presence of irregular breath patterns following sighs. Regrettably, in our preliminary study, we were unable to detect these alterations due to the limited number of mice and the documented substantial variability in their respiratory patterns. Indeed, these authors noted that despite all the mice in their study having midfacial hypoplasia, a shorter cranial base, and nasal septum deviation, an augmented frequency of spontaneous apneas was observed only in a subgroup of the studied BMP7-KO mice.

Furthermore, given that these respiratory characteristics, along with the observed craniofacial abnormalities, are commonly associated with the development and onset of OSAs in pediatric patients[303], it is reasonable to infer that these findings are indicative of nasal airway obstructions, even in the context of mice. Consequently, we classified the apneic events that occurred during sleep into CSA or OSA, depending on the presence or absence of diaphragm contraction, respectively. We noted that almost all apneic events occurring during NREM sleep were of central origin in both BMP7-KO and BMP7-WT mice, whereas we observed occurrences of both CSA and OSA during REM sleep. Notably, despite a great inter-subject variability, BMP7-KO mice appeared to exhibit an increased occurrence rate of CSA during NREM sleep, as well as an augmented frequency of both

CSA (absent in BMP7-WT mice) and OSA during REM sleep in comparison to BMP7-WT mice.

This experimental protocol acknowledges some limitations. Since it serves as an initial study, we employed a limited number of animals of the same sex (3 male BMP7-KO and 3 male BMP7-WT mice). Furthermore, as elucidated more comprehensively in the "10. Discussion" section, as for the experiments conducted at the University of Bologna (Italy) in the mouse model of DS and CDD, there are other notable constraints. These encompass the technical difficulties related to DIA electrode implantation, the lack of oximeters for gauging the extent of arterial blood desaturation, and the inability to assess muscle weakness. Additionally, in this particular strain of mice, characterized by cranial bones that are extremely delicate and thinner than those of wild-type mice, even the implantation of EEG and EMG electrodes and the long-term stability of the structure integrating them onto the skull prove to be intricate and demanding. However, given the short duration of the experimental protocol (5-7 days from the surgery to the recording sessions), we successfully obtained high-quality signals for sleep stage discrimination and apnea categorization.

In conclusion, while further experiments are necessary to definitively establish the existence of respiratory disruptions, particularly those of an obstructive nature., the present investigation serves as a cornerstone for forthcoming research. Indeed, future studies, encompassing a larger sample size and involving mice of both sexes, will be crucial in evaluating the potential presence of sleep and breathing impairments in BMP7-KO mice.

CONCLUSIONS

Sleep apnea represents a research topic of great interest due to its widespread occurrence and significant health implications. Indeed, the understanding of its pathogenesis and developing possible therapies are primary objectives of biomedical research and having reliable mouse models at our disposal would greatly facilitate the achievement of these goals.

This study effectively illustrates that mice are valuable models for the investigation of SBDs. Indeed, by the simultaneous detection of sleep states and diaphragm activity, we found that mice, like humans, exhibited OSAs and varying degrees of airway obstruction. Notably, we demonstrated, for the first time, a higher prevalence of sleep apneas with an obstructive component in both TS and CDKL5-KO mice, which respectively recapitulate the core aspects of human DS and CDD. Therefore, we suggest that these mouse models serve as reliable candidates as models of REM sleep-related OSA. However, although BMP7-KO mice, a model of PRS, seem to exhibit a similar pattern to other examined murine models, further in-depth investigations are necessary to solidify this understanding.

In conclusion, the successful identification of these two novel animal models (TS and CDKL5-KO mice) holds the potential to pave the way for deepening our knowledge of the mechanisms, pathophysiology, genetics, and cardiovascular consequences of OSAs. For instance, forthcoming research will aim to investigate the alterations induced by these conditions in terms of the composition of cell populations, gene expression, protein synthesis, transcriptomics, and connectivity within the brain areas responsible for breathing regulation during sleep. Moreover, future studies may develop a reliable system for measuring blood saturation levels in mice to explore the possible changes in blood oxygen concentration during apneas and subsequently elucidate the impact of OSA-related cardiovascular impairments in DS and CDD patients. Finally, these two mouse models present exceptional utility in expediting the development of targeted therapeutic interventions. This may include innovative techniques, such as the chemogenetic and optogenetic stimulation of brain nuclei involved in the control of upper airway patency and tongue movements, all within the perspective of clinical applications.

LIST OF ABBREVIATIONS

BMP7-KO or $BMP7^{fl/fl}$:Wnt1-Cre	Mice with a neural crest-specific deletion of BMP7
A, B, and C	Constants depending on the nature of the substance (formula)
BF	Basal forebrain
BMP	Bone morphogenetic protein
BMP7-WT or $BMP7^{fl/fl}$	Mice carrying loxP sites flanking the first coding exon of the BMP7 gene
CDD	CDKL5 deficiency disorder
CDKL5	Cyclin-dependent kinase-like 5
CDKL5-KO	CDKL5-knockout
CDKL5-WT	Wild-type mice
CO_2	Carbon dioxide
CPAP	Continuous positive airway pressure
CPG	Central pattern generator
CSA	Central sleep apnea
CSF	Cerebrospinal fluid
cVRG	Caudal ventral respiratory group
DIA	Diaphragm electromyogram
DPGi	Dorsal paragigantocellular reticular nucleus
DR	Dorsal raphe
DS	Down Syndrome
ECG	Electrocardiography
EEG	Electroencephalography

EMG	Electromyogram / nuchal electromyogram
EOG	Electrooculogram
EU	Euploid mouse
FCR	Functional residual capacity
fR	Breathing frequency
GABA	Gamma-aminobutyric acid
h	Relative humidity of the system (formula)
HCVR	Hypercapnic ventilatory response
HOVR	Hypoxic ventilatory response
HP	Heart period
HR	Heart rate
Hsa21	Chromosome 21
ICSD-3	Third Edition of the International Classification of Sleep Disorders
ISF	Interstitial fluid
KFn	Kölliker-Fuse nucleus
LC	Locus coeruleus
LH	Lateral hypothalamus
LPGi	Lateral paragigantocellular nucleus
MCH	Melanin-concentrating hormone
MnPO	Median preoptic nucleus
MR	Median raphe
nNOS	Nitric oxide synthase
NREM (sleep)	Non-rapid-eye-movements (sleep)
NTS	Nucleus tractus solitarii

OSA	Obstructive sleep apnea
P	Water vapor pressure associated with a specific temperature (formula)
P_A	Water vapor pressure associated with the animal's temperature (formula)
$PaCO_2$	Arterial carbon dioxide
PaO_2	Arterial concentration of oxygen
PB	Parabrachial nucleus
P_B	Barometric pressure (formula)
P_{Ch}	Water vapor pressure associated with the animal chamber (formula)
PCR	Polymerase chain reaction
pFL (or PF)	Parafacial respiratory group
PH	Posterior hypothalamus
PiCo	Post-inspiratory Complex
P_K	Pressure deflection associated with the calibration volume (formula)
POA	Preoptic area
PPT/LDT	Pedunculopontine and laterodorsal tegmental nuclei
preBötC	PreBötzinger Complex
PRS	Pierre Robin sequence
P_T	Pressure deflection associated with the breath of interest (formula)
PZ	Parafacial zone
REM (sleep)	Rapid-eye-movements (sleep)
RTN	Retrotrapezoid nucleus
rVRG	Rostral ventral respiratory group
SBD	Sleep-related breathing disorder

SCN	Suprachiasmatic nucleus
SEM	Standard Error of the Mean
SLD	Sublaterodorsal nucleus
sub-OSA	Sub-obstructive sleep apnea
SWA	Slow-wave activity
T	Temperature of interest (formula)
T_A	Temperature associated with the animal's body (formula)
T_{Ch}	Temperature associated with the chamber (formula)
Te	Expiratory time
TGF-β	Transforming growth factor-β
Ti	Inspiratory time
TMN	Tuberomammillary nucleus
TS	Ts65Dn mouse
T_{TOT}	Ventilatory period or total breath duration
V_E	Minute ventilation
VENT	Ventilatory signal
VII	Facial nerve
V_K	Volume of air injected during the calibration of the system (formula)
vlPAG/LPT	Ventrolateral periaqueductal gray matter and the lateral pontine tegmentum
VLPO	Ventrolateral preoptic area
VMM	Ventromedial medulla
VRG	Ventral respiratory group
V_T	Tidal volume
VTA	Ventral tegmental area

W	Wakefulness
WBP	Whole-body plethysmography
ΔHP	Difference in heart period

BIBLIOGRAPHY

1. Hirshkowitz, M. Normal human sleep: an overview. *Med Clin North Am* **88**, 551–565, vii (2004).
2. Frank, M. G. & Heller, H. C. The Function(s) of Sleep. *Handb Exp Pharmacol* **253**, 3–34 (2019).
3. Campbell, S. S. & Tobler, I. Animal sleep: a review of sleep duration across phylogeny. *Neurosci Biobehav Rev* **8**, 269–300 (1984).
4. Mohanty, N. P., Wagener, C., Herrel, A. & Thaker, M. The ecology of sleep in non-avian reptiles. *Biol Rev Camb Philos Soc* **97**, 505–526 (2022).
5. Miyazaki, S., Liu, C.-Y. & Hayashi, Y. Sleep in vertebrate and invertebrate animals, and insights into the function and evolution of sleep. *Neurosci Res* **118**, 3–12 (2017).
6. Hendricks, J. C., Sehgal, A. & Pack, A. I. The need for a simple animal model to understand sleep. *Prog Neurobiol* **61**, 339–351 (2000).
7. Hor, H. & Tafti, M. Physiology. How much sleep do we need? *Science* **325**, 825–826 (2009).
8. Medic, G., Wille, M. & Hemels, M. E. Short- and long-term health consequences of sleep disruption. *Nat Sci Sleep* **9**, 151–161 (2017).
9. Chattu, V. K. *et al.* The Global Problem of Insufficient Sleep and Its Serious Public Health Implications. *Healthcare* **7**, 1 (2019).
10. Andersen, M. L. *et al.* Distinct effects of acute and chronic sleep loss on DNA damage in rats. *Prog Neuropsychopharmacol Biol Psychiatry* **33**, 562–567 (2009).
11. Banks, S. & Dinges, D. F. Behavioral and Physiological Consequences of Sleep Restriction. *J Clin Sleep Med* **3**, 519–528 (2007).
12. Killgore, W. D. S. Effects of sleep deprivation on cognition. *Prog Brain Res* **185**, 105–129 (2010).
13. Killick, R., Banks, S. & Liu, P. Y. Implications of Sleep Restriction and Recovery on Metabolic Outcomes. *J Clin Endocrinol Metab* **97**, 3876–3890 (2012).

14. Kayser, M. S., Yue, Z. & Sehgal, A. A critical period of sleep for development of courtship circuitry and behavior in Drosophila. *Science* **344**, 269–274 (2014).

15. Markwald, R. R. *et al.* Impact of insufficient sleep on total daily energy expenditure, food intake, and weight gain. *Proc Natl Acad Sci U S A* **110**, 5695–5700 (2013).

16. Savage, V. M. & West, G. B. A quantitative, theoretical framework for understanding mammalian sleep. *Proc Natl Acad Sci U S A* **104**, 1051–1056 (2007).

17. Born, J. & Wilhelm, I. System consolidation of memory during sleep. *Psychol Res* **76**, 192–203 (2012).

18. Havekes, R. & Abel, T. The tired hippocampus: The molecular impact of sleep deprivation on hippocampal function. *Curr Opin Neurobiol* **44**, 13–19 (2017).

19. Tononi, G. & Cirelli, C. Sleep and the Price of Plasticity: From Synaptic and Cellular Homeostasis to Memory Consolidation and Integration. *Neuron* **81**, 12–34 (2014).

20. Tononi, G. & Cirelli, C. Sleep function and synaptic homeostasis. *Sleep Med Rev* **10**, 49–62 (2006).

21. Benington, J. H. & Craig Heller, H. Restoration of brain energy metabolism as the function of sleep. *Progress in Neurobiology* **45**, 347–360 (1995).

22. Petit, J.-M., Burlet-Godinot, S., Magistretti, P. J. & Allaman, I. Glycogen metabolism and the homeostatic regulation of sleep. *Metab Brain Dis* **30**, 263–279 (2015).

23. Borbély, A. A. & Achermann, P. Concepts and models of sleep regulation: an overview. *J Sleep Res* **1**, 63–79 (1992).

24. Mackiewicz, M. *et al.* Macromolecule biosynthesis: a key function of sleep. *Physiol Genomics* **31**, 441–457 (2007).

25. Vazquez, J., Hall, S. C., Witkowska, H. E. & Greco, M. A. Rapid alterations in cortical protein profiles underlie spontaneous sleep and wake bouts. *J Cell Biochem* **105**, 1472–1484 (2008).

26. Ramm, P. & Smith, C. T. Rates of cerebral protein synthesis are linked to slow wave sleep in the rat. *Physiol Behav* **48**, 749–753 (1990).

27. Nakanishi, H. *et al.* Positive correlations between cerebral protein synthesis rates and deep sleep in Macaca mulatta. *Eur J Neurosci* **9**, 271–279 (1997).

28. Giuditta, A., Rutigliano, B. & Vitale-Neugebauer, A. Influence of synchronized sleep on the biosynthesis of RNA in neuronal and mixed fractions isolated from rabbit cerebral cortex. *J Neurochem* **35**, 1267–1272 (1980).

29. Giuditta, A., Rutigliano, B. & Vitale-Neugebauer, A. Influence of synchronized sleep on the biosynthesis of RNA in two nuclear classes isolated from rabbit cerebral cortex. *J Neurochem* **35**, 1259–1266 (1980).

30. Taishi, P. *et al.* Conditions that affect sleep alter the expression of molecules associated with synaptic plasticity. *Am J Physiol Regul Integr Comp Physiol* **281**, R839-845 (2001).

31. Seibt, J. *et al.* Protein synthesis during sleep consolidates cortical plasticity in vivo. *Curr Biol* **22**, 676–682 (2012).

32. Vecsey, C. G. *et al.* Genomic analysis of sleep deprivation reveals translational regulation in the hippocampus. *Physiol Genomics* **44**, 981–991 (2012).

33. Tudor, J. C. *et al.* Sleep deprivation impairs memory by attenuating mTORC1-dependent protein synthesis. *Sci Signal* **9**, ra41 (2016).

34. Cirelli, C., Gutierrez, C. M. & Tononi, G. Extensive and divergent effects of sleep and wakefulness on brain gene expression. *Neuron* **41**, 35–43 (2004).

35. Basheer, R., Brown, R., Ramesh, V., Begum, S. & McCarley, R. W. Sleep deprivation-induced protein changes in basal forebrain: implications for synaptic plasticity. *J Neurosci Res* **82**, 650–658 (2005).

36. Xie, L. *et al.* Sleep drives metabolite clearance from the adult brain. *Science* **342**, 373–377 (2013).

37. Iliff, J. J. *et al.* A paravascular pathway facilitates CSF flow through the brain parenchyma and the clearance of interstitial solutes, including amyloid β. *Sci Transl Med* **4**, 147ra111 (2012).

38. Iliff, J. J. *et al.* Cerebral arterial pulsation drives paravascular CSF-interstitial fluid exchange in the murine brain. *J Neurosci* **33**, 18190–18199 (2013).

39. Eide, P. K. & Ringstad, G. MRI with intrathecal MRI gadolinium contrast medium administration: a possible method to assess glymphatic function in human brain. *Acta Radiol Open* **4**, 2058460115609635 (2015).

40. Kiviniemi, V. *et al.* Ultra-fast magnetic resonance encephalography of physiological brain activity - Glymphatic pulsation mechanisms? *J Cereb Blood Flow Metab* **36**, 1033–1045 (2016).

41. Lundgaard, I. *et al.* Glymphatic clearance controls state-dependent changes in brain lactate concentration. *J Cereb Blood Flow Metab* **37**, 2112–2124 (2017).

42. Aukland, K. & Reed, R. K. Interstitial-lymphatic mechanisms in the control of extracellular fluid volume. *Physiol Rev* **73**, 1–78 (1993).

43. Aspelund, A. *et al.* A dural lymphatic vascular system that drains brain interstitial fluid and macromolecules. *J Exp Med* **212**, 991–999 (2015).

44. Funato, H. *et al.* Forward-genetics analysis of sleep in randomly mutagenized mice. *Nature* **539**, 378–383 (2016).

45. Haas, L. F. Hans Berger (1873-1941), Richard Caton (1842-1926), and electroencephalography. *J Neurol Neurosurg Psychiatry* **74**, 9 (2003).

46. Loomis, A. L., Harvey, E. N. & Hobart, G. A. Cerebral states during sleep, as studied by human brain potentials. *Journal of Experimental Psychology* **21**, 127–144 (1937).

47. Aserinsky, E. & Kleitman, N. Regularly occurring periods of eye motility, and concomitant phenomena, during sleep. *Science* **118**, 273–274 (1953).

48. Jouvet, M., Michel, F. & Courjon, J. Sur un stade d'activité électrique cérébrale rapide au cours du sommeil physiologique. *C R Soc Biol (Paris)* (1959).

49. Hirshkowitz, M. Polysomnography Challenges. *Sleep Medicine Clinics* **11**, 403–411 (2016).

50. Kushida, C. A. *et al.* Practice parameters for the indications for polysomnography and related procedures: An update for 2005. *Sleep* **28**, 499–521 (2005).

51. Billiard, M. Normal sleep. in *Sleep Medicine* (eds. Högl, B., Comella, C. L. & Smith, H. R.) 9–24 (Cambridge University Press, 2008). doi:10.1017/CBO9780511545085.003.

52. Rechtschaffen, A. & Kales, A. *A Manual of Standardized Terminology, Techniques and Scoring System for Sleep Stages of Human Subjects*. (Brain Information Service/Brain Research Institute, University of California, 1968).

53. Iber, C., Ancoli-Israel, S., Chesson, A. L. & Quan, S. F. *The AASM manual for the scoring of sleep and associated events: rules, terminology and technical specifications*. vol. 1 (American academy of sleep medicine Westchester, IL, 2007).

54. Alvente, S., Matteoli, G., Miglioranza, E., Zoccoli, G. & Bastianini, S. How to study sleep apneas in mouse models of human pathology. *J Neurosci Methods* **395**, 109923 (2023).

55. Paterson, L. M., Nutt, D. J. & Wilson, S. J. Sleep and its disorders in translational medicine. *J Psychopharmacol* **25**, 1226–1234 (2011).

56. Saper, C. B., Fuller, P. M., Pedersen, N. P., Lu, J. & Scammell, T. E. Sleep state switching. *Neuron* **68**, 1023–1042 (2010).

57. Bastianini, S. *et al.* SCOPRISM: a new algorithm for automatic sleep scoring in mice. *J Neurosci Methods* **235**, 277–284 (2014).

58. Scammell, T. E., Arrigoni, E. & Lipton, J. O. Neural Circuitry of Wakefulness and Sleep. *Neuron* **93**, 747–765 (2017).

59. Toth, L. A. & Bhargava, P. Animal models of sleep disorders. *Comp Med* **63**, 91–104 (2013).

60. Mitler, M. M., Lund, R., Sokolove, P. G., Pittendrigh, C. S. & Dement, W. C. Sleep and activity rhythms in mice: a description of circadian patterns and unexpected disruptions in sleep. *Brain Res* **131**, 129–145 (1977).

61. Baekey, D. M., Feng, P., Decker, M. J. & Strohl, K. P. Breathing and Sleep: Measurement Methods, Genetic Influences, and Developmental Impacts. *ILAR Journal* **50**, 248–261 (2009).

62. Wright, K. P., Badia, P. & Wauquier, A. Topographical and temporal patterns of brain activity during the transition from wakefulness to sleep. *Sleep* **18**, 880–889 (1995).

63. Takahashi, K., Kayama, Y., Lin, J. S. & Sakai, K. Locus coeruleus neuronal activity during the sleep-waking cycle in mice. *Neuroscience* **169**, 1115–1126 (2010).

64. Fisher, S. P., Foster, R. G. & Peirson, S. N. The circadian control of sleep. *Handb Exp Pharmacol* 157–183 (2013) doi:10.1007/978-3-642-25950-0_7.

65. Borbély, A. A., Daan, S., Wirz-Justice, A. & Deboer, T. The two-process model of sleep regulation: a reappraisal. *J Sleep Res* **25**, 131–143 (2016).

66. Borbély, A. A., Baumann, F., Brandeis, D., Strauch, I. & Lehmann, D. Sleep deprivation: effect on sleep stages and EEG power density in man. *Electroencephalogr Clin Neurophysiol* **51**, 483–495 (1981).

67. Lancel, M., van Riezen, H. & Glatt, A. Effects of circadian phase and duration of sleep deprivation on sleep and EEG power spectra in the cat. *Brain Res* **548**, 206–214 (1991).

68. Borbély, A. A. & Achermann, P. Sleep homeostasis and models of sleep regulation. *J Biol Rhythms* **14**, 557–568 (1999).

69. Weaver, D. R. The suprachiasmatic nucleus: a 25-year retrospective. *J Biol Rhythms* **13**, 100–112 (1998).

70. Morin, L. P. Neuroanatomy of the extended circadian rhythm system. *Exp Neurol* **243**, 4–20 (2013).

71. Luppi, P. H., Aston-Jones, G., Akaoka, H., Chouvet, G. & Jouvet, M. Afferent projections to the rat locus coeruleus demonstrated by retrograde and anterograde tracing with cholera-toxin B subunit and Phaseolus vulgaris leucoagglutinin. *Neuroscience* **65**, 119–160 (1995).

72. Schwarz, L. A. *et al.* Viral-genetic tracing of the input-output organization of a central noradrenaline circuit. *Nature* **524**, 88–92 (2015).

73. Aston-Jones, G. & Cohen, J. D. An integrative theory of locus coeruleus-norepinephrine function: adaptive gain and optimal performance. *Annu Rev Neurosci* **28**, 403–450 (2005).

74. Weissbourd, B. *et al.* Presynaptic partners of dorsal raphe serotonergic and GABAergic neurons. *Neuron* **83**, 645–662 (2014).

75. Eban-Rothschild, A., Rothschild, G., Giardino, W. J., Jones, J. R. & de Lecea, L. VTA dopaminergic neurons regulate ethologically relevant sleep-wake behaviors. *Nat Neurosci* **19**, 1356–1366 (2016).

76. Ferris, M. J. *et al.* Dopamine transporters govern diurnal variation in extracellular dopamine tone. *Proc Natl Acad Sci U S A* **111**, E2751-2759 (2014).

77. Yu, X. *et al.* Wakefulness Is Governed by GABA and Histamine Cotransmission. *Neuron* **87**, 164–178 (2015).

78. Anaclet, C. *et al.* Basal forebrain control of wakefulness and cortical rhythms. *Nat Commun* **6**, 8744 (2015).

79. Xu, M. *et al.* Basal forebrain circuit for sleep-wake control. *Nat Neurosci* **18**, 1641–1647 (2015).

80. Zant, J. C. *et al.* Cholinergic Neurons in the Basal Forebrain Promote Wakefulness by Actions on Neighboring Non-Cholinergic Neurons: An Opto-Dialysis Study. *J Neurosci* **36**, 2057–2067 (2016).

81. Boucetta, S., Cissé, Y., Mainville, L., Morales, M. & Jones, B. E. Discharge profiles across the sleep-waking cycle of identified cholinergic, GABAergic, and glutamatergic neurons in the pontomesencephalic tegmentum of the rat. *J Neurosci* **34**, 4708–4727 (2014).

82. Kaur, S. *et al.* Glutamatergic signaling from the parabrachial nucleus plays a critical role in hypercapnic arousal. *J Neurosci* **33**, 7627–7640 (2013).

83. Mochizuki, T. *et al.* Orexin receptor 2 expression in the posterior hypothalamus rescues sleepiness in narcoleptic mice. *Proc Natl Acad Sci U S A* **108**, 4471–4476 (2011).

84. Hasegawa, E., Yanagisawa, M., Sakurai, T. & Mieda, M. Orexin neurons suppress narcolepsy via 2 distinct efferent pathways. *J Clin Invest* **124**, 604–616 (2014).

85. de Lecea, L. *et al.* The hypocretins: hypothalamus-specific peptides with neuroexcitatory activity. *Proc Natl Acad Sci U S A* **95**, 322–327 (1998).

86. Sakurai, T. *et al.* Orexins and orexin receptors: a family of hypothalamic neuropeptides and G protein-coupled receptors that regulate feeding behavior. *Cell* **92**, 573–585 (1998).

87. Peyron, C. *et al.* Neurons containing hypocretin (orexin) project to multiple neuronal systems. *J Neurosci* **18**, 9996–10015 (1998).

88. Nambu, T. *et al.* Distribution of orexin neurons in the adult rat brain. *Brain Res* **827**, 243–260 (1999).

89. Schöne, C., Apergis-Schoute, J., Sakurai, T., Adamantidis, A. & Burdakov, D. Coreleased orexin and glutamate evoke nonredundant spike outputs and computations in histamine neurons. *Cell Rep* **7**, 697–704 (2014).

90. Yamanaka, A. *et al.* Hypothalamic orexin neurons regulate arousal according to energy balance in mice. *Neuron* **38**, 701–713 (2003).

91. Mahler, S. V., Moorman, D. E., Smith, R. J., James, M. H. & Aston-Jones, G. Motivational activation: a unifying hypothesis of orexin/hypocretin function. *Nat Neurosci* **17**, 1298–1303 (2014).

92. Bonnavion, P., Jackson, A. C., Carter, M. E. & de Lecea, L. Antagonistic interplay between hypocretin and leptin in the lateral hypothalamus regulates stress responses. *Nat Commun* **6**, 6266 (2015).

93. Lu, J., Jhou, T. C. & Saper, C. B. Identification of wake-active dopaminergic neurons in the ventral periaqueductal gray matter. *J Neurosci* **26**, 193–202 (2006).

94. Wang, H.-L. & Morales, M. Pedunculopontine and laterodorsal tegmental nuclei contain distinct populations of cholinergic, glutamatergic and GABAergic neurons in the rat. *Eur J Neurosci* **29**, 340–358 (2009).

95. Herrera, C. G. *et al.* Hypothalamic feedforward inhibition of thalamocortical network controls arousal and consciousness. *Nat Neurosci* **19**, 290–298 (2016).

96. Venner, A., Anaclet, C., Broadhurst, R. Y., Saper, C. B. & Fuller, P. M. A Novel Population of Wake-Promoting GABAergic Neurons in the Ventral Lateral Hypothalamus. *Curr Biol* **26**, 2137–2143 (2016).

97. Krueger, J. M. *et al.* Involvement of cytokines in slow wave sleep. *Prog Brain Res* **193**, 39–47 (2011).

98. Halassa, M. M. *et al.* Astrocytic modulation of sleep homeostasis and cognitive consequences of sleep loss. *Neuron* **61**, 213–219 (2009).

99. Schmitt, L. I., Sims, R. E., Dale, N. & Haydon, P. G. Wakefulness affects synaptic and network activity by increasing extracellular astrocyte-derived adenosine. *J Neurosci* **32**, 4417–4425 (2012).

100. Porkka-Heiskanen, T. *et al.* Adenosine: a mediator of the sleep-inducing effects of prolonged wakefulness. *Science* **276**, 1265–1268 (1997).

101. Fredholm, B. B., Bättig, K., Holmén, J., Nehlig, A. & Zvartau, E. E. Actions of caffeine in the brain with special reference to factors that contribute to its widespread use. *Pharmacol Rev* **51**, 83–133 (1999).

102. v. Economo, C. Beitrag zur Cytoarchitektonik des Operculum Rolando. *Z. f. d. g. Neur. u. Psych.* **130**, 775–780 (1930).

103. McGinty, D. J. & Sterman, M. B. Sleep suppression after basal forebrain lesions in the cat. *Science* **160**, 1253–1255 (1968).

104. Szymusiak, R. & McGinty, D. Sleep-related neuronal discharge in the basal forebrain of cats. *Brain Res* **370**, 82–92 (1986).

105. Sherin, J. E., Shiromani, P. J., McCarley, R. W. & Saper, C. B. Activation of ventrolateral preoptic neurons during sleep. *Science* **271**, 216–219 (1996).

106. Alam, M. A., Kumar, S., McGinty, D., Alam, M. N. & Szymusiak, R. Neuronal activity in the preoptic hypothalamus during sleep deprivation and recovery sleep. *J Neurophysiol* **111**, 287–299 (2014).

107. Sherin, J. E., Elmquist, J. K., Torrealba, F. & Saper, C. B. Innervation of histaminergic tuberomammillary neurons by GABAergic and galaninergic neurons in the ventrolateral preoptic nucleus of the rat. *J Neurosci* **18**, 4705–4721 (1998).

108. Uschakov, A., Gong, H., McGinty, D. & Szymusiak, R. Efferent projections from the median preoptic nucleus to sleep- and arousal-regulatory nuclei in the rat brain. *Neuroscience* **150**, 104–120 (2007).

109. Saito, Y. C. *et al.* GABAergic neurons in the preoptic area send direct inhibitory projections to orexin neurons. *Front Neural Circuits* **7**, 192 (2013).

110. Hassani, O. K., Lee, M. G., Henny, P. & Jones, B. E. Discharge profiles of identified GABAergic in comparison to cholinergic and putative glutamatergic basal forebrain neurons across the sleep-wake cycle. *J Neurosci* **29**, 11828–11840 (2009).

111. Manns, I. D., Alonso, A. & Jones, B. E. Discharge properties of juxtacellularly labeled and immunohistochemically identified cholinergic basal forebrain neurons recorded in association with the electroencephalogram in anesthetized rats. *J Neurosci* **20**, 1505–1518 (2000).

112. Kim, T. *et al.* Cortically projecting basal forebrain parvalbumin neurons regulate cortical gamma band oscillations. *Proc Natl Acad Sci U S A* **112**, 3535–3540 (2015).

113. Batini, C., Moruzzi, G., Palestini, M., Rossi, G. F. & Zanchetti, A. Presistent patterns of wakefulness in the pretrigeminal midpontine preparation. *Science* **128**, 30–32 (1958).

114. Anaclet, C. *et al.* The GABAergic parafacial zone is a medullary slow wave sleep-promoting center. *Nat Neurosci* **17**, 1217–1224 (2014).

115. Gerashchenko, D. *et al.* Identification of a population of sleep-active cerebral cortex neurons. *Proc Natl Acad Sci U S A* **105**, 10227–10232 (2008).

116. Morairty, S. R. *et al.* A role for cortical nNOS/NK1 neurons in coupling homeostatic sleep drive to EEG slow wave activity. *Proc Natl Acad Sci U S A* **110**, 20272–20277 (2013).

117. Hobson, J. A., McCarley, R. W. & Wyzinski, P. W. Sleep cycle oscillation: reciprocal discharge by two brainstem neuronal groups. *Science* **189**, 55–58 (1975).

118. Van Dort, C. J. *et al.* Optogenetic activation of cholinergic neurons in the PPT or LDT induces REM sleep. *Proc Natl Acad Sci U S A* **112**, 584–589 (2015).

119. Boissard, R. *et al.* The rat ponto-medullary network responsible for paradoxical sleep onset and maintenance: a combined microinjection and functional neuroanatomical study. *Eur J Neurosci* **16**, 1959–1973 (2002).

120. Schenkel, E. & Siegel, J. M. REM sleep without atonia after lesions of the medial medulla. *Neurosci Lett* **98**, 159–165 (1989).

121. Holmes, C. J. & Jones, B. E. Importance of cholinergic, GABAergic, serotonergic and other neurons in the medial medullary reticular formation for sleep-wake states studied by cytotoxic lesions in the cat. *Neuroscience* **62**, 1179–1200 (1994).

122. Luppi, P.-H. *et al.* Brainstem mechanisms of paradoxical (REM) sleep generation. *Pflugers Arch* **463**, 43–52 (2012).

123. Lu, J., Sherman, D., Devor, M. & Saper, C. B. A putative flip-flop switch for control of REM sleep. *Nature* **441**, 589–594 (2006).

124. Crochet, S. & Sakai, K. Effects of microdialysis application of monoamines on the EEG and behavioural states in the cat mesopontine tegmentum. *Eur J Neurosci* **11**, 3738–3752 (1999).

125. Luebke, J. I. *et al.* Serotonin hyperpolarizes cholinergic low-threshold burst neurons in the rat laterodorsal tegmental nucleus in vitro. *Proc Natl Acad Sci U S A* **89**, 743–747 (1992).

126. Williams, J. A. & Reiner, P. B. Noradrenaline hyperpolarizes identified rat mesopontine cholinergic neurons in vitro. *J Neurosci* **13**, 3878–3883 (1993).

127. Sapin, E. *et al.* Localization of the brainstem GABAergic neurons controlling paradoxical (REM) sleep. *PLoS One* **4**, e4272 (2009).

128. Hayashi, Y. *et al.* Cells of a common developmental origin regulate REM/non-REM sleep and wakefulness in mice. *Science* **350**, 957–961 (2015).

129. Weber, F. *et al.* Control of REM sleep by ventral medulla GABAergic neurons. *Nature* **526**, 435–438 (2015).

130. Goutagny, R. *et al.* Role of the dorsal paragigantocellular reticular nucleus in paradoxical (rapid eye movement) sleep generation: a combined electrophysiological and anatomical study in the rat. *Neuroscience* **152**, 849–857 (2008).

131. Lu, J. *et al.* Selective activation of the extended ventrolateral preoptic nucleus during rapid eye movement sleep. *J Neurosci* **22**, 4568–4576 (2002).

132. Jego, S. *et al.* Optogenetic identification of a rapid eye movement sleep modulatory circuit in the hypothalamus. *Nat Neurosci* **16**, 1637–1643 (2013).

133. Tsunematsu, T. *et al.* Optogenetic manipulation of activity and temporally controlled cell-specific ablation reveal a role for MCH neurons in sleep/wake regulation. *J Neurosci* **34**, 6896–6909 (2014).

134. Vetrivelan, R. *et al.* Melanin-concentrating hormone neurons specifically promote rapid eye movement sleep in mice. *Neuroscience* **336**, 102–113 (2016).

135. Adamantidis, A. R., Zhang, F., Aravanis, A. M., Deisseroth, K. & de Lecea, L. Neural substrates of awakening probed with optogenetic control of hypocretin neurons. *Nature* **450**, 420–424 (2007).

136. Mieda, M. *et al.* Differential roles of orexin receptor-1 and -2 in the regulation of non-REM and REM sleep. *J Neurosci* **31**, 6518–6526 (2011).

137. Sasaki, K. *et al.* Pharmacogenetic modulation of orexin neurons alters sleep/wakefulness states in mice. *PLoS One* **6**, e20360 (2011).

138. Hassani, O. K., Lee, M. G. & Jones, B. E. Melanin-concentrating hormone neurons discharge in a reciprocal manner to orexin neurons across the sleep-wake cycle. *Proc Natl Acad Sci U S A* **106**, 2418–2422 (2009).

139. Welsh, D. K., Takahashi, J. S. & Kay, S. A. Suprachiasmatic nucleus: cell autonomy and network properties. *Annu Rev Physiol* **72**, 551–577 (2010).

140. Colwell, C. S. Linking neural activity and molecular oscillations in the SCN. *Nat Rev Neurosci* **12**, 553–569 (2011).

141. Buhr, E. D., Yoo, S.-H. & Takahashi, J. S. Temperature as a universal resetting cue for mammalian circadian oscillators. *Science* **330**, 379–385 (2010).

142. Buhr, E. D. & Takahashi, J. S. Molecular components of the Mammalian circadian clock. *Handb Exp Pharmacol* 3–27 (2013) doi:10.1007/978-3-642-25950-0_1.

143. Siepka, S. M., Yoo, S.-H., Park, J., Lee, C. & Takahashi, J. S. Genetics and neurobiology of circadian clocks in mammals. *Cold Spring Harb Symp Quant Biol* **72**, 251–259 (2007).

144. Dibner, C., Schibler, U. & Albrecht, U. The mammalian circadian timing system: organization and coordination of central and peripheral clocks. *Annu Rev Physiol* **72**, 517–549 (2010).

145. Takahashi, J. S. Transcriptional architecture of the mammalian circadian clock. *Nat Rev Genet* **18**, 164–179 (2017).

146. Deurveilher, S. & Semba, K. Indirect projections from the suprachiasmatic nucleus to major arousal-promoting cell groups in rat: implications for the circadian control of behavioural state. *Neuroscience* **130**, 165–183 (2005).

147. Del Negro, C. A., Funk, G. D. & Feldman, J. L. Breathing matters. *Nat Rev Neurosci* **19**, 351–367 (2018).

148. Patwa, A. & Shah, A. Anatomy and physiology of respiratory system relevant to anaesthesia. *Indian J Anaesth* **59**, 533–541 (2015).

149. Donner, M. W., Bosnia, J. F. & Robertson, D. L. Anatomy and physiology of the pharynx. *Gastrointest Radiol* **10**, 197–212 (1985).

150. Sowho, M., Amatoury, J., Kirkness, J. P. & Patil, S. P. Sleep and respiratory physiology in adults. *Clin Chest Med* **35**, 469–481 (2014).

151. Heinzer, R. C. & Sériès, F. Chapter 23 - Normal Physiology of the Upper and Lower Airways. in *Principles and Practice of Sleep Medicine (Fifth Edition)* (eds. Kryger, M. H., Roth, T. & Dement, W. C.) 259–268 (W.B. Saunders, 2011). doi:10.1016/B978-1-4160-6645-3.00023-2.

152. Krohn, F. *et al.* The integrated brain network that controls respiration. *Elife* **12**, e83654 (2023).

153. De Troyer, A. & Estenne, M. Coordination between rib cage muscles and diaphragm during quiet breathing in humans. *J Appl Physiol Respir Environ Exerc Physiol* **57**, 899–906 (1984).

154. De Troyer, A., Legrand, A., Gevenois, P. A. & Wilson, T. A. Mechanical advantage of the human parasternal intercostal and triangularis sterni muscles. *J Physiol* **513 (Pt 3)**, 915–925 (1998).

155. De Troyer, A., Kirkwood, P. A. & Wilson, T. A. Respiratory action of the intercostal muscles. *Physiol Rev* **85**, 717–756 (2005).

156. van Dishoeck, H. A. E. Elektrogramm der Nasenflügelmuskeln und Nasenwiderstandskurve. *Acta Oto-Laryngologica* **25**, 285–295 (1937).

157. Strohl, K. P. Respiratory activation of the facial nerve and alar muscles in anaesthetized dogs. *J Physiol* **363**, 351–362 (1985).

158. Vaiman, M., Eviatar, E. & Segal, S. Intranasal electromyography in evaluation of the nasal valve. *Rhinology* **41**, 134–141 (2003).

159. Fuller, D. D., Williams, J. S., Janssen, P. L. & Fregosi, R. F. Effect of co-activation of tongue protrudor and retractor muscles on tongue movements and pharyngeal airflow mechanics in the rat. *J Physiol* **519 Pt 2**, 601–613 (1999).

160. Gestreau, C., Dutschmann, M., Obled, S. & Bianchi, A. L. Activation of XII motoneurons and premotor neurons during various oropharyngeal behaviors. *Respir Physiol Neurobiol* **147**, 159–176 (2005).

161. Mong, F. S., Chen, Y. C. & Lu, C. H. Dendritic ramifications of trigeminal motor neurons innervating jaw-closing muscles of rats. *J Neurol Sci* **86**, 251–264 (1988).

162. Gesell, R. & White, F. Recruitment of muscular activity and the central neurone after-discharge of hyperpnea. *American Journal of Physiology-Legacy Content* **122**, 48–56 (1938).

163. Insalaco, G. *et al.* Thyroarytenoid muscle activity during loaded and nonloaded breathing in adult humans. *J Appl Physiol (1985)* **70**, 2410–2416 (1991).

164. Hutchison, A. A. *et al.* Laryngeal and diaphragmatic muscle activities and airflow patterns after birth in premature lambs. *J Appl Physiol (1985)* **75**, 121–131 (1993).

165. Amis, T. C., Brancatisano, A. & Tully, A. Thyroid cartilage movements during breathing. *J Appl Physiol (1985)* **78**, 441–448 (1995).

166. Welch, J. F., Kipp, S. & Sheel, A. W. Respiratory muscles during exercise: mechanics, energetics, and fatigue. *Current Opinion in Physiology* **10**, 102–109 (2019).

167. de Britto, A. A. & Moraes, D. J. A. Non-chemosensitive parafacial neurons simultaneously regulate active expiration and airway patency under hypercapnia in rats. *J Physiol* **595**, 2043–2064 (2017).

168. Huckstepp, R. T. R., Cardoza, K. P., Henderson, L. E. & Feldman, J. L. Role of parafacial nuclei in control of breathing in adult rats. *J Neurosci* **35**, 1052–1067 (2015).

169. Sateia, M. J. International classification of sleep disorders-third edition: highlights and modifications. *Chest* **146**, 1387–1394 (2014).

170. Davis, E. M. & O'Donnell, C. P. Rodent models of sleep apnea. *Respir Physiol Neurobiol* **188**, 355–361 (2013).

171. Gautier, H., Remmers, J. E. & Bartlett, D. Control of the duration of expiration. *Respir Physiol* **18**, 205–221 (1973).

172. Dutschmann, M., Jones, S. E., Subramanian, H. H., Stanic, D. & Bautista, T. G. The physiological significance of postinspiration in respiratory control. *Prog Brain Res* **212**, 113–130 (2014).

173. Dutschmann, M., Bautista, T. G., Trevizan-Baú, P., Dhingra, R. R. & Furuya, W. I. The pontine Kölliker-Fuse nucleus gates facial, hypoglossal, and vagal upper airway related motor activity. *Respir Physiol Neurobiol* **284**, 103563 (2021).

174. Anderson, T. M. *et al.* A novel excitatory network for the control of breathing. *Nature* **536**, 76–80 (2016).

175. Smith, J. C., Ellenberger, H. H., Ballanyi, K., Richter, D. W. & Feldman, J. L. Pre-Bötzinger complex: a brainstem region that may generate respiratory rhythm in mammals. *Science* **254**, 726–729 (1991).

176. Gray, P. A., Janczewski, W. A., Mellen, N., McCrimmon, D. R. & Feldman, J. L. Normal breathing requires preBötzinger complex neurokinin-1 receptor-expressing neurons. *Nat Neurosci* **4**, 927–930 (2001).

177. Tan, W. *et al.* Silencing preBötzinger complex somatostatin-expressing neurons induces persistent apnea in awake rat. *Nat Neurosci* **11**, 538–540 (2008).

178. Pisanski, A. & Pagliardini, S. The parafacial respiratory group and the control of active expiration. *Respir Physiol Neurobiol* **265**, 153–160 (2019).

179. Pagliardini, S. *et al.* Active expiration induced by excitation of ventral medulla in adult anesthetized rats. *J Neurosci* **31**, 2895–2905 (2011).

180. Dutschmann, M. & Herbert, H. The Kölliker-Fuse nucleus gates the postinspiratory phase of the respiratory cycle to control inspiratory off-switch and upper airway resistance in rat. *Eur J Neurosci* **24**, 1071–1084 (2006).

181. Porter, W. T. The Path of the Respiratory Impulse from the Bulb to the Phrenic Nuclei. *J Physiol* **17**, 455–485 (1895).

182. Ellenberger, H. H. & Feldman, J. L. Monosynaptic transmission of respiratory drive to phrenic motoneurons from brainstem bulbospinal neurons in rats. *J Comp Neurol* **269**, 47–57 (1988).

183. Butler, J. E., Hudson, A. L. & Gandevia, S. C. The neural control of human inspiratory muscles. *Prog Brain Res* **209**, 295–308 (2014).

184. Shinozaki, Y. *et al.* Structural and functional identification of two distinct inspiratory neuronal populations at the level of the phrenic nucleus in the rat cervical spinal cord. *Brain Struct Funct* **224**, 57–72 (2019).

185. Jensen, V. N., Alilain, W. J. & Crone, S. A. Role of Propriospinal Neurons in Control of Respiratory Muscles and Recovery of Breathing Following Injury. *Front Syst Neurosci* **13**, 84 (2019).

186. Schottelkotte, K. M. & Crone, S. A. Forebrain control of breathing: Anatomy and potential functions. *Front Neurol* **13**, 1041887 (2022).

187. Douglas, N. J. Chapter 22 - Respiratory Physiology: Understanding the Control of Ventilation. in *Principles and Practice of Sleep Medicine (Fifth Edition)* (eds. Kryger, M. H., Roth, T. & Dement, W. C.) 250–258 (W.B. Saunders, 2011). doi:10.1016/B978-1-4160-6645-3.00022-0.

188. Guyenet, P. G. & Wang, H. Pre-Bötzinger neurons with preinspiratory discharges 'in vivo' express NK1 receptors in the rat. *J Neurophysiol* **86**, 438–446 (2001).

189. Yang, C. F. & Feldman, J. L. Efferent projections of excitatory and inhibitory preBötzinger Complex neurons. *J Comp Neurol* **526**, 1389–1402 (2018).

190. Wu, J. *et al.* A V0 core neuronal circuit for inspiration. *Nat Commun* **8**, 544 (2017).

191. Chamberlin, N. L., Eikermann, M., Fassbender, P., White, D. P. & Malhotra, A. Genioglossus premotoneurons and the negative pressure reflex in rats. *J Physiol* **579**, 515–526 (2007).

192. Tan, W., Pagliardini, S., Yang, P., Janczewski, W. A. & Feldman, J. L. Projections of preBötzinger complex neurons in adult rats. *J Comp Neurol* **518**, 1862–1878 (2010).

193. Koshiya, N. *et al.* Anatomical and functional pathways of rhythmogenic inspiratory premotor information flow originating in the pre-Bötzinger complex in the rat medulla. *Neuroscience* **268**, 194–211 (2014).

194. Guo, H. *et al.* Whole-Brain Monosynaptic Inputs to Hypoglossal Motor Neurons in Mice. *Neurosci Bull* **36**, 585–597 (2020).

195. Biancardi, V. *et al.* Mapping of the excitatory, inhibitory, and modulatory afferent projections to the anatomically defined active expiratory oscillator in adult male rats. *J Comp Neurol* **529**, 853–884 (2021).

196. Trevizan-Baú, P. *et al.* Reciprocal connectivity of the periaqueductal gray with the ponto-medullary respiratory network in rat. *Brain Res* **1757**, 147255 (2021).

197. Yackle, K. *et al.* Breathing control center neurons that promote arousal in mice. *Science* **355**, 1411–1415 (2017).

198. Yang, C. F., Kim, E. J., Callaway, E. M. & Feldman, J. L. Monosynaptic Projections to Excitatory and Inhibitory preBötzinger Complex Neurons. *Front Neuroanat* **14**, 58 (2020).

199. Trevizan-Baú, P. *et al.* Forebrain projection neurons target functionally diverse respiratory control areas in the midbrain, pons, and medulla oblongata. *J Comp Neurol* **529**, 2243–2264 (2021).

200. Damasceno, R. S., Takakura, A. C. & Moreira, T. S. Regulation of the chemosensory control of breathing by Kölliker-Fuse neurons. *Am J Physiol Regul Integr Comp Physiol* **307**, R57-67 (2014).

201. Dick, T. E., Bellingham, M. C. & Richter, D. W. Pontine respiratory neurons in anesthetized cats. *Brain Res* **636**, 259–269 (1994).

202. Ezure, K. & Tanaka, I. Distribution and medullary projection of respiratory neurons in the dorsolateral pons of the rat. *Neuroscience* **141**, 1011–1023 (2006).

203. Ezure, K., Tanaka, I. & Saito, Y. Brainstem and spinal projections of augmenting expiratory neurons in the rat. *Neurosci Res* **45**, 41–51 (2003).

204. Loewy, A. D. & Burton, H. Nuclei of the solitary tract: efferent projections to the lower brain stem and spinal cord of the cat. *J Comp Neurol* **181**, 421–449 (1978).

205. Herbert, H., Moga, M. M. & Saper, C. B. Connections of the parabrachial nucleus with the nucleus of the solitary tract and the medullary reticular formation in the rat. *J Comp Neurol* **293**, 540–580 (1990).

206. McGovern, A. E. *et al.* Distinct brainstem and forebrain circuits receiving tracheal sensory neuron inputs revealed using a novel conditional anterograde transsynaptic viral tracing system. *J Neurosci* **35**, 7041–7055 (2015).

207. Rosin, D. L., Chang, D. A. & Guyenet, P. G. Afferent and efferent connections of the rat retrotrapezoid nucleus. *J Comp Neurol* **499**, 64–89 (2006).

208. Bochorishvili, G., Stornetta, R. L., Coates, M. B. & Guyenet, P. G. Pre-Bötzinger complex receives glutamatergic innervation from galaninergic and other retrotrapezoid nucleus neurons. *J Comp Neurol* **520**, 1047–1061 (2012).

209. Silva, J. N., Tanabe, F. M., Moreira, T. S. & Takakura, A. C. Neuroanatomical and physiological evidence that the retrotrapezoid nucleus/parafacial region regulates expiration in adult rats. *Respir Physiol Neurobiol* **227**, 9–22 (2016).

210. Oliveira, L. M., Takakura, A. C. & Moreira, T. S. Forebrain and Hindbrain Projecting-neurons Target the Post-inspiratory Complex Cholinergic Neurons. *Neuroscience* **476**, 102–115 (2021).

211. Fulwiler, C. E. & Saper, C. B. Subnuclear organization of the efferent connections of the parabrachial nucleus in the rat. *Brain Res* **319**, 229–259 (1984).

212. Song, G., Wang, H., Xu, H. & Poon, C.-S. Kölliker–Fuse neurons send collateral projections to multiple hypoxia-activated and nonactivated structures in rat brainstem and spinal cord. *Brain Struct Funct* **217**, 835–858 (2012).

213. Geerling, J. C., Yokota, S., Rukhadze, I., Roe, D. & Chamberlin, N. L. Kölliker-Fuse GABAergic and glutamatergic neurons project to distinct targets. *J Comp Neurol* **525**, 1844–1860 (2017).

214. Ellenberger, H. H., Vera, P. L., Haselton, J. R., Haselton, C. L. & Schneiderman, N. Brainstem projections to the phrenic nucleus: an anterograde and retrograde HRP study in the rabbit. *Brain Res Bull* **24**, 163–174 (1990).

215. Yokota, S., Tsumori, T., Ono, K. & Yasui, Y. Glutamatergic pathways from the Kölliker-Fuse nucleus to the phrenic nucleus in the rat. *Brain Res* **995**, 118–130 (2004).

216. Yokota, S., Oka, T., Tsumori, T., Nakamura, S. & Yasui, Y. Glutamatergic neurons in the Kölliker-Fuse nucleus project to the rostral ventral respiratory group and phrenic nucleus: a combined retrograde tracing and in situ hybridization study in the rat. *Neurosci Res* **59**, 341–346 (2007).

217. Núñez-Abades, P. A., Portillo, F. & Pásaro, R. Characterisation of afferent projections to the nucleus ambiguus of the rat by means of fluorescent double labelling. *J Anat* **172**, 1–15 (1990).

218. Yokota, S., Kaur, S., VanderHorst, V. G., Saper, C. B. & Chamberlin, N. L. Respiratory-related outputs of glutamatergic, hypercapnia-responsive parabrachial neurons in mice. *J Comp Neurol* **523**, 907–920 (2015).

219. Lipski, J., Zhang, X., Kruszewska, B. & Kanjhan, R. Morphological study of long axonal projections of ventral medullary inspiratory neurons in the rat. *Brain Res* **640**, 171–184 (1994).

220. Yokota, S., Oka, T., Asano, H. & Yasui, Y. Orexinergic fibers are in contact with Kölliker-Fuse nucleus neurons projecting to the respiration-related nuclei in the medulla oblongata and spinal cord of the rat. *Brain Res* **1648**, 512–523 (2016).

221. Holstege, G. Anatomical study of the final common pathway for vocalization in the cat. *J Comp Neurol* **284**, 242–252 (1989).

222. Jones, S. E., Stanić, D. & Dutschmann, M. Dorsal and ventral aspects of the most caudal medullary reticular formation have differential roles in modulation and formation of the respiratory motor pattern in rat. *Brain Struct Funct* **221**, 4353–4368 (2016).

223. Gerrits, P. O. & Holstege, G. Pontine and medullary projections to the nucleus retroambiguus: a wheat germ agglutinin-horseradish peroxidase and autoradiographic tracing study in the cat. *J Comp Neurol* **373**, 173–185 (1996).

224. Toor, R. U. A. S. *et al.* Neurons in the Intermediate Reticular Nucleus Coordinate Postinspiratory Activity, Swallowing, and Respiratory-Sympathetic Coupling in the Rat. *J Neurosci* **39**, 9757–9766 (2019).

225. Anderson, T. M. & Ramirez, J.-M. Respiratory rhythm generation: triple oscillator hypothesis. *F1000Res* **6**, 139 (2017).

226. Hülsmann, S. The post-inspiratory complex (PiCo), what is the evidence? *J Physiol* **599**, 357–359 (2021).

227. Ashhad, S., Kam, K., Del Negro, C. A. & Feldman, J. L. Breathing Rhythm and Pattern and Their Influence on Emotion. *Annu Rev Neurosci* **45**, 223–247 (2022).

228. Lima, J. D. *et al.* Cholinergic neurons in the pedunculopontine tegmental nucleus modulate breathing in rats by direct projections to the retrotrapezoid nucleus. *J Physiol* **597**, 1919–1934 (2019).

229. Janczewski, W. A. & Feldman, J. L. Distinct rhythm generators for inspiration and expiration in the juvenile rat. *J Physiol* **570**, 407–420 (2006).

230. Silva, J. N. *et al.* Inhibition of the pontine Kölliker-Fuse nucleus reduces genioglossal activity elicited by stimulation of the retrotrapezoid chemoreceptor neurons. *Neuroscience* **328**, 9–21 (2016).

231. Janczewski, W. A., Onimaru, H., Homma, I. & Feldman, J. L. Opioid-resistant respiratory pathway from the preinspiratory neurones to abdominal muscles: in vivo and in vitro study in the newborn rat. *J Physiol* **545**, 1017–1026 (2002).

232. de Britto, A. A., Magalhães, K. S., da Silva, M. P., Paton, J. F. R. & Moraes, D. J. A. Active expiratory oscillator regulates nasofacial and oral motor activities in rats. *Exp Physiol* **105**, 379–392 (2020).

233. Leirão, I. P., Silva, C. A., Gargaglioni, L. H. & da Silva, G. S. F. Hypercapnia-induced active expiration increases in sleep and enhances ventilation in unanaesthetized rats. *J Physiol* **596**, 3271–3283 (2018).

234. Onimaru, H. & Homma, I. A novel functional neuron group for respiratory rhythm generation in the ventral medulla. *J Neurosci* **23**, 1478–1486 (2003).

235. Thoby-Brisson, M. *et al.* Genetic identification of an embryonic parafacial oscillator coupling to the preBötzinger complex. *Nat Neurosci* **12**, 1028–1035 (2009).

236. Oku, Y., Masumiya, H. & Okada, Y. Postnatal developmental changes in activation profiles of the respiratory neuronal network in the rat ventral medulla. *J Physiol* **585**, 175–186 (2007).

237. van der Heijden, M. E. & Zoghbi, H. Y. Development of the brainstem respiratory circuit. *Wiley Interdiscip Rev Dev Biol* **9**, e366 (2020).

238. Andrews, C. G. & Pagliardini, S. Expiratory activation of abdominal muscle is associated with improved respiratory stability and an increase in minute ventilation in REM epochs of adult rats. *J Appl Physiol (1985)* **119**, 968–974 (2015).

239. Saini, J. K. & Pagliardini, S. Breathing During Sleep in the Postnatal Period of Rats: The Contribution of Active Expiration. *Sleep* **40**, (2017).

240. Saini, J. K., Janes, T. A., MacLean, J. E. & Pagliardini, S. Expiratory activity during sleep in children. *J Sleep Res* **31**, e13539 (2022).

241. Morris, K. F. *et al*. Carotid chemoreceptors tune breathing via multipath routing: reticular chain and loop operations supported by parallel spike train correlations. *J Neurophysiol* **119**, 700–722 (2018).

242. Silva, J. N., Oliveira, L. M., Souza, F. C., Moreira, T. S. & Takakura, A. C. Distinct pathways to the parafacial respiratory group to trigger active expiration in adult rats. *Am J Physiol Lung Cell Mol Physiol* **317**, L402–L413 (2019).

243. Zoccal, D. B. *et al*. Interaction between the retrotrapezoid nucleus and the parafacial respiratory group to regulate active expiration and sympathetic activity in rats. *Am J Physiol Lung Cell Mol Physiol* **315**, L891–L909 (2018).

244. Wellman, A. & White, D. P. Chapter 100 - Central Sleep Apnea and Periodic Breathing. in *Principles and Practice of Sleep Medicine (Fifth Edition)* (eds. Kryger, M. H., Roth, T. & Dement, W. C.) 1140–1152 (W.B. Saunders, 2011). doi:10.1016/B978-1-4160-6645-3.00100-6.

245. Orem, J. The nature of the wakefulness stimulus for breathing. *Prog Clin Biol Res* **345**, 23–30; discussion 31 (1990).

246. Verbraecken, J. A. & De Backer, W. A. Upper Airway Mechanics. *Respiration* **78**, 121–133 (2009).

247. Khoo, M. C. K. Determinants of ventilatory instability and variability. *Respiration Physiology* **122**, 167–182 (2000).

248. Horner, R. L. Chapter 21 - Respiratory Physiology: Central Neural Control of Respiratory Neurons and Motoneurons during Sleep. in *Principles and Practice of*

Sleep Medicine (Fifth Edition) (eds. Kryger, M. H., Roth, T. & Dement, W. C.) 237–249 (W.B. Saunders, 2011). doi:10.1016/B978-1-4160-6645-3.00021-9.

249. Worsnop, C., Kay, A., Pierce, R., Kim, Y. & Trinder, J. Activity of respiratory pump and upper airway muscles during sleep onset. *J Appl Physiol (1985)* **85**, 908–920 (1998).
250. Lo, Y.-L. *et al.* Influence of wakefulness on pharyngeal airway muscle activity. *Thorax* **62**, 799–805 (2007).
251. Amici, R. *et al.* Sleep and bodily functions: the physiological interplay between body homeostasis and sleep homeostasis. *Arch Ital Biol* **152**, 66–78 (2014).
252. Horner, R. L., Kozar, L. F., Kimoff, R. J. & Phillipson, E. A. Effects of sleep on the tonic drive to respiratory muscle and the threshold for rhythm generation in the dog. *J Physiol* **474**, 525–537 (1994).
253. Orem, J., Lovering, A. T., Dunin-Barkowski, W. & Vidruk, E. H. Endogenous excitatory drive to the respiratory system in rapid eye movement sleep in cats. *J Physiol* **527 Pt 2**, 365–376 (2000).
254. Dempsey, J. A., Veasey, S. C., Morgan, B. J. & O'Donnell, C. P. Pathophysiology of sleep apnea. *Physiol Rev* **90**, 47–112 (2010).
255. Dempsey, J. A. Crossing the apnoeic threshold: causes and consequences. *Exp Physiol* **90**, 13–24 (2005).
256. Tangel, D. J., Mezzanotte, W. S. & White, D. P. Influence of sleep on tensor palatini EMG and upper airway resistance in normal men. *Journal of Applied Physiology* **70**, 2574–2581 (1991).
257. Wiegand, L., Zwillich, C. W., Wiegand, D. & White, D. P. Changes in upper airway muscle activation and ventilation during phasic REM sleep in normal men. *Journal of Applied Physiology* **71**, 488–497 (1991).
258. Naifeh, K. H. & Kamiya, J. The Nature of Respiratory Changes Associated with Sleep Onset. *Sleep* **4**, 49–59 (1981).

259. Trinder, J., Whitworth, F., Kay, A. & Wilkin, P. Respiratory instability during sleep onset. *Journal of Applied Physiology* **73**, 2462–2469 (1992).

260. Brebbia, D. R. & Altshuler, K. Z. Oxygen consumption rate and electroencephalographic stage of sleep. *Science* **150**, 1621–1623 (1965).

261. White, D. P., Weil, J. V. & Zwillich, C. W. Metabolic rate and breathing during sleep. *J Appl Physiol (1985)* **59**, 384–391 (1985).

262. Hudgel, D. W. & Devadatta, P. Decrease in functional residual capacity during sleep in normal humans. *Journal of Applied Physiology* **57**, 1319–1322 (1984).

263. Ballard, R. D. *et al.* Influence of sleep on lung volume in asthmatic patients and normal subjects. *Journal of Applied Physiology* **68**, 2034–2041 (1990).

264. Casey, K. R., Cantillo, K. O. & Brown, L. K. Sleep-Related Hypoventilation/Hypoxemic Syndromes. *Chest* **131**, 1936–1948 (2007).

265. Skatrud, J. B. & Dempsey, J. A. Airway resistance and respiratory muscle function in snorers during NREM sleep. *Journal of Applied Physiology* **59**, 328–335 (1985).

266. Gould, G. A. *et al.* Breathing Pattern and Eye Movement Density during REM Sleep in Humans. *Am Rev Respir Dis* **138**, 874–877 (1988).

267. Douglas, N. J., White, D. P., Pickett, C. K., Weil, J. V. & Zwillich, C. W. Respiration during sleep in normal man. *Thorax* **37**, 840–844 (1982).

268. Stradling, J. R., Chadwick, G. A. & Frew, A. J. Changes in ventilation and its components in normal subjects during sleep. *Thorax* **40**, 364–370 (1985).

269. Berthon-Jones, M. & Sullivan, C. E. Ventilatory and arousal responses to hypoxia in sleeping humans. *Am Rev Respir Dis* **125**, 632–639 (1982).

270. Douglas, N. J., White, D. P., Weil, J. V., Pickett, C. K. & Zwillich, C. W. Hypercapnic ventilatory response in sleeping adults. *Am Rev Respir Dis* **126**, 758–762 (1982).

271. Kara, T., Narkiewicz, K. & Somers, V. K. Chemoreflexes--physiology and clinical implications. *Acta Physiol Scand* **177**, 377–384 (2003).

272. Smith, C. A., Nakayama, H. & Dempsey, J. A. The essential role of carotid body chemoreceptors in sleep apnea. *Can J Physiol Pharmacol* **81**, 774–779 (2003).

273. Hedemark, L. L. & Kronenberg, R. S. Ventilatory and heart rate responses to hypoxia and hypercapnia during sleep in adults. *J Appl Physiol Respir Environ Exerc Physiol* **53**, 307–312 (1982).

274. Aroucha Lyra, M. C. *et al.* Prevalence of sleep-disordered breathing and associations with malocclusion in children. *J Clin Sleep Med* **16**, 1007–1012 (2020).

275. Peppard, P. E. *et al.* Increased prevalence of sleep-disordered breathing in adults. *Am J Epidemiol* **177**, 1006–1014 (2013).

276. Kim, E. J. *et al.* Upper airway changes in severe obstructive sleep apnea: upper airway length and volumetric analyses using 3D MDCT. *Acta Otolaryngol* **131**, 527–532 (2011).

277. Meltzer, L. J., Johnson, C., Crosette, J., Ramos, M. & Mindell, J. A. Prevalence of diagnosed sleep disorders in pediatric primary care practices. *Pediatrics* **125**, e1410-1418 (2010).

278. Heinzer, R. *et al.* Prevalence of sleep-disordered breathing in the general population: the HypnoLaus study. *Lancet Respir Med* **3**, 310–318 (2015).

279. GBD 2015 Obesity Collaborators *et al.* Health Effects of Overweight and Obesity in 195 Countries over 25 Years. *N Engl J Med* **377**, 13–27 (2017).

280. Javaheri, S. *et al.* Sleep Apnea: Types, Mechanisms, and Clinical Cardiovascular Consequences. *J Am Coll Cardiol* **69**, 841–858 (2017).

281. Thorpy, M. International Classification of Sleep Disorders. in *Sleep Disorders Medicine: Basic Science, Technical Considerations and Clinical Aspects* (ed. Chokroverty, S.) 475–484 (Springer, 2017). doi:10.1007/978-1-4939-6578-6_27.

282. Senaratna, C. V. *et al.* Prevalence of obstructive sleep apnea in the general population: A systematic review. *Sleep Med Rev* **34**, 70–81 (2017).

283. Maiolino, G. *et al.* Treating sleep disorders to improve blood pressure control and cardiovascular prevention: a dream come true?-a narrative review. *J Thorac Dis* **12**, S225–S234 (2020).

284. Nespoli, L., Caprioglio, A., Brunetti, L. & Nosetti, L. Obstructive sleep apnea syndrome in childhood. *Early Hum Dev* **89 Suppl 3**, S33-37 (2013).

285. Alzoubaidi, M. & Mokhlesi, B. Obstructive sleep apnea during rapid eye movement sleep: clinical relevance and therapeutic implications. *Curr Opin Pulm Med* **22**, 545–554 (2016).

286. Bradley, T. D. & Floras, J. S. Obstructive sleep apnoea and its cardiovascular consequences. *Lancet* **373**, 82–93 (2009).

287. Thorpy, M. J. Classification of sleep disorders. *Neurotherapeutics* **9**, 687–701 (2012).

288. Donovan, L. M. & Kapur, V. K. Prevalence and Characteristics of Central Compared to Obstructive Sleep Apnea: Analyses from the Sleep Heart Health Study Cohort. *Sleep* **39**, 1353–1359 (2016).

289. Wang, D., Yee, B. J., Grunstein, R. R. & Chung, F. Chronic Opioid Use and Central Sleep Apnea, Where Are We Now and Where To Go? A State of the Art Review. *Anesth Analg* **132**, 1244–1253 (2021).

290. Lévy, P., Naughton, M. T., Tamisier, R., Cowie, M. R. & Bradley, T. D. Sleep apnoea and heart failure. *Eur Respir J* **59**, 2101640 (2022).

291. Randerath, W. *et al.* Definition, discrimination, diagnosis and treatment of central breathing disturbances during sleep. *Eur Respir J* **49**, 1600959 (2017).

292. Naughton, M. T. Cheyne-Stokes respiration: friend or foe? *Thorax* **67**, 357–360 (2012).

293. Hall, M. J. *et al.* Cycle length of periodic breathing in patients with and without heart failure. *Am J Respir Crit Care Med* **154**, 376–381 (1996).

294. Bloch, K. E. *et al.* Nocturnal periodic breathing during acclimatization at very high altitude at Mount Muztagh Ata (7,546 m). *Am J Respir Crit Care Med* **182**, 562–568 (2010).

295. Nicholson, A. N., Smith, P. A., Stone, B. M., Bradwell, A. R. & Coote, J. H. Altitude insomnia: studies during an expedition to the Himalayas. *Sleep* **11**, 354–361 (1988).

296. Alattar, M. A. & Scharf, S. M. Opioid-associated central sleep apnea: a case series. *Sleep Breath* **13**, 201–206 (2009).

297. Farney, R. J., Walker, J. M., Cloward, T. V. & Rhondeau, S. Sleep-disordered breathing associated with long-term opioid therapy. *Chest* **123**, 632–639 (2003).

298. Gipson, K., Lu, M. & Kinane, T. B. Sleep-Disordered Breathing in Children. *Pediatr Rev* **40**, 3–13 (2019).

299. Jordan, A. S., McSharry, D. G. & Malhotra, A. Adult obstructive sleep apnoea. *Lancet* **383**, 736–747 (2014).

300. Lyons, O. D. & Bradley, T. D. Heart Failure and Sleep Apnea. *Canadian Journal of Cardiology* **31**, 898–908 (2015).

301. Mendelson, M. *et al.* Effects of exercise training on sleep apnoea in patients with coronary artery disease: a randomised trial. *Eur Respir J* **48**, 142–150 (2016).

302. Dehlink, E. & Tan, H.-L. Update on paediatric obstructive sleep apnoea. *J Thorac Dis* **8**, 224–235 (2016).

303. Cielo, C. M., Montalva, F. M. & Taylor, J. A. Craniofacial disorders associated with airway obstruction in the neonate. *Semin Fetal Neonatal Med* **21**, 254–262 (2016).

304. Bozzini, M. F. R. & Di Francesco, R. C. Managing obstructive sleep apnoea in children: the role of craniofacial morphology. *Clinics (Sao Paulo)* **71**, 664–666 (2016).

305. Skotko, B. G. *et al.* A predictive model for obstructive sleep apnea and Down syndrome. *Am J Med Genet A* **173**, 889–896 (2017).

306. Bauters, F., Rietzschel, E. R., Hertegonne, K. B. C. & Chirinos, J. A. The Link Between Obstructive Sleep Apnea and Cardiovascular Disease. *Curr Atheroscler Rep* **18**, 1 (2016).

307. Drager, L. F. *et al.* Translational approaches to understanding metabolic dysfunction and cardiovascular consequences of obstructive sleep apnea. *Am J Physiol Heart Circ Physiol* **309**, H1101-1111 (2015).

308. Baltzis, D., Bakker, J. P., Patel, S. R. & Veves, A. Obstructive Sleep Apnea and Vascular Diseases. *Compr Physiol* **6**, 1519–1528 (2016).

309. Baguet, J.-P., Barone-Rochette, G., Tamisier, R., Levy, P. & Pépin, J.-L. Mechanisms of cardiac dysfunction in obstructive sleep apnea. *Nat Rev Cardiol* **9**, 679–688 (2012).

310. Mokhlesi, B. & Punjabi, N. M. ‘REM-related’ obstructive sleep apnea: an epiphenomenon or a clinically important entity? *Sleep* **35**, 5–7 (2012).

311. Mokhlesi, B. REM-related obstructive sleep apnea: to treat or not to treat? *J Clin Sleep Med* **8**, 249–250 (2012).

312. Grace, K. P., Hughes, S. W. & Horner, R. L. Identification of the mechanism mediating genioglossus muscle suppression in REM sleep. *Am J Respir Crit Care Med* **187**, 311–319 (2013).

313. Rishi, A. R. & Rishi, M. A. Rapid eye movement related obstructive sleep apnea: Where do we stand? *Respir Investig* **59**, 589–595 (2021).

314. Haba-Rubio, J., Janssens, J.-P., Rochat, T. & Sforza, E. Rapid eye movement-related disordered breathing: clinical and polysomnographic features. *Chest* **128**, 3350–3357 (2005).

315. Koo, B. B., Patel, S. R., Strohl, K. & Hoffstein, V. Rapid eye movement-related sleep-disordered breathing: influence of age and gender. *Chest* **134**, 1156–1161 (2008).

316. O’Connor, C., Thornley, K. S. & Hanly, P. J. Gender differences in the polysomnographic features of obstructive sleep apnea. *Am J Respir Crit Care Med* **161**, 1465–1472 (2000).

317. Findley, L. J., Wilhoit, S. C. & Suratt, P. M. Apnea duration and hypoxemia during REM sleep in patients with obstructive sleep apnea. *Chest* **87**, 432–436 (1985).

318. Varga, A. W. & Mokhlesi, B. REM obstructive sleep apnea: risk for adverse health outcomes and novel treatments. *Sleep Breath* **23**, 413–423 (2019).

319. Lejeune, J., Gautier, M. & Turpin, R. [Study of somatic chromosomes from 9 mongoloid children]. *C R Hebd Seances Acad Sci* **248**, 1721–1722 (1959).

320. Antonarakis, S. E. Parental origin of the extra chromosome in trisomy 21 as indicated by analysis of DNA polymorphisms. Down Syndrome Collaborative Group. *N Engl J Med* **324**, 872–876 (1991).

321. Antonarakis, S. E., Avramopoulos, D., Blouin, J. L., Talbot, C. C. & Schinzel, A. A. Mitotic errors in somatic cells cause trisomy 21 in about 4.5% of cases and are not associated with advanced maternal age. *Nat Genet* **3**, 146–150 (1993).

322. Barlow, G. M. *et al.* Down syndrome congenital heart disease: a narrowed region and a candidate gene. *Genet Med* **3**, 91–101 (2001).

323. Galdzicki, Z., Siarey, R., Pearce, R., Stoll, J. & Rapoport, S. I. On the cause of mental retardation in Down syndrome: extrapolation from full and segmental trisomy 16 mouse models. *Brain Res Brain Res Rev* **35**, 115–145 (2001).

324. Hassold, T. & Hunt, P. To err (meiotically) is human: the genesis of human aneuploidy. *Nat Rev Genet* **2**, 280–291 (2001).

325. Lyle, R. *et al.* Genotype-phenotype correlations in Down syndrome identified by array CGH in 30 cases of partial trisomy and partial monosomy chromosome 21. *Eur J Hum Genet* **17**, 454–466 (2009).

326. Papavassiliou, P. *et al.* The phenotype of persons having mosaicism for trisomy 21/Down syndrome reflects the percentage of trisomic cells present in different tissues. *Am J Med Genet A* **149A**, 573–583 (2009).

327. Morris, J. K., Alberman, E., Mutton, D. & Jacobs, P. Cytogenetic and epidemiological findings in Down syndrome: England and Wales 1989-2009. *Am J Med Genet A* **158A**, 1151–1157 (2012).

328. Langdon, J. & Down, H. Observations on an ethnic classification of idiots. *Heredity* **21**, 695–697 (1966).

329. Presson, A. P. *et al.* Current estimate of Down Syndrome population prevalence in the United States. *J Pediatr* **163**, 1163–1168 (2013).

330. de Graaf, G., Buckley, F. & Skotko, B. G. Estimates of the live births, natural losses, and elective terminations with Down syndrome in the United States. *Am J Med Genet A* **167A**, 756–767 (2015).

331. Chapman, R. S. & Hesketh, L. J. Behavioral phenotype of individuals with Down syndrome. *Ment Retard Dev Disabil Res Rev* **6**, 84–95 (2000).

332. Vicari, S. Motor development and neuropsychological patterns in persons with Down syndrome. *Behav Genet* **36**, 355–364 (2006).

333. Bartesaghi, R., Guidi, S. & Ciani, E. Is it possible to improve neurodevelopmental abnormalities in Down syndrome? *Rev Neurosci* **22**, 419–455 (2011).

334. Asim, A., Kumar, A., Muthuswamy, S., Jain, S. & Agarwal, S. Down syndrome: an insight of the disease. *J Biomed Sci* **22**, 41 (2015).

335. Antonarakis, S. E. *et al.* Down syndrome. *Nat Rev Dis Primers* **6**, 9 (2020).

336. Freeman, S. B. *et al.* Population-based study of congenital heart defects in Down syndrome. *Am J Med Genet* **80**, 213–217 (1998).

337. Freeman, S. B. *et al.* Congenital gastrointestinal defects in Down syndrome: a report from the Atlanta and National Down Syndrome Projects. *Clin Genet* **75**, 180–184 (2009).

338. Noble, J. Natural history of Down's syndrome: a brief review for those involved in antenatal screening. *J Med Screen* **5**, 172–177 (1998).

339. Nadel, L. Down's syndrome: a genetic disorder in biobehavioral perspective. *Genes Brain Behav* **2**, 156–166 (2003).

340. Lott, I. T. Neurological phenotypes for Down syndrome across the life span. *Prog Brain Res* **197**, 101–121 (2012).

341. Barca, D. *et al.* Intellectual disability and epilepsy in down syndrome. *Maedica (Bucur)* **9**, 344–350 (2014).

342. Hartley, D. *et al.* Down syndrome and Alzheimer's disease: Common pathways, common goals. *Alzheimers Dement* **11**, 700–709 (2015).

343. Arumugam, A. *et al.* Down syndrome-A narrative review with a focus on anatomical features. *Clin Anat* **29**, 568–577 (2016).

344. Whooten, R., Schmitt, J. & Schwartz, A. Endocrine manifestations of Down syndrome. *Curr Opin Endocrinol Diabetes Obes* **25**, 61–66 (2018).

345. Capone, G. *et al.* Co-occurring medical conditions in adults with Down syndrome: A systematic review toward the development of health care guidelines. Part II. *Am J Med Genet A* **182**, 1832–1845 (2020).

346. Bull, M. J. *et al.* Health Supervision for Children and Adolescents With Down Syndrome. *Pediatrics* **149**, e2022057010 (2022).

347. de Miguel-Díez, J., Villa-Asensi, J. R. & Alvarez-Sala, J. L. Prevalence of sleep-disordered breathing in children with Down syndrome: polygraphic findings in 108 children. *Sleep* **26**, 1006–1009 (2003).

348. Austeng, M. E. *et al.* Obstructive sleep apnea in younger school children with Down syndrome. *Int J Pediatr Otorhinolaryngol* **78**, 1026–1029 (2014).

349. Hill, C. M. *et al.* Prevalence and predictors of obstructive sleep apnoea in young children with Down syndrome. *Sleep Med* **27–28**, 99–106 (2016).

350. Maris, M., Verhulst, S., Wojciechowski, M., Van de Heyning, P. & Boudewyns, A. Prevalence of Obstructive Sleep Apnea in Children with Down Syndrome. *Sleep* **39**, 699–704 (2016).

351. Young, T. *et al.* The occurrence of sleep-disordered breathing among middle-aged adults. *N Engl J Med* **328**, 1230–1235 (1993).

352. Trois, M. S. *et al.* Obstructive sleep apnea in adults with Down syndrome. *J Clin Sleep Med* **5**, 317–323 (2009).

353. Cornacchia, M., Sethness, J., Alapat, P., Lin, Y.-H. & Peacock, C. The Prevalence of OSA Among an Adult Population With Down Syndrome Referred to a Medical Clinic. *Am J Intellect Dev Disabil* **124**, 4–10 (2019).

354. Landete, P. *et al.* Obstructive sleep apnea in adults with Down syndrome. *Am J Med Genet A* **182**, 2832–2840 (2020).

355. Lin, S. C., Davey, M. J., Horne, R. S. C. & Nixon, G. M. Screening for obstructive sleep apnea in children with Down syndrome. *J Pediatr* **165**, 117–122 (2014).

356. Goffinski, A. *et al.* Obstructive sleep apnea in young infants with Down syndrome evaluated in a Down syndrome specialty clinic. *Am J Med Genet A* **167A**, 324–330 (2015).

357. Rosen, D. Management of obstructive sleep apnea associated with Down syndrome and other craniofacial dysmorphologies. *Curr Opin Pulm Med* **17**, 431–436 (2011).

358. Symonds, J. D. *et al.* Incidence and phenotypes of childhood-onset genetic epilepsies: a prospective population-based national cohort. *Brain* **142**, 2303–2318 (2019).

359. Montini, E. *et al.* Identification and characterization of a novel serine-threonine kinase gene from the Xp22 region. *Genomics* **51**, 427–433 (1998).

360. Zhu, Y.-C. & Xiong, Z.-Q. Molecular and Synaptic Bases of CDKL5 Disorder. *Dev Neurobiol* **79**, 8–19 (2019).

361. Williamson, S. L. *et al.* A novel transcript of cyclin-dependent kinase-like 5 (CDKL5) has an alternative C-terminus and is the predominant transcript in brain. *Hum Genet* **131**, 187–200 (2012).

362. Kalscheuer, V. M. *et al.* Disruption of the serine/threonine kinase 9 gene causes severe X-linked infantile spasms and mental retardation. *Am J Hum Genet* **72**, 1401–1411 (2003).

363. Tao, J. *et al.* Mutations in the X-linked cyclin-dependent kinase-like 5 (CDKL5/STK9) gene are associated with severe neurodevelopmental retardation. *Am J Hum Genet* **75**, 1149–1154 (2004).

364. Weaving, L. S. *et al.* Mutations of CDKL5 cause a severe neurodevelopmental disorder with infantile spasms and mental retardation. *Am J Hum Genet* **75**, 1079–1093 (2004).

365. Scala, E. *et al.* CDKL5/STK9 is mutated in Rett syndrome variant with infantile spasms. *J Med Genet* **42**, 103–107 (2005).

366. Hanefeld, F. The clinical pattern of the Rett syndrome. *Brain Dev* **7**, 320–325 (1985).

367. Fehr, S. *et al.* The CDKL5 disorder is an independent clinical entity associated with early-onset encephalopathy. *Eur J Hum Genet* **21**, 266–273 (2013).

368. Jakimiec, M., Paprocka, J. & Śmigiel, R. CDKL5 Deficiency Disorder-A Complex Epileptic Encephalopathy. *Brain Sci* **10**, 107 (2020).

369. Devinsky, O. *et al.* Open-label use of highly purified CBD (Epidiolex®) in patients with CDKL5 deficiency disorder and Aicardi, Dup15q, and Doose syndromes. *Epilepsy Behav* **86**, 131–137 (2018).

370. Olson, H. E. *et al.* Cyclin-Dependent Kinase-Like 5 Deficiency Disorder: Clinical Review. *Pediatr Neurol* **97**, 18–25 (2019).

371. Mangatt, M. *et al.* Prevalence and onset of comorbidities in the CDKL5 disorder differ from Rett syndrome. *Orphanet J Rare Dis* **11**, 39 (2016).

372. Leonard, H. *et al.* CDKL5 deficiency disorder: clinical features, diagnosis, and management. *Lancet Neurol* **21**, 563–576 (2022).

373. Zhao, Y. *et al.* Clinical features and gene mutational spectrum of CDKL5-related diseases in a cohort of Chinese patients. *BMC Med Genet* **15**, 24 (2014).

374. Bahi-Buisson, N. & Bienvenu, T. CDKL5-Related Disorders: From Clinical Description to Molecular Genetics. *Mol Syndromol* **2**, 137–152 (2012).

375. Bahi-Buisson, N. *et al.* Key clinical features to identify girls with CDKL5 mutations. *Brain* **131**, 2647–2661 (2008).

376. Mei, D. *et al.* Xp22.3 genomic deletions involving the CDKL5 gene in girls with early onset epileptic encephalopathy. *Epilepsia* **51**, 647–654 (2010).

377. Amin, S. *et al.* Caregiver's perception of epilepsy treatment, quality of life and comorbidities in an international cohort of CDKL5 patients. *Hippokratia* **21**, 130–135 (2017).

378. Bush, P. G. & Williams, A. J. Incidence of the Robin Anomalad (Pierre Robin syndrome). *British Journal of Plastic Surgery* **36**, 434–437 (1983).

379. Izumi, K., Konczal, L. L., Mitchell, A. L. & Jones, M. C. Underlying genetic diagnosis of Pierre Robin sequence: retrospective chart review at two children's hospitals and a systematic literature review. *J Pediatr* **160**, 645-650.e2 (2012).

380. Robin, P. A fall of the base of the tongue considered as a new cause of nasopharyngeal respiratory impairment: Pierre Robin sequence, a translation. 1923. *Plast Reconstr Surg* **93**, 1301–1303 (1994).

381. Gangopadhyay, N., Mendonca, D. A. & Woo, A. S. Pierre robin sequence. *Semin Plast Surg* **26**, 76–82 (2012).

382. Shprintzen, R. J. The implications of the diagnosis of Robin sequence. *Cleft Palate Craniofac J* **29**, 205–209 (1992).

383. Jakobsen, L. P. *et al.* The genetic basis of the Pierre Robin Sequence. *Cleft Palate Craniofac J* **43**, 155–159 (2006).

384. Baxter, D. & Shanks, A. L. Pierre Robin Syndrome. in *StatPearls* (StatPearls Publishing, 2023).

385. Jakobsen, L. P. *et al.* Pierre Robin sequence may be caused by dysregulation of SOX9 and KCNJ2. *J Med Genet* **44**, 381–386 (2007).

386. Weaver, T. E. *et al.* Continuous positive airway pressure treatment of sleepy patients with milder obstructive sleep apnea: results of the CPAP Apnea Trial North American Program (CATNAP) randomized clinical trial. *Am J Respir Crit Care Med* **186**, 677–683 (2012).

387. Sin, D. D., Logan, A. G., Fitzgerald, F. S., Liu, P. P. & Bradley, T. D. Effects of continuous positive airway pressure on cardiovascular outcomes in heart failure patients with and without Cheyne-Stokes respiration. *Circulation* **102**, 61–66 (2000).

388. Naughton, M. T., Liu, P. P., Bernard, D. C., Goldstein, R. S. & Bradley, T. D. Treatment of congestive heart failure and Cheyne-Stokes respiration during sleep by continuous positive airway pressure. *Am J Respir Crit Care Med* **151**, 92–97 (1995).

389. Javaheri, S., Javaheri, S. & Javaheri, A. Sleep Apnea, Heart Failure, and Pulmonary Hypertension. *Curr Heart Fail Rep* **10**, 315–320 (2013).

390. Bratton, D. J., Stradling, J. R., Barbé, F. & Kohler, M. Effect of CPAP on blood pressure in patients with minimally symptomatic obstructive sleep apnoea: a meta-

analysis using individual patient data from four randomised controlled trials. *Thorax* **69**, 1128–1135 (2014).

391. Bakker, J. P. *et al.* Blood pressure improvement with continuous positive airway pressure is independent of obstructive sleep apnea severity. *J Clin Sleep Med* **10**, 365–369 (2014).
392. Fava, C. *et al.* Effect of CPAP on blood pressure in patients with OSA/hypopnea a systematic review and meta-analysis. *Chest* **145**, 762–771 (2014).
393. Liu, L., Cao, Q., Guo, Z. & Dai, Q. Continuous Positive Airway Pressure in Patients With Obstructive Sleep Apnea and Resistant Hypertension: A Meta-Analysis of Randomized Controlled Trials. *J Clin Hypertens (Greenwich)* **18**, 153–158 (2016).
394. McEvoy, R. D. *et al.* CPAP for Prevention of Cardiovascular Events in Obstructive Sleep Apnea. *N Engl J Med* **375**, 919–931 (2016).
395. Craig, S. *et al.* Continuous positive airway pressure treatment for obstructive sleep apnoea reduces resting heart rate but does not affect dysrhythmias: a randomised controlled trial. *J Sleep Res* **18**, 329–336 (2009).
396. Ryan, C. M., Usui, K., Floras, J. S. & Bradley, T. D. Effect of continuous positive airway pressure on ventricular ectopy in heart failure patients with obstructive sleep apnoea. *Thorax* **60**, 781–785 (2005).
397. Fein, A. S. *et al.* Treatment of obstructive sleep apnea reduces the risk of atrial fibrillation recurrence after catheter ablation. *J Am Coll Cardiol* **62**, 300–305 (2013).
398. Neilan, T. G. *et al.* Effect of sleep apnea and continuous positive airway pressure on cardiac structure and recurrence of atrial fibrillation. *J Am Heart Assoc* **2**, e000421 (2013).
399. Holmqvist, F. *et al.* Impact of obstructive sleep apnea and continuous positive airway pressure therapy on outcomes in patients with atrial fibrillation-Results from the Outcomes Registry for Better Informed Treatment of Atrial Fibrillation (ORBIT-AF). *Am Heart J* **169**, 647-654.e2 (2015).

400. Wu, X. *et al.* Treatment of OSA reduces the risk of repeat revascularization after percutaneous coronary intervention. *Chest* **147**, 708–718 (2015).

401. Marin, J. M., Carrizo, S. J., Vicente, E. & Agusti, A. G. N. Long-term cardiovascular outcomes in men with obstructive sleep apnoea-hypopnoea with or without treatment with continuous positive airway pressure: an observational study. *Lancet* **365**, 1046–1053 (2005).

402. Campos-Rodriguez, F. *et al.* Cardiovascular mortality in women with obstructive sleep apnea with or without continuous positive airway pressure treatment: a cohort study. *Ann Intern Med* **156**, 115–122 (2012).

403. Chirinos, J. A. *et al.* CPAP, weight loss, or both for obstructive sleep apnea. *N Engl J Med* **370**, 2265–2275 (2014).

404. Iftikhar, I. H., Kline, C. E. & Youngstedt, S. D. Effects of exercise training on sleep apnea: a meta-analysis. *Lung* **192**, 175–184 (2014).

405. Redolfi, S. *et al.* Attenuation of obstructive sleep apnea and overnight rostral fluid shift by physical activity. *Am J Respir Crit Care Med* **191**, 856–858 (2015).

406. Barbé, F. *et al.* Effect of continuous positive airway pressure on the incidence of hypertension and cardiovascular events in nonsleepy patients with obstructive sleep apnea: a randomized controlled trial. *JAMA* **307**, 2161–2168 (2012).

407. Peker, Y. *et al.* Effect of Positive Airway Pressure on Cardiovascular Outcomes in Coronary Artery Disease Patients with Nonsleepy Obstructive Sleep Apnea. The RICCADSA Randomized Controlled Trial. *Am J Respir Crit Care Med* **194**, 613–620 (2016).

408. Meyer, A. C. *et al.* Airway interventions in children with Pierre Robin Sequence. *Otolaryngol Head Neck Surg* **138**, 782–787 (2008).

409. Anderson, K. D., Cole, A., Chuo, C. B. & Slator, R. Home management of upper airway obstruction in Pierre Robin sequence using a nasopharyngeal airway. *Cleft Palate Craniofac J* **44**, 269–273 (2007).

410. Phillips, C. L. *et al.* Health outcomes of continuous positive airway pressure versus oral appliance treatment for obstructive sleep apnea: a randomized controlled trial. *Am J Respir Crit Care Med* **187**, 879–887 (2013).

411. Mackay, D. R. Controversies in the diagnosis and management of the Robin sequence. *J Craniofac Surg* **22**, 415–420 (2011).

412. Robison, J. G. & Otteson, T. D. Increased prevalence of obstructive sleep apnea in patients with cleft palate. *Arch Otolaryngol Head Neck Surg* **137**, 269–274 (2011).

413. Roy, S., Munson, P. D., Zhao, L., Holinger, L. D. & Patel, P. K. CT analysis after distraction osteogenesis in Pierre Robin Sequence. *Laryngoscope* **119**, 380–386 (2009).

414. Sedaghat, A. R. *et al.* Characterization of obstructive sleep apnea before and after tongue-lip adhesion in children with micrognathia. *Cleft Palate Craniofac J* **49**, 21–26 (2012).

415. Resnick, C. M., Dentino, K., Katz, E., Mulliken, J. B. & Padwa, B. L. Effectiveness of Tongue-lip Adhesion for Obstructive Sleep Apnea in Infants With Robin Sequence Measured by Polysomnography. *Cleft Palate Craniofac J* **53**, 584–588 (2016).

416. Jacobowitz, O., Schwartz, A. R., Lovett, E. G., Ranuzzi, G. & Malhotra, A. Design and rationale for the treating Obstructive Sleep Apnea using Targeted Hypoglossal Nerve Stimulation (OSPREY) trial. *Contemp Clin Trials* **119**, 106804 (2022).

417. Schwartz, A. R. *et al.* Acute upper airway responses to hypoglossal nerve stimulation during sleep in obstructive sleep apnea. *Am J Respir Crit Care Med* **185**, 420–426 (2012).

418. Mouse Genome Sequencing Consortium *et al.* Initial sequencing and comparative analysis of the mouse genome. *Nature* **420**, 520–562 (2002).

419. Cinelli, E. *et al.* Neuronal mechanisms of respiratory pattern generation are evolutionary conserved. *J Neurosci* **33**, 9104–9112 (2013).

420. Reznik, G. K. Comparative anatomy, physiology, and function of the upper respiratory tract. *Environ Health Perspect* **85**, 171–176 (1990).

421. Fleury Curado, T. *et al.* Sleep-disordered breathing in C57BL/6J mice with diet-induced obesity. *Sleep* **41**, zsy089 (2018).

422. Fleury Curado, T. A. *et al.* Silencing of Hypoglossal Motoneurons Leads to Sleep Disordered Breathing in Lean Mice. *Front Neurol* **9**, 962 (2018).

423. Chemelli, R. M. *et al.* Narcolepsy in orexin knockout mice: molecular genetics of sleep regulation. *Cell* **98**, 437–451 (1999).

424. Fung, S. J., Yamuy, J., Sampogna, S., Morales, F. R. & Chase, M. H. Hypocretin (orexin) input to trigeminal and hypoglossal motoneurons in the cat: a double-labeling immunohistochemical study. *Brain Res* **903**, 257–262 (2001).

425. Krout, K. E., Mettenleiter, T. C. & Loewy, A. D. Single CNS neurons link both central motor and cardiosympathetic systems: a double-virus tracing study. *Neuroscience* **118**, 853–866 (2003).

426. Young, J. K. *et al.* Orexin stimulates breathing via medullary and spinal pathways. *J Appl Physiol (1985)* **98**, 1387–1395 (2005).

427. Nakamura, A., Zhang, W., Yanagisawa, M., Fukuda, Y. & Kuwaki, T. Vigilance state-dependent attenuation of hypercapnic chemoreflex and exaggerated sleep apnea in orexin knockout mice. *J Appl Physiol (1985)* **102**, 241–248 (2007).

428. Amendola, E. *et al.* Mapping pathological phenotypes in a mouse model of CDKL5 disorder. *PLoS One* **9**, e91613 (2014).

429. Lo Martire, V. *et al.* CDKL5 deficiency entails sleep apneas in mice. *J Sleep Res* **26**, 495–497 (2017).

430. Peng, Y.-J. *et al.* Complementary roles of gasotransmitters CO and H2S in sleep apnea. *Proc Natl Acad Sci U S A* **114**, 1413–1418 (2017).

431. Dauger, S. *et al.* Phox2b controls the development of peripheral chemoreceptors and afferent visceral pathways. *Development* **130**, 6635–6642 (2003).

432. Durand, E. *et al.* Sleep-disordered breathing in newborn mice heterozygous for the transcription factor Phox2b. *Am J Respir Crit Care Med* **172**, 238–243 (2005).

433. Real, C. *et al.* Sleep apneas are increased in mice lacking monoamine oxidase A. *Sleep* **30**, 1295–1302 (2007).

434. Baum, D. M. *et al.* New Zealand Obese Mice as a Translational Model of Obesity-related Obstructive Sleep Apnea Syndrome. *Am J Respir Crit Care Med* **198**, 1336–1339 (2018).

435. Berger, S. *et al.* Intranasal Leptin Relieves Sleep-disordered Breathing in Mice with Diet-induced Obesity. *Am J Respir Crit Care Med* **199**, 773–783 (2019).

436. Freire, C. *et al.* Intranasal Leptin Prevents Opioid-induced Sleep-disordered Breathing in Obese Mice. *Am J Respir Cell Mol Biol* **63**, 502–509 (2020).

437. Kim, L. J. *et al.* Leptin Receptor Blockade Attenuates Hypertension, but Does Not Affect Ventilatory Response to Hypoxia in a Model of Polygenic Obesity. *Front Physiol* **12**, 688375 (2021).

438. Davisson, M. T., Schmidt, C. & Akeson, E. C. Segmental trisomy of murine chromosome 16: a new model system for studying Down syndrome. *Prog Clin Biol Res* **360**, 263–280 (1990).

439. Gropp, A., Kolbus, U. & Giers, D. Systematic approach to the study of trisomy in the mouse. II. *Cytogenet Cell Genet* **14**, 42–62 (1975).

440. Webb, S., Anderson, R. H., Lamers, W. H. & Brown, N. A. Mechanisms of deficient cardiac septation in the mouse with trisomy 16. *Circ Res* **84**, 897–905 (1999).

441. Herault, Y. *et al.* Rodent models in Down syndrome research: impact and future opportunities. *Dis Model Mech* **10**, 1165–1186 (2017).

442. Lana-Elola, E., Watson-Scales, S. D., Fisher, E. M. C. & Tybulewicz, V. L. J. Down syndrome: searching for the genetic culprits. *Dis Model Mech* **4**, 586–595 (2011).

443. Reeves, R. H. *et al.* A mouse model for Down syndrome exhibits learning and behaviour deficits. *Nat Genet* **11**, 177–184 (1995).

444. Richtsmeier, J. T., Zumwalt, A., Carlson, E. J., Epstein, C. J. & Reeves, R. H. Craniofacial phenotypes in segmentally trisomic mouse models for Down syndrome. *Am J Med Genet* **107**, 317–324 (2002).

445. Fructuoso, M. *et al.* Increased levels of inflammatory plasma markers and obesity risk in a mouse model of Down syndrome. *Free Radic Biol Med* **114**, 122–130 (2018).

446. Das, D. *et al.* Increased incidence of intermittent hypoxemia in the Ts65Dn mouse model of Down syndrome. *Neurosci Lett* **604**, 91–96 (2015).

447. Colas, D. *et al.* Sleep and EEG features in genetic models of Down syndrome. *Neurobiol Dis* **30**, 1–7 (2008).

448. Hector, R. D. *et al.* Characterisation of CDKL5 Transcript Isoforms in Human and Mouse. *PLoS One* **11**, e0157758 (2016).

449. Wang, I.-T. J. *et al.* Loss of CDKL5 disrupts kinome profile and event-related potentials leading to autistic-like phenotypes in mice. *Proc Natl Acad Sci U S A* **109**, 21516–21521 (2012).

450. Jhang, C.-L., Huang, T.-N., Hsueh, Y.-P. & Liao, W. Mice lacking cyclin-dependent kinase-like 5 manifest autistic and ADHD-like behaviors. *Hum Mol Genet* **26**, 3922–3934 (2017).

451. Tang, S. *et al.* Loss of CDKL5 in Glutamatergic Neurons Disrupts Hippocampal Microcircuitry and Leads to Memory Impairment in Mice. *J Neurosci* **37**, 7420–7437 (2017).

452. Okuda, K. *et al.* CDKL5 controls postsynaptic localization of GluN2B-containing NMDA receptors in the hippocampus and regulates seizure susceptibility. *Neurobiol Dis* **106**, 158–170 (2017).

453. Farley, F. W., Soriano, P., Steffen, L. S. & Dymecki, S. M. Widespread recombinase expression using FLPeR (flipper) mice. *Genesis* **28**, 106–110 (2000).

454. Tang, S.-H. E., Silva, F. J., Tsark, W. M. K. & Mann, J. R. A Cre/loxP-deleter transgenic line in mouse strain 129S1/SvImJ. *Genesis* **32**, 199–202 (2002).

455. Trazzi, S. *et al.* HDAC4: a key factor underlying brain developmental alterations in CDKL5 disorder. *Hum Mol Genet* **25**, 3887–3907 (2016).

456. Ricciardi, S. *et al.* CDKL5 ensures excitatory synapse stability by reinforcing NGL-1-PSD95 interaction in the postsynaptic compartment and is impaired in patient iPSC-derived neurons. *Nat Cell Biol* **14**, 911–923 (2012).

457. Fuchs, C. *et al.* Loss of CDKL5 impairs survival and dendritic growth of newborn neurons by altering AKT/GSK-3β signaling. *Neurobiol Dis* **70**, 53–68 (2014).

458. Fuchs, C. *et al.* Inhibition of GSK3β rescues hippocampal development and learning in a mouse model of CDKL5 disorder. *Neurobiol Dis* **82**, 298–310 (2015).

459. Galvani, G. *et al.* Inhibition of microglia overactivation restores neuronal survival in a mouse model of CDKL5 deficiency disorder. *J Neuroinflammation* **18**, 155 (2021).

460. Fuchs, C. *et al.* Heterozygous CDKL5 Knockout Female Mice Are a Valuable Animal Model for CDKL5 Disorder. *Neural Plast* **2018**, 9726950 (2018).

461. Gennaccaro, L. *et al.* Age-Related Cognitive and Motor Decline in a Mouse Model of CDKL5 Deficiency Disorder is Associated with Increased Neuronal Senescence and Death. *Aging Dis* **12**, 764–785 (2021).

462. Urist, M. R. Bone: formation by autoinduction. *Science* **150**, 893–899 (1965).

463. Urist, M. R., Mikulski, A. & Lietze, A. Solubilized and insolubilized bone morphogenetic protein. *Proc Natl Acad Sci U S A* **76**, 1828–1832 (1979).

464. Bessa, P. C., Casal, M. & Reis, R. L. Bone morphogenetic proteins in tissue engineering: the road from the laboratory to the clinic, part I (basic concepts). *Journal of Tissue Engineering and Regenerative Medicine* **2**, 1–13 (2008).

465. Reddi, A. H. BMPs: from bone morphogenetic proteins to body morphogenetic proteins. *Cytokine Growth Factor Rev* **16**, 249–250 (2005).

466. Tsumaki, N. & Yoshikawa, H. The role of bone morphogenetic proteins in endochondral bone formation. *Cytokine Growth Factor Rev* **16**, 279–285 (2005).

467. White, P. M. *et al.* Neural crest stem cells undergo cell-intrinsic developmental changes in sensitivity to instructive differentiation signals. *Neuron* **29**, 57–71 (2001).

468. Chen, H. *et al.* BMP10 is essential for maintaining cardiac growth during murine cardiogenesis. *Development* **131**, 2219–2231 (2004).

469. Kishigami, S. & Mishina, Y. BMP signaling and early embryonic patterning. *Cytokine Growth Factor Rev* **16**, 265–278 (2005).

470. Callis, T. E., Cao, D. & Wang, D.-Z. Bone morphogenetic protein signaling modulates myocardin transactivation of cardiac genes. *Circ Res* **97**, 992–1000 (2005).

471. Knight, P. G. & Glister, C. TGF-beta superfamily members and ovarian follicle development. *Reproduction* **132**, 191–206 (2006).

472. Reddi, A. H. Cartilage-derived morphogenetic proteins and cartilage morphogenesis. *Microsc Res Tech* **43**, 131–136 (1998).

473. Kang, Q. *et al.* Characterization of the distinct orthotopic bone-forming activity of 14 BMPs using recombinant adenovirus-mediated gene delivery. *Gene Ther* **11**, 1312–1320 (2004).

474. Simic, P. & Vukicevic, S. Bone morphogenetic proteins in development and homeostasis of kidney. *Cytokine Growth Factor Rev* **16**, 299–308 (2005).

475. Wyatt, A. W., Osborne, R. J., Stewart, H. & Ragge, N. K. Bone morphogenetic protein 7 (BMP7) mutations are associated with variable ocular, brain, ear, palate, and skeletal anomalies. *Hum Mutat* **31**, 781–787 (2010).

476. Yu, Q. *et al.* BMP7 Gene involved in nonsyndromic orofacial clefts in Western Han Chinese. *Med Oral Patol Oral Cir Bucal* **20**, e298-304 (2015).

477. Zouvelou, V. *et al.* Generation and functional characterization of mice with a conditional BMP7 allele. *Int J Dev Biol* **53**, 597–603 (2009).

478. Kouskoura, T. *et al.* The etiology of cleft palate formation in BMP7-deficient mice. *PLoS One* **8**, e59463 (2013).

479. Dooley, C. M. *et al.* The gene regulatory basis of genetic compensation during neural crest induction. *PLoS Genet* **15**, e1008213 (2019).

480. Etchevers, H. C., Dupin, E. & Le Douarin, N. M. The diverse neural crest: from embryology to human pathology. *Development* **146**, dev169821 (2019).

481. Roth, D. M., Bayona, F., Baddam, P. & Graf, D. Craniofacial Development: Neural Crest in Molecular Embryology. *Head Neck Pathol* **15**, 1–15 (2021).

482. Danielian, P. S., Muccino, D., Rowitch, D. H., Michael, S. K. & McMahon, A. P. Modification of gene activity in mouse embryos in utero by a tamoxifen-inducible form of Cre recombinase. *Curr Biol* **8**, 1323–1326 (1998).

483. Kouskoura, T. *et al.* Dislocated Tongue Muscle Attachment and Cleft Palate Formation. *J Dent Res* **95**, 453–459 (2016).

484. Baddam, P. *et al.* Neural crest-specific deletion of Bmp7 leads to midfacial hypoplasia, nasal airway obstruction, and disordered breathing modelling Obstructive Sleep Apnea. *Dis Model Mech* **14**, dmm047738, dmm.047738 (2021).

485. Drorbaugh, J. E. & Fenn, W. O. A barometric method for measuring ventilation in newborn infants. *Pediatrics* **16**, 81–87 (1955).

486. Mortola, J. P. & Frappell, P. B. On the barometric method for measurements of ventilation, and its use in small animals. *Can J Physiol Pharmacol* **76**, 937–944 (1998).

487. Stephenson, R. & Gucciardi, E. J. Theoretical and practical considerations in the application of whole body plethysmography to sleep research. *Eur J Appl Physiol* **87**, 207–219 (2002).

488. Lim, R. *et al.* Measuring respiratory function in mice using unrestrained whole-body plethysmography. *J Vis Exp* e51755 (2014) doi:10.3791/51755.

489. Crone, S. A. *et al.* Irregular Breathing in Mice following Genetic Ablation of V2a Neurons. *J Neurosci* **32**, 7895–7906 (2012).

490. Berteotti, C. *et al.* Effect of ambient temperature on sleep breathing phenotype in mice: the role of orexins. *The Journal of experimental biology* **223**, (2020).

491. Giannakopoulou, C. E. *et al.* Regulation of breathing pattern by IL-10. *Am J Physiol Regul Integr Comp Physiol* **317**, R190–R202 (2019).

492. Chapin, J. L. Ventilatory response of the unrestrained and unanesthetized hamster to CO2. *Am J Physiol* **179**, 146–148 (1954).

493. Bastianini, S. *et al.* Accurate discrimination of the wake-sleep states of mice using non-invasive whole-body plethysmography. *Sci Rep* **7**, 41698 (2017).

494. Nakamura, A., Fukuda, Y. & Kuwaki, T. Sleep apnea and effect of chemostimulation on breathing instability in mice. *J Appl Physiol (1985)* **94**, 525–532 (2003).

495. Bartolucci, M. L. *et al.* Obstructive sleep apneas naturally occur in mice during REM sleep and are highly prevalent in a mouse model of Down syndrome. *Neurobiol Dis* **159**, 105508 (2021).

496. Hernandez, A. B. *et al.* Novel whole body plethysmography system for the continuous characterization of sleep and breathing in a mouse. *J Appl Physiol (1985)* **112**, 671–680 (2012).

497. Bastianini, S. *et al.* Post-sigh sleep apneas in mice: Systematic review and data-driven definition. *J Sleep Res* **28**, e12845 (2019).

498. Friedman, L. *et al.* Ventilatory behavior during sleep among A/J and C57BL/6J mouse strains. *J Appl Physiol (1985)* **97**, 1787–1795 (2004).

499. Stettner, G. M. *et al.* Spontaneous central apneas occur in the C57BL/6J mouse strain. *Respir Physiol Neurobiol* **160**, 21–27 (2008).

500. Yamauchi, M. *et al.* Post-sigh breathing behavior and spontaneous pauses in the C57BL/6J (B6) mouse. *Respir Physiol Neurobiol* **162**, 117–125 (2008).

501. Gillombardo, C. B. *et al.* C57BL/6J mouse apolipoprotein A2 gene is deterministic for apnea. *Respir Physiol Neurobiol* **235**, 88–94 (2017).

502. Silvani, A. *et al.* Sleep modulates hypertension in leptin-deficient obese mice. *Hypertension* **53**, 251–255 (2009).

503. Bastianini, S. *et al.* Histamine Transmission Modulates the Phenotype of Murine Narcolepsy Caused by Orexin Neuron Deficiency. *PLoS One* **10**, e0140520 (2015).

504. Moore, C. S. *et al.* Increased male reproductive success in Ts65Dn 'Down syndrome' mice. *Mamm Genome* **21**, 543–549 (2010).

505. Reinholdt, L. G. *et al.* Molecular characterization of the translocation breakpoints in the Down syndrome mouse model Ts65Dn. *Mamm Genome* **22**, 685–691 (2011).

506. Franken, P., Malafosse, A. & Tafti, M. Genetic determinants of sleep regulation in inbred mice. *Sleep* **22**, 155–169 (1999).

507. Silvani, A. *et al.* Cardiorespiratory anomalies in mice lacking CB1 cannabinoid receptors. *PLoS One* **9**, e100536 (2014).

508. Drorbaugh, J. E. & Fenn, W. O. A barometric method for measuring ventilation in newborn infants. *Pediatrics* **16**, 81–87 (1955).

509. Seeley, R. J. & MacDougald, O. A. Mice as experimental models for human physiology: when several degrees in housing temperature matter. *Nature Metabolism 2021 3:4* **3**, 443–445 (2021).

510. Antoine C. Sur les variations de tempéreture des gaz et des vapeurs qui conservent la même quantité de chaleur sous des tensions différentes. *Comptes Rendus des Séances de l'Académie des Sciences* **106**, 56–60 (1888).

511. Thomson, G. W. The Antoine equation for vapor-pressure data. *Chemical reviews* **38**, 1–39 (1946).

512. Shamim-Uzzaman, Q. A., Singh, S. & Chowdhuri, S. Hypopnea definitions, determinants and dilemmas: a focused review. *Sleep Science and Practice* **2**, 7 (2018).

513. Curran-Everett, D. Multiple comparisons: philosophies and illustrations. *Am J Physiol Regul Integr Comp Physiol* **279**, R1-8 (2000).

514. Léger, D. & Stepnowsky, C. The economic and societal burden of excessive daytime sleepiness in patients with obstructive sleep apnea. *Sleep Med Rev* **51**, 101275 (2020).

515. Trzepizur, W., Cortese, R. & Gozal, D. Murine models of sleep apnea: functional implications of altered macrophage polarity and epigenetic modifications in adipose and vascular tissues. *Metabolism* **84**, 44–55 (2018).

516. Brennick, M. J. *et al.* Altered upper airway and soft tissue structures in the New Zealand Obese mouse. *Am J Respir Crit Care Med* **179**, 158–169 (2009).

517. Brennick, M. J., Kuna, S. T., Pickup, S., Cater, J. & Schwab, R. J. Respiratory modulation of the pharyngeal airway in lean and obese mice. *Respir Physiol Neurobiol* **175**, 296–302 (2011).

518. McSharry, D. G. *et al.* Physiological mechanisms of upper airway hypotonia during REM sleep. *Sleep* **37**, 561–569 (2014).

519. Mokhlesi, B. *et al.* Obstructive sleep apnea during REM sleep and hypertension. results of the Wisconsin Sleep Cohort. *Am J Respir Crit Care Med* **190**, 1158–1167 (2014).

520. Anttalainen, U. *et al.* Prolonged partial upper airway obstruction during sleep - an underdiagnosed phenotype of sleep-disordered breathing. *Eur Clin Respir J* **3**, 31806 (2016).

521. Lal, C., White, D. R., Joseph, J. E., van Bakergem, K. & LaRosa, A. Sleep-Disordered Breathing in Down Syndrome. *Chest* **147**, 570–579 (2015).

522. Ferri, R. *et al.* Respiratory patterns during sleep in Down's syndrome:importance of central apnoeas. *J Sleep Res* **6**, 134–141 (1997).

523. Ridore, S., Debbarma, S., Nazir, R., Bennett, D. S. & Sedky, K. Obstructive Sleep Apnea in Individuals with Down Syndrome: A Meta-Analytic Literature Review. *JSDR* **1**, 1–15 (2017).

524. Bonsignore, M. R., Romano, S., Marrone, O., Chiodi, M. & Bonsignore, G. Different heart rate patterns in obstructive apneas during NREM sleep. *Sleep* **20**, 1167–1174 (1997).

525. Silvani, A., Calandra-Buonaura, G., Dampney, R. A. L. & Cortelli, P. Brain-heart interactions: physiology and clinical implications. *Philos Trans A Math Phys Eng Sci* **374**, 20150181 (2016).

526. Fan, Z., Ahn, M., Roth, H. L., Li, L. & Vaughn, B. V. Sleep Apnea and Hypoventilation in Patients with Down Syndrome: Analysis of 144 Polysomnogram Studies. *Children (Basel)* **4**, 55 (2017).

527. Simpson, R., Oyekan, A. A., Ehsan, Z. & Ingram, D. G. Obstructive sleep apnea in patients with Down syndrome: current perspectives. *Nat Sci Sleep* **10**, 287–293 (2018).

528. Thottam, P. J., Choi, S., Simons, J. P. & Kitsko, D. J. Effect of Adenotonsillectomy on Central and Obstructive Sleep Apnea in Children with Down Syndrome. *Otolaryngol Head Neck Surg* **153**, 644–648 (2015).

529. Hagebeuk, E. E. O., van den Bossche, R. A. S. & de Weerd, A. W. Respiratory and sleep disorders in female children with atypical Rett syndrome caused by mutations in the CDKL5 gene. *Dev Med Child Neurol* **55**, 480–484 (2013).

530. Hagebeuk, E. E. O., Smits, A. & de Weerd, A. Long time polysomnographic sleep and breathing evaluations in children with CDKL5 deficiency disorder. *Sleep Med* **103**, 173–179 (2023).

531. LoMauro, A. & Aliverti, A. Sex and gender in respiratory physiology. *Eur Respir Rev* **30**, 210038 (2021).

532. Torres-Tamayo, N. *et al.* 3D analysis of sexual dimorphism in size, shape and breathing kinematics of human lungs. *J Anat* **232**, 227–237 (2018).

533. Gargaglioni, L. H., Marques, D. A. & Patrone, L. G. A. Sex differences in breathing. *Comp Biochem Physiol A Mol Integr Physiol* **238**, 110543 (2019).

534. Behan, M. & Thomas, C. F. Sex hormone receptors are expressed in identified respiratory motoneurons in male and female rats. *Neuroscience* **130**, 725–734 (2005).

535. Popovic, R. M. & White, D. P. Upper airway muscle activity in normal women: influence of hormonal status. *J Appl Physiol (1985)* **84**, 1055–1062 (1998).

536. Berthon-Jones, M. & Sullivan, C. E. Ventilation and arousal responses to hypercapnia in normal sleeping humans. *J Appl Physiol Respir Environ Exerc Physiol* **57**, 59–67 (1984).

537. White, D. P., Douglas, N. J., Pickett, C. K., Weil, J. V. & Zwillich, C. W. Hypoxic ventilatory response during sleep in normal premenopausal women. *Am Rev Respir Dis* **126**, 530–533 (1982).

538. Cowley, P. M. *et al.* Functional and biochemical characterization of soleus muscle in Down syndrome mice: insight into the muscle dysfunction seen in the human condition. *Am J Physiol Regul Integr Comp Physiol* **303**, R1251-1260 (2012).

539. Segklia, A. *et al.* Bmp7 regulates the survival, proliferation, and neurogenic properties of neural progenitor cells during corticogenesis in the mouse. *PLoS One* **7**, e34088 (2012).

540. Seifert, E. L., Knowles, J. & Mortola, J. P. Continuous circadian measurements of ventilation in behaving adult rats. *Respir Physiol* **120**, 179–183 (2000).

541. Dejours, P. *Principles of comparative respiratory physiology*. (Elsevier/North-Holland Biomedical Press, 1981).